Superpartner Mass Spectrum and Cosmological Implications from Orbifolds

Dissertation

zur Erlangung des Doktorgrades

des Departments Physik

der Universität Hamburg

vorgelegt von

Kai Schmidt-Hoberg

aus Hamburg

Hamburg

2007

Gutachter der Dissertation:	Prof. Dr. W. Buchmüller
	Prof. Dr. J. Louis
Gutachter der Disputation:	Prof. Dr. W. Buchmüller
	Prof. Dr. J. Bartels
Datum der Disputation:	19. 06. 2007
Vorsitzender des Prüfungsausschusses:	Prof. Dr. C. Hagner
Vorsitzender des Promotionsausschusses:	Prof. Dr. G. Huber
Dekan der Fakultät MIN:	Prof. Dr. A. Frühwald

Abstract

This thesis is devoted to orbifolded quantum field theories in six spacetime dimensions. Within the framework of $T^2/\mathbb{Z}_2$ and $T^2/\left(\mathbb{Z}_2 \times \mathbb{Z}_2^{\mathrm{PS}} \times \mathbb{Z}_2^{\mathrm{GG}}\right)$ we calculate the Casimir energy, which yields an essential contribution to the modulus potential. Turning to more phenomenological aspects, we study gaugino-mediated supersymmetry breaking in a six-dimensional $SO(10)$ orbifold GUT model where quarks and leptons are mixtures of brane and bulk fields. We derive bounds on the soft supersymmetry breaking parameters and calculate the superparticle mass spectrum. Higgs fields are bulk fields, and in general their masses differ from those of squarks and sleptons at the unification scale. As a consequence, at different points in parameter space, the gravitino, a neutralino or a scalar lepton can be the lightest or next-to-lightest superparticle. We investigate the constraints from primordial nucleosynthesis on the different scenarios. While neutralino dark matter and gravitino dark matter with a $\widetilde{\nu}$ next-to-lightest superparticle are consistent for a wide range of parameters, gravitino dark matter with a $\widetilde{\tau}$ next-to-lightest superparticle is strongly constrained.

Zusammenfassung

Diese Arbeit beschäftigt sich mit Quantenfeldtheorien auf sechsdimensionalen Orbifolds. Wir berechnen die Casimir-Energie auf den kompakten extradimensionalen Räumen $T^2/\mathbb{Z}_2$ und $T^2/\left(\mathbb{Z}_2 \times \mathbb{Z}_2^{\mathrm{PS}} \times \mathbb{Z}_2^{\mathrm{GG}}\right)$. Als eine phänomenologische Anwendung solcher Theorien studieren wir Gaugino-Mediation in einem sechsdimensionalen $SO(10)$ Orbifold GUT Modell, in welchem Quarks und Leptonen Mischungen aus Brane- und Bulkfeldern sind. Wir leiten Schranken an die weichen supersymmetriebrechenden Terme ab und bestimmen das Massenspektrum der supersymmetrischen Teilchen. Die Higgs-Felder sind Bulkfelder und haben im allgemeinen andere Massen an der GUT Skala als die Squarks und Sleptonen. Daraus ergibt sich, daß in unterschiedlichen Bereichen des Parameterraumes ein Neutralino, ein Gravitino oder ein skalares Lepton das leichteste beziehungsweise zweitleichteste Superteilchen sein kann. Wir untersuchen die Einschränkungen verschiedener Szenarien, die sich durch die korrekte Vorhersage der Produktion leichter Elemente im frühen Universum ergeben. Während Neutralinos zum einen und Gravitinos mit einem Sneutrino als zweitleichtestem Superteilchen zum anderen über einen großen Parameterbereich gute Kandidaten für die Dunkle Materie darstellen, ist ein Szenario, in dem Dunkle Materie aus Gravitinos mit einem Stau als zweitleichtestem Superteilchen besteht, starken Einschränkungen unterworfen.

Contents

I. Introduction

A few months before the start of the Large Hadron Collider (LHC), high energy physics finds itself in a peculiar situation: On the one hand, most results from laboratory experiments confirm the expectations of the standard model of particle physics, on the other hand there are many theoretical arguments which suggest that the standard model should not be considered the fundamental theory of nature. Recent cosmological data support these theoretical considerations. In particular it seems impossible to incorporate the by now well-established cosmological concordance model with dark matter and dark energy dominating the energy density of our universe. While there are quite simple extensions of the standard model which can provide viable dark matter candidates, the existence of dark energy will most likely require a deeper understanding of quantum gravity and might force us to go beyond the familiar framework of quantum field theory. All this leads to the conclusion that the standard model, though spectacularly successful at energies currently accessible at colliders, should be regarded as a low-energy effective theory only. An immediate question resulting from this conclusion concerns the energy scale up to which the standard model is valid. Certainly a new framework will be required at the Planck scale, where quantum gravitational effects become important. However there are many reasons to believe that new effects set in at a much smaller scale. In fact, theoretical considerations suggest that there will be some deviations from the standard model at an energy scale as low as 1 TeV – precisely the region that will be experimentally tested at the LHC.

But what kind of 'new physics' is the LHC likely to find? Guided by the idea that the standard model should be embedded into a more fundamental framework such as string theory, one may hope to find imprints of this fundamental theory. However, as the string scale is far beyond the energy scale which will be probed at the LHC we would not expect these signatures to show any 'stringyness'. Rather we would expect some signals which result from the low-energy limit of string theory. With this in mind it seems sensible to look for implications this limit might have for collider searches. When trying to connect string theory with our world at low energies, we have to account for the fact that we experience only four spacetime dimensions, while string theory is intrinsically higher-dimensional. Consequently, to recover the four spacetime dimensions we are used to, the additional spacetime dimensions have to be hidden somehow. One possibility to achieve this is via compactification of the extra dimensions, where the inverse radius of compactification – the compactification scale – has to be large enough in order to be compatible with current experiments. Although these extra-dimensions are essentially invisible, they can have a profound influence on the particle spectrum and symmetries at low energies.

Another ingredient which, like additional spacetime dimensions, is almost inevitable

in string theory is supersymmetry. Although there is as yet no experimental evidence for it, theories with low-energy supersymmetry have emerged as the strongest candidates for physics beyond the standard model. The motivations for supersymmetric theories are manifold. Besides solving several long standing problems of particle physics it also provides a candidate particle for cold dark matter in form of the lightest supersymmetric particle (LSP) if R-parity is conserved. In this thesis we will not elaborate on the basics of supersymmetry but simply assume an elementary knowledge. The reader who is not familiar with this subject is referred to one of the following introductory articles [1, 2].

The complexity of string theory allows explicit calculations only in a very limited number of cases and makes it difficult to extract detailed phenomenological implications. Besides it is not clear how exactly the additional space-like dimensions should be compactified. There are however suggestions that some of these extra dimensions could be larger than others [3]. If one assumes a string compactification which is highly anisotropic, there exists an energy region in which the description in terms of an intermediate higher dimensional field theory with typically one or two extra dimensions seems appropriate. The main focus of this thesis will be on such higher-dimensional field theories with two additional spacetime dimensions. In particular we will be interested in phenomenological implications for particle physics and cosmology. At this stage it should be noted that although we motivated these higher-dimensional field theories as an intermediate step between string theory and the standard model, they can also be seen as an extension to the standard model with an unknown high energy completion, which is the line of thinking we will be following here.

In the course of this thesis we will see that in order to obtain a viable phenomenology we have to employ a particular compactification scheme which was originally invented in string theory [4, 5]. The resulting compact spaces are known as orbifolds and unlike a smooth internal manifold they possess points where the metric becomes singular. Recently these orbifolds have become popular in a purely field theoretic context [6–12]. What are the properties which make these orbifolded field theories so popular? The symmetries and the particle content of the standard model as well as the apparent unification of gauge couplings hint towards grand unified theories (GUTs). These grand unified theories can naturally explain the observed patterns of quarks and leptons, but in the standard four-dimensional setup they give no clues as to why these patterns show large hierarchies in masses and mixings. In contrast, orbifold GUTs are attractive candidates for unified theories explaining the masses and mixings of fermions. In addition, features such as the doublet-triplet splitting and the absence of dimension-five operators for proton decay, which are difficult to realise in four-dimensional grand unified theories, are easily obtained.

Although the orbifold constructions are phenomenologically quite attractive, they suffer from a problem which is generic in all higher-dimensional theories: the size and shape of the compact space correspond to the vacuum expectation values of massless scalar fields, called moduli fields, and these expectation values are not determined at the classical level. However, in order to avoid phenomenological problems the size and shape moduli have to be 'stabilised', i.e. they have to acquire a well-defined vacuum expecta-

tion value through a non-trivial potential. There are classical as well as quantum effects which can potentially lead to such a stabilisation. One quantum contribution to the potential which is generically present in theories with compact spaces depends on the properties of the extra-dimensional space [13,14]. We will evaluate the resulting 'Casimir energy' in Chapter III and discuss its rôle for the stabilisation of the extra-dimensional volume.

If supersymmetry is realised in nature, it must be broken. While it is unclear what kind of breaking mechanism should be considered, it is desirable that the breaking is spontaneous rather than explicit to preserve the appealing features of supersymmetry. As of now it is generally believed that supersymmetry should be broken in a "hidden sector" to lift the superpartner masses to a phenomenologically acceptable range. A very natural way to achieve a separation between different sectors is through the introduction of branes in a higher dimensional spacetime. Higher-dimensional locality then forbids direct couplings between fields that live on different branes.[1] Gaugino mediation [16,17] is an attractive way to achieve supersymmetry breaking in such higher-dimensional theories. The main idea of gaugino mediation is that gauge and possibly Higgs fields live in the bulk whereas matter fields are confined to four-dimensional branes. Supersymmetry is broken on an additional, spatially separated brane by the non-vanishing F-term vacuum expectation value of a chiral gauge singlet. Gauginos and Higgs fields acquire soft supersymmetry breaking masses at tree-level, since they are bulk fields, whereas the corresponding terms for squarks and sleptons are strongly suppressed at the compactification scale. However, in order to translate these masses at the compactification scale into measurable quantities at the electroweak scale, one has to employ renormalisation group techniques and the running leads to non-vanishing masses for the squarks and sleptons too.

In order to obtain specific predictions for the superpartner mass spectrum, it seems sensible to combine models which explain the fermion masses and mixings with models for supersymmetry breaking. In Chapter IV we consider an $SO(10)$ theory in six dimensions, proposed in [11,18–20], in combination with gaugino-mediated supersymmetry breaking. The orbifold compactification of the two extra dimensions has four fixed points corresponding to four-dimensional branes. On three of them, three quark-lepton generations are localised. The standard model leptons and down-type quarks are linear combinations of these localised fermions and a partial fourth generation living in the bulk. This leads to the observed large neutrino mixings. On the fourth brane, we assume the gauge-singlet field of gaugino mediation to develop an F-term vacuum expectation value leading to the breakdown of supersymmetry. Within this setup we calculate the soft supersymmetry breaking terms at the compactification scale and constrain their values by means of naïve dimensional analysis [21]. These terms serve as boundary conditions for a renormalisation group analysis which leads to the determination of the low-energy superparticle mass spectrum.

[1] However, as argued in [15], this does not imply a sequestered form of the four-dimensional Kähler potential in general.

Varying the boundary conditions at the compactification scale, it turns out that there are different candidates for the lightest supersymmetric particle in the framework of gaugino mediation. One of them is the gravitino, whose mass only has to respect a lower bound in gaugino mediation [22]. In addition to the gravitino, a neutralino or a scalar lepton, $\widetilde{\tau}$ or $\widetilde{\nu}$, could be the LSP. However, since a scalar lepton is excluded as LSP [23, 24], it can only be the next-to-lightest superparticle (NLSP) with the gravitino as LSP, which is consistent with the lower bound on the gravitino mass. One then obtains the $\widetilde{G}$-$\widetilde{\tau}$ and the $\widetilde{G}$-$\widetilde{\nu}$ scenarios with $\widetilde{\tau}$ and $\widetilde{\nu}$ as NLSP, respectively. The $\widetilde{G}$-$\widetilde{\tau}$ scenario is particularly interesting, since it may allow to determine the gravitino mass and spin at colliders [25–30]. It is well known, however, to be strongly constrained by primordial nucleosynthesis (BBN) [31–35]. In Chapter V we therefore study the impact of such cosmological constraints on the $\widetilde{G}$-$\widetilde{\tau}$ scenario and compare it with the other dark matter scenarios within the setup of gaugino mediation.

To summarise, this thesis is organised as follows. In the next chapter, we will briefly introduce the concept of an orbifold and discuss how supersymmetry as well as gauge symmetry breaking can be achieved by the compactification. We will also supply the necessary background that we need to calculate the Casimir energy in Chapter III. Chapter IV is devoted to the calculation of the low-energy superpartner mass spectrum within the framework of gaugino mediation while Chapter V will mainly be concerned with cosmological constraints on the gaugino mediation scenario. Whereas the results of Chapter III are unpublished as of now, Chapters IV and V are mainly based on our references [36] and [37] respectively. For the convenience of the reader we close each chapter with a short summary and concluding remarks. Last not least we will discuss the impact of this work and point out possible future directions.

II. Orbifold Compactifications

The idea that the unification of fundamental forces may be related to the existence of extra-dimensions has intrigued many physicists ever since the pioneering works of Kaluza and Klein were published in the 1920s [38, 39]. Nevertheless, it took several decades before in the mid 1980s it was realised that ten-dimensional string theory provides a consistent quantum theory of gravity coupled to matter [40,41], and therefore is a strong candidate for a higher-dimensional unified theory incorporating the ideas of Kaluza and Klein. More recently the framework of higher-dimensional theories became an important research topic also for particle phenomenologists. The tremendous interest was triggered by the fact that these theories offer new possible solutions to long standing problems of particle physics such as the naturalness and the hierarchy problem [42].

One obvious phenomenological constraint which was already discussed in the introduction is that the extra dimensions have to be hidden in some way in order to mimic the four-dimensional world we live in. The simplest realisation of a spacetime that looks four-dimensional from a low energy perspective is a product space where four of these dimensions are large while the additional dimensions form a small compact manifold. A simple example of such a compact manifold is an n-dimensional torus, where n is the number of extra dimensions. Of course the radius of compactification has to be small enough so that the extra dimensions are unaccessible by current experiments. However, even for small radii there is a serious drawback which makes the resulting theory unsuitable as a candidate for a physical theory. The problem lies within the spinor representation in higher dimensional spacetimes. The minimal dimension of a spinor grows rapidly with spacetime-dimension which makes it impossible to construct a theory which is chiral from the four-dimensional point of view, when all spinor components survive the compactification procedure. It was realised that this problem could be circumvented by using a particular compactification scheme, known as orbifold compactification. In this scheme the resulting compact space is not a smooth manifold but a space which possesses singular points.

Originally orbifold compactifications were used in the context of string theory [4, 5] but most field theory orbifold models which are on the market by now are not derived from specific string constructions. This is why a careful discussion of the consistency of these field theoretic orbifolds is required, since they are not directly embedded in the consistent framework of string theories.

In this thesis we will be concerned with two-dimensional toroidal orbifold compactifications corresponding to a six-dimensional spacetime in the full setup. An orbifold is a generalisation of a manifold which locally looks like a quotient space of $\mathbb{R}^n$. While the mathematical definition is wider, in physics the notion of an orbifold usually refers to a

space which is constructed from a regular manifold by modding out a non-freely acting discrete symmetry.[1] At fixed points of the discrete symmetry the metric on the orbifold becomes singular. At non-singular points however, the orbifold is locally indistinguishable from the regular manifold and inherits many of its properties. Therefore we will briefly discuss this regular manifold before we move on to the orbifold construction.

1. The Torus $\mathbf{T^2}$

The two-dimensional torus T^2 is specified by its underlying lattice which in turn depends on three independent real parameters. These are given by the two lengths of the lattice vectors $L_1 \equiv 2\pi R_y$, $L_2 = 2\pi R_z$ and the angle θ between them (see Figure II.1). Points

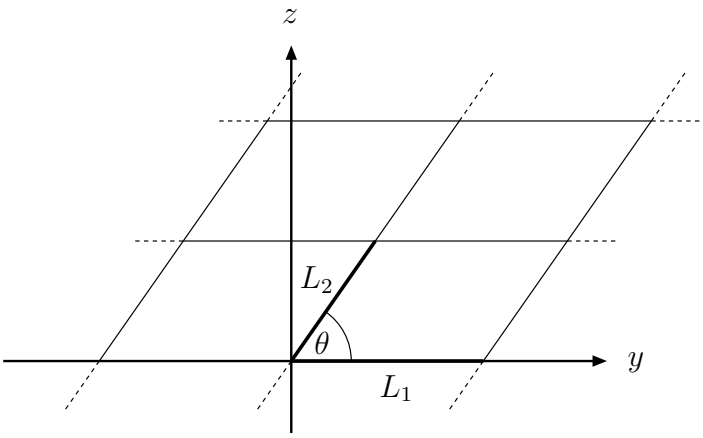

Figure II.1.: Lattice of the Torus with the three moduli L_1, L_2 and θ.

which differ by a lattice vector are identified, leading to the periodicity of the torus,

$$(y, z) \cong (y + nL_2 \cos\theta + mL_1, z + nL_2 \sin\theta)\,, \tag{II.1}$$

where (y, z) are the extra-dimensional coordinates and $m, n \in \mathbb{Z}$. Sometimes it is more convenient to express the shape and size of the torus in terms of the area modulus $\mathcal{A} = L_1 L_2 \sin\theta$ and the shape modulus $\tau = \frac{L_2}{L_1} e^{i\theta}$.

Fields which live on the product space $\mathcal{M}^4 \times T^2$ have to fulfill certain boundary conditions in order to be consistent with the periodicity of the torus: They have to be equal at the identified points up to a global or local symmetry transformation of the Lagrangian. For example a periodic scalar field $\Phi(x, y, z)$ satisfies

[1] Not all orbifolds in the mathematical sense can globally be written as a regular manifold modded out by some symmetry.

$$\Phi(x, y + nL_2 \cos\theta + mL_1, z + nL_2 \sin\theta) = \Phi(x, y, z)\,. \tag{II.2}$$

There can also be more general boundary conditions including a complex phase, which is known as a Scherk-Schwarz twist [43].

1.1. Mode Expansion on $\mathbf{T^2}$

The dependence of a field on the extra-dimensional coordinates (y, z) can be expanded in terms of eigenfunctions of the extra-dimensional Laplacian according to

$$\Phi(x, y, z) = \sum_{m,n=-\infty}^{\infty} \phi_{(m,n)}(x) \cdot f_{m,n}(y, z)\,. \tag{II.3}$$

The explicit form of the expansion depends on the boundary conditions of the six-dimensional field $\Phi(x, y, z)$. For periodic boundary conditions as in (II.2) the mode expansion can be written as

$$\Phi(x, y, z) = \frac{1}{\sqrt{\mathcal{A}}} \sum_{m,n=-\infty}^{\infty} \phi_{(m,n)}(x) \cdot \exp\left\{ i \left(m \frac{y - z\cot\theta}{R_y} + n \frac{z}{R_z \sin\theta} \right) \right\}\,. \tag{II.4}$$

Here the normalisation is chosen such that the fields $\phi_{(m,n)}(x)$ have a canonical kinetic term when integrating over the extra dimensions to obtain the effective four-dimensional theory. Performing this integration we obtain an infinite tower of massive four-dimensional fields - the well-known Kaluza-Klein tower. In the periodic case the mass for the mode $\phi_{(m,n)}(x)$ is given by

$$\mathcal{M}^2_{m,n} = \frac{1}{\sin^2\theta} \left(\frac{m^2}{R_y^2} + \frac{n^2}{R_z^2} - \frac{2mn\cos\theta}{R_y R_z} \right) = \frac{4\pi^2}{\mathcal{A}\tau_2} \left| n - m\tau \right|^2\,. \tag{II.5}$$

We see that the Kaluza-Klein spectrum is sensitive to the volume as well as to the shape of the extra-dimensional space. For $\theta = \pi/2$ the Kaluza-Klein masses reduce to their well known form for a rectangular torus lattice. As can be seen from (II.5) the Kaluza-Klein masses are inversely proportional to the size of the extra dimensions in the rectangular case. Since the size of the extra dimensions is usually considered to be very small, the corresponding Kaluza-Klein masses are very heavy, leaving only the massless zero mode in the low energy effective action.

2. The Orbifold $\mathbf{T^2/\mathbb{Z}_2}$

Having briefly discussed the covering space let us come to the construction of $T^2/\mathbb{Z}_2$, the orbifold we will be mainly concerned with in this thesis. Note that unlike $\mathbb{Z}_N$ rotations

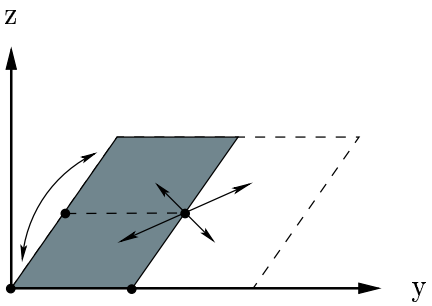

(a) *Construction of the $T^2/\mathbb{Z}_2$ orbifold through implementing the $\mathbb{Z}_2$-symmetry and gluing the edges.*

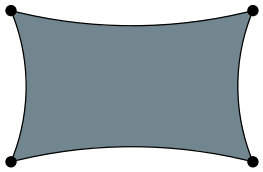

(b) *The resulting pillow with the four corners corresponding to the four fixed points*

Figure II.2.: The $\mathbb{Z}_2$-Transformation acting on the Torus.

with $N > 2$, the reflection is always a symmetry of the lattice for any value of the moduli $\mathcal{A}$ and τ and hence they are also moduli of the resulting orbifold.

When orbifolding a quantum field theory, the symmetry group acts on coordinate space as well as on field space. We first implement the $\mathbb{Z}_2$-symmetry on the internal manifold by identifying points which are mapped onto each other by the reflection r

$$r : (y, z) \mapsto -(y, z) \,. \tag{II.6}$$

This action has four fixed points,

$$P_1 = (0, 0) \,, \tag{II.7a}$$
$$P_2 = (\pi R_y, 0) \,, \tag{II.7b}$$
$$P_3 = (\pi R_y \cos\theta, \pi R_z \sin\theta) \,, \tag{II.7c}$$
$$P_4 = (\pi R_y (1 + \cos\theta), \pi R_z \sin\theta) \,. \tag{II.7d}$$

The fundamental domain is halved and the edges are identified as sketched in Figure II.2. Embedded into three-dimensional space, the resulting object can be thought of as a 'pillow' with four corners, corresponding to the four fixed points. These fixed points lead to many new phenomena in orbifolded theories which are absent in theories that are formulated on the original manifold. In particular 'brane fields' can be localised at these fixed points leading to many new possibilities for model building. Furthermore quantum corrections of bulk fields in general lead to divergences localised at the fixed points [44]. These divergences have to be renormalised by field operators on the branes, inducing a running of the brane couplings with the renormalisation scale. Therefore they cannot be set to zero at all scales and should be considered free parameters of the theory which should be included in the action already at tree level. This means that in addition to the intrinsic brane fields there are also brane localised terms of bulk fields.

However, these brane terms are volume suppressed in comparison to the corresponding bulk terms, and therefore they are usually considered small perturbations.

Because the orbifold reflection (II.6) is a symmetry of the higher-dimensional Laplacian, it has a natural action on its eigenfunctions. The action of the symmetry group on field space can be written as [45]

$$r : \Phi_i(x,y,z) \mapsto R_{ij}\Phi_j(x,-y,-z) \quad , \quad R^2 = \mathbb{1}\,, \tag{II.8}$$

where R is a matrix representation of the $\mathbb{Z}_2$ symmetry group with eigenvalues ± 1 and Φ a vector which comprises all fields in the theory. In the diagonal basis, fields can be classified by their respective eigenvalues, leading to a set of even and odd fields:

$$r : \Phi_i(x,y,z) \mapsto \pm\Phi_i(x,-y,-z)\,. \tag{II.9}$$

In the following we will see that the phenomenological consequences of this seemingly innocent orbifold action are quite profound.

2.1. Mode Expansion on $\mathbf{T^2/\mathbb{Z}_2}$

Using the orbifold action on fields (II.9), the toroidal mode expansion (II.4) can be restricted to the orbifolded case. Special care has to be taken about the normalisation in order to ensure a canonical kinetic term for the Kaluza-Klein modes. For later convenience we will give this mode expansion explicitly. In the following we will restrict ourselves to a rectangular torus lattice. In this case the Kaluza-Klein modes for even and odd fields can be written as[2]

$$\Phi_+(x,y,z) = \frac{1}{\sqrt{2\pi^2 R_y R_z 2^{\delta_{n,0}\delta_{m,0}}}} \left[\delta_{0,m}\sum_{n\geq 0} + \sum_{m>0}\sum_{n=-\infty}^{\infty}\right] \phi_+^{(m,n)}(x) \times \cos\left(\frac{my}{R_y} + \frac{nz}{R_z}\right)\,, \tag{II.10a}$$

$$\Phi_-(x,y,z) = \frac{1}{\sqrt{2\pi^2 R_y R_z}} \left[\delta_{0,m}\sum_{n\geq 0} + \sum_{m>0}\sum_{n=-\infty}^{\infty}\right] \phi_+^{(m,n)}(x) \times \sin\left(\frac{my}{R_y} + \frac{nz}{R_z}\right)\,, \tag{II.10b}$$

respectively. From these expressions we immediately see that roughly half of the Kaluza-Klein states are projected out at the fixed points. Only even fields retain a zero mode while the lightest mode of an odd field already has a mass of order the compactification scale. This is the main feature of orbifolded field theories: By assigning appropriate boundary conditions, unwanted fields can be removed from the low energy spectrum. It is this feature which allows for novel solutions to long-standing problems of particle

[2] cf. Appendix for details.

physics. For example we can now construct a theory which is chiral in four dimensions simply by assigning different parities to the left- and right-handed components of a Dirac spinor. Furthermore the matrix R can utilise all of the symmetries of the bulk theory, including gauge symmetries. Hence when choosing appropriate boundary conditions, gauge symmetries as well as supersymmetry can be broken or reduced at the fixed points without the introduction of a complicated Higgs sector or other additional fields. Another generic feature of orbifolded theories is the existence of 'split multiplets', i.e., incomplete representations of the underlying GUT symmetry. This is why orbifolds have been extensively used in the context of grand unified theories as first suggested by Kawamura [6, 7]. Many problems of four-dimensional GUTs such as the doublet-triplet splitting problem or the (in)stability of the proton can be easily cured in this higher-dimensional setup.

In Chapter IV we will work within the framework of a supersymmetric orbifold GUT model which exhibits all these features. It is an $SO(10)$ gauge theory compactified on $T^2/(\mathbb{Z}_2 \times \mathbb{Z}_2^{\rm PS} \times \mathbb{Z}_2^{\rm GG})$. But before we familiarise the reader with the rather specific field content of this model, we will concentrate on one basic ingredient which we will need in the next chapter - the $SO(10)$ vector multiplet which resides in the bulk of the theory.

2.2. From $\mathcal{N} = 2$ to $\mathcal{N} = 1$ Supersymmetry

In this section we briefly review how to implement the orbifold symmetry on the six-dimensional vector multiplet such that a viable four-dimensional theory at low energies emerges.[3] The first thing we should note at this stage is that the minimal amount of supersymmetry in six dimensions corresponds to $\mathcal{N} = 2$ extended supersymmetry in four dimensions. However, it is well known that such extended supersymmetric theories do not lead to a viable phenomenology. Therefore something needs to be done in order to arrive at a theory which is acceptable from a phenomenological point of view.

The gauge fields A_M with $(M = \mu, 5, 6)$ and gauginos $\lambda_{1,2}$ of the six-dimensional vector multiplet can be conveniently grouped into four-dimensional $\mathcal{N} = 1$ vector and chiral multiplets:

$$V = (A_\mu, \lambda_1), \quad \Psi = (A_{5,6}, \lambda_2)\ . \tag{II.11}$$

Here V as well as Ψ are matrices in the adjoint representation of $SO(10)$. To promote the $\mathbb{Z}_2$-symmetry to a symmetry of our theory, we have to specify the $\mathbb{Z}_2$-parities of the fields as in (II.9). The unwanted extended supersymmetry can then be broken at the fixed points by choosing appropriate parities for the different fields. However, since we require the theory to be invariant under the parity transformation of the fields, the choice of parity assignments is restricted. For example invariance of the action implies that since the derivatives $\partial_{5,6}$ are odd under reflection, the two Weyl fermions λ_1 and λ_2 must have opposite parities. Taking such consistency conditions into account we

[3] For more details see e.g. [11].

can write the parity transformation of the six-dimensional fields under the reflection $(y, z) \to (-y, -z)$ as

$$\mathbb{Z}_2: \quad PV(x,-y,-z)P^{-1} = +V(x,y,z)\ , \tag{II.12a}$$
$$\mathbb{Z}_2: \quad P\Psi(x,-y,-z)P^{-1} = -\Psi(x,y,z)\ , \tag{II.12b}$$

where P is a matrix representation of the orbifold symmetry, $P^2 = 1$. Here we choose this matrix to act trivially in group space, $P = \mathbb{1}$. With these assignments only the vector multiplet V remains in the low energy spectrum while the zero modes of the chiral field Ψ are projected out. In this way the orbifold compactification leads to an effective four-dimensional gauge theory with $\mathcal{N} = 1$ supersymmetry.

However, with the given parity assignments the full $SO(10)$ gauge group survives the compactification. The simplest possibility to achieve supersymmetry as well as gauge symmetry breaking is to introduce additional $\mathbb{Z}_2$-symmetries into the theory.

3. The Orbifold $\mathbf{T^2/(\mathbb{Z}_2 \times \mathbb{Z}_2^{PS} \times \mathbb{Z}_2^{GG})}$

To achieve a breaking of the $SO(10)$ gauge group we compactify the theory on an internal space with two additional reflection symmetries, one around the point $y' = y + \frac{\pi}{2}R_y$ and the other around the point $z' = z + \frac{\pi}{2}R_z$. The construction of this orbifold is sketched in Figure II.3. The resulting space again has four fixed points, $O_{\text{I}} = (0,0)$, $O_{\text{PS}} = (\pi R_5/2, 0)$, $O_{\text{GG}} = (0, \pi R_6/2)$ and $O_{\text{fl}} = (\pi R_5/2, \pi R_6/2)$, but the fundamental domain is a factor four smaller because of the two additional reflection symmetries. However, the main difference to the orbifold $T^2/\mathbb{Z}_2$ we considered before is the non-trivial action of the two additional parities on the $SO(10)$ generators.

3.1. Breaking of the SO(10) Gauge Symmetry

Local breaking of $SO(10)$ to the Pati-Salam group $G_{\text{PS}} = SU(4) \times SU(2) \times SU(2)$ and to the extended Georgi-Glashow group $G_{\text{GG}} = SU(5) \times U(1)_X$ is achieved by acting with the additional two $\mathbb{Z}_2$-symmetries on the gauge fields,

$$\mathbb{Z}_2^{\text{PS}}: \quad P_{\text{PS}}V(x,-y+\pi R_5/2,-z)P_{\text{PS}}^{-1} = \eta^V_{\text{PS}}V(x,y+\pi R_5/2,z) \tag{II.13a}$$
$$\mathbb{Z}_2^{\text{GG}}: \quad P_{\text{GG}}V(x,-y,-z+\pi R_6/2)P_{\text{GG}}^{-1} = \eta^V_{\text{GG}}V(x,y,z+\pi R_6/2)\ . \tag{II.13b}$$

Here the P_i are matrices acting non-trivially on the $SO(10)$ generators. In the vector representation they can be taken as [11]

$$P_{\text{PS}} = \begin{pmatrix} \sigma_2 & 0 & 0 & 0 & 0 \\ 0 & \sigma_2 & 0 & 0 & 0 \\ 0 & 0 & \sigma_2 & 0 & 0 \\ 0 & 0 & 0 & \sigma_2 & 0 \\ 0 & 0 & 0 & 0 & \sigma_2 \end{pmatrix}\ , \tag{II.14a}$$

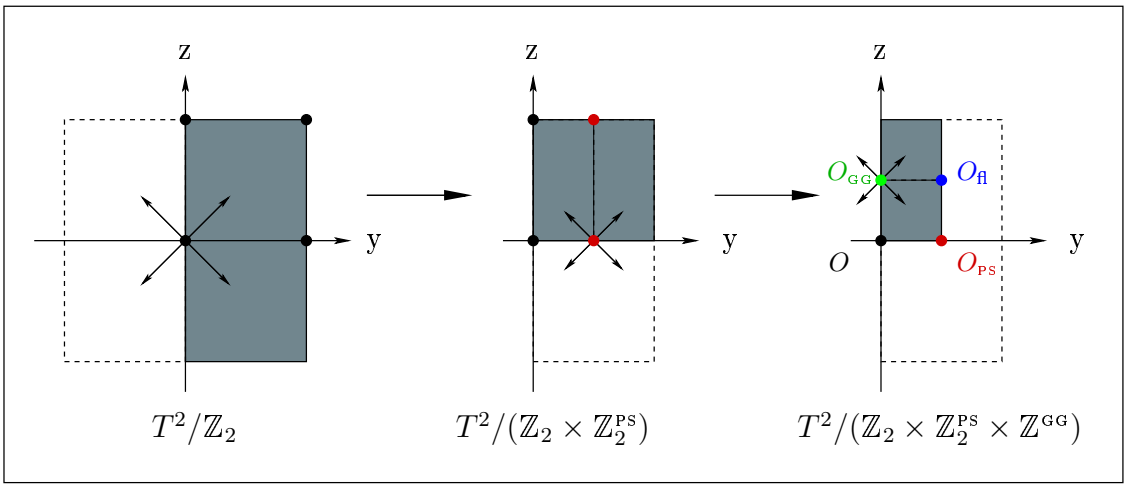

Figure II.3.: Implementation of the three $\mathbb{Z}_2$ symmetries on the two-dimensional torus T^2 leading to the Orbifold $T^2/\left(\mathbb{Z}_2 \times \mathbb{Z}_2^{PS} \times \mathbb{Z}_2^{GG}\right)$. The different coloured dots mark the inequivalent fixed points of this orbifold, as explained in the text.

$$P_{GG} = \begin{pmatrix} -\sigma_0 & 0 & 0 & 0 & 0 \\ 0 & -\sigma_0 & 0 & 0 & 0 \\ 0 & 0 & -\sigma_0 & 0 & 0 \\ 0 & 0 & 0 & \sigma_0 & 0 \\ 0 & 0 & 0 & 0 & \sigma_0 \end{pmatrix}, \tag{II.14b}$$

with σ_0 and σ_2 two-dimensional Pauli matrices[4]. The corresponding parities are chosen to be $\eta^V_{PS} = \eta^V_{GG} = +1$. Combining the $\mathbb{Z}_2$ symmetries, there is a fourth relation

$$P_{fl} V(x, -y + \pi R_5/2, -z + \pi R_6/2) P_{fl}^{-1} = V(x, y + \pi R_5/2, z + \pi R_6/2) \tag{II.15}$$

resulting in an additional subgroup $G_{fl} = SU(5)' \times U(1)'$ [12]. The given parity assignments lead to the following pattern of remaining gauge symmetries: At O_I the full $SO(10)$ survives, whereas at the other fixed points, O_{PS}, O_{GG} and O_{fl}, $SO(10)$ is broken to its three GUT subgroups G_{PS}, G_{GG} and flipped $SU(5)$, G_{fl}, respectively. The intersection of these GUT groups yields the standard model group with an additional $U(1)$ factor, $G_{SM'} = SU(3)_C \times SU(2)_L \times U(1)_Y \times U(1)_X$, as unbroken gauge symmetry below the compactification scale.

3.2. Mode Expansion on $\mathbf{T^2/\left(\mathbb{Z}_2 \times \mathbb{Z}_2^{PS} \times \mathbb{Z}_2^{GG}\right)}$

The additional reflection symmetries also change the Kaluza-Klein expansion. For later convenience we give this expansion explicitly for fields which are non-vanishing at the

[4] For notations and conventions see [11]

	$(V_\mu,\, \lambda_1)$				$(V_{5,6},\, \lambda_2)$		
$G'_{\rm SM}$	$\mathbb{Z}_2$	$\mathbb{Z}_2^{\rm GG}$	$\mathbb{Z}_2^{\rm PS}$	$\mathcal{M}^2_{m,n}$	$\mathbb{Z}_2$	$\mathbb{Z}_2^{\rm GG}$	$\mathbb{Z}_2^{\rm PS}$
$(\mathbf{8},\mathbf{1};0,0)$	$+$	$+$	$+$	$4\left(\frac{m^2}{R_y^2}+\frac{n^2}{R_z^2}\right)$	$-$	$-$	$-$
$(\mathbf{3},\mathbf{2};-5,0)$	$+$	$+$	$-$	$4\left(\frac{m^2}{R_y^2}+\frac{(n+1/2)^2}{R_z^2}\right)$	$-$	$-$	$+$
$(\bar{\mathbf{3}},\mathbf{2};5,0)$	$+$	$+$	$-$	$4\left(\frac{m^2}{R_y^2}+\frac{(n+1/2)^2}{R_z^2}\right)$	$-$	$-$	$+$
$(\mathbf{1},\mathbf{3};0,0)$	$+$	$+$	$+$	$4\left(\frac{m^2}{R_y^2}+\frac{n^2}{R_z^2}\right)$	$-$	$-$	$-$
$(\mathbf{1},\mathbf{1};0,0)$	$+$	$+$	$+$	$4\left(\frac{m^2}{R_y^2}+\frac{n^2}{R_z^2}\right)$	$-$	$-$	$-$
$(\mathbf{3},\mathbf{2};1,4)$	$+$	$-$	$-$	$4\left(\frac{(m+1/2)^2}{R_y^2}+\frac{(n+1/2)^2}{R_z^2}\right)$	$-$	$+$	$+$
$(\bar{\mathbf{3}};\mathbf{1},-4,4)$	$+$	$-$	$+$	$4\left(\frac{(m+1/2)^2}{R_y^2}+\frac{n^2}{R_z^2}\right)$	$-$	$+$	$-$
$(\mathbf{1},\mathbf{1};6,4)$	$+$	$-$	$+$	$4\left(\frac{(m+1/2)^2}{R_y^2}+\frac{n^2}{R_z^2}\right)$	$-$	$+$	$-$
$(\bar{\mathbf{3}},\mathbf{2};-1,-4)$	$+$	$-$	$-$	$4\left(\frac{(m+1/2)^2}{R_y^2}+\frac{(n+1/2)^2}{R_z^2}\right)$	$-$	$+$	$+$
$(\mathbf{3},\mathbf{1};4,-4)$	$+$	$-$	$+$	$4\left(\frac{(m+1/2)^2}{R_y^2}+\frac{n^2}{R_z^2}\right)$	$-$	$+$	$-$
$(\mathbf{1},\mathbf{1};-6,-4)$	$+$	$-$	$+$	$4\left(\frac{(m+1/2)^2}{R_y^2}+\frac{n^2}{R_z^2}\right)$	$-$	$+$	$-$
$(\mathbf{1},\mathbf{1};0,0)$	$+$	$+$	$+$	$4\left(\frac{m^2}{R_y^2}+\frac{n^2}{R_z^2}\right)$	$-$	$-$	$-$

Table II.1.: Decomposition of the 45-plet of $SO(10)$ into multiplets of the extended standard model gauge group $G'_{\rm SM} = SU(3) \times SU(2) \times U(1)_Y \times U(1)_X$ and corresponding parity assignments. For later convenience we also give the Kaluza-Klein masses $\mathcal{M}^2_{m,n}$.

fixed point $O = (0, 0)$,

$$\Phi_{+++}(x,y,z) = \frac{1}{\sqrt{2\pi R_y R_z 2^{\delta_{n,0}\delta_{m,0}}}} \left[\delta_{0,m}\sum_{n=0}^{\infty} + \sum_{m=1}^{\infty}\sum_{n=-\infty}^{\infty}\right] \phi_{+++}^{(2m,2n)}(x) \times \cos\left(\frac{2my}{R_y} + \frac{2nz}{R_z}\right), \tag{II.16a}$$

$$\Phi_{++-}(x,y,z) = \frac{1}{\sqrt{2\pi R_y R_z}} \left[\delta_{0,m}\sum_{n=0}^{\infty} + \sum_{m=1}^{\infty}\sum_{n=-\infty}^{\infty}\right] \phi_{++-}^{(2m,2n+1)}(x) \times \cos\left(\frac{2my}{R_y} + \frac{(2n+1)z}{R_z}\right), \tag{II.16b}$$

$$\Phi_{+-+}(x,y,z) = \frac{1}{\sqrt{2\pi R_y R_z}} \left[\sum_{m=0}^{\infty}\sum_{n=-\infty}^{\infty}\right] \phi_{+-+}^{(2m+1,2n)}(x) \times \cos\left(\frac{(2m+1)y}{R_y} + \frac{(2n)z}{R_z}\right), \tag{II.16c}$$

$$\Phi_{+--}(x,y,z) = \frac{1}{\sqrt{2\pi R_y R_z}} \left[\sum_{m=0}^{\infty}\sum_{n=-\infty}^{\infty}\right] \phi_{+--}^{(2m+1,2n+1)}(x) \times \cos\left(\frac{(2m+1)y}{R_y} + \frac{(2n+1)z}{R_z}\right). \tag{II.16d}$$

Only fields for which all parities are positive have zero modes. In the case we considered here, they form an $\mathcal{N} = 1$ massless vector multiplet in the adjoint representation of the unbroken extended standard model gauge group, as can be seen in Table II.1.

Summary and Concluding Remarks

In this chapter we have introduced the concept of orbifold compactifications and provided a basis for applications in the forthcoming chapters. In particular the explicit mode expansions will prove useful in the calculation of the Casimir energy. We have seen that orbifolded theories offer promising breaking schemes for supersymmetry as well as gauge symmetries and in addition imply the existence of branes, four-dimensional subspaces to which fields can be confined. All these features allow for novel solutions to many problems of high energy physics and constitute a rich phenomenology, which we are going to explore in the remainder of this work.

III. Stabilisation and Casimir Energy

We argued in the introduction that possible extra dimensions have to be small in order to be consistent with current experiments. An obvious question which results from this phenomenological constraint is the following: If we happen to live in such a higher-dimensional world, what determines the size of the extra dimensions and how is this size maintained?

To address this question in a more mathematical way we note that when we naïvely compactify a higher-dimensional theory, the volume of the compact space will correspond to a massless scalar field in the low-energy theory. This means that the potential of the field is flat and therefore the corresponding volume is arbitrary. What we encounter here is a special case of the modulus problem, a generic problem of higher-dimensional theories such as string theory which has attracted much attention recently. It is this arbitrariness which immediately leads to phenomenological problems: In addition to the problem that the extra dimensions are not small, the massless field would also contribute to Newton's law and result in a fifth force [46], which is not acceptable from a phenomenological point of view. Therefore the volume of the extra dimensions has to be fixed at some small value. It is intuitively clear that a stabilisation at non-trivial values occurs dynamically, if there are attractive and repulsive forces which balance each other at some finite volume. These stabilisation forces can be of classical origin, e.g. they can be due to a scalar bulk field which has different interactions with different branes. A prominent example of such a stabilisation mechanism can be found in [47]. In this chapter we will be concerned with another interesting possibility namely that quantum effects induce a non-trivial potential for the volume modulus.

1. The Energy of the Vacuum

The prediction of the Casimir force in 1948 [48] followed by its experimental verification in 1956 [49, 50] has stimulated investigations about the zero-point energy in quantum field theory. These investigations in turn generalised the concept of the Casimir effect to include not only electromagnetic interactions but also other quantum fields. The occurrence of divergent zero-point energies in quantum field theories can be traced back to the concept of canonical field quantisation, because this quantisation scheme does not fix the ordering of non-commuting field operators in the Hamiltonian. In order to arrive at a well defined theory this ambiguity is usually circumvented by the procedure of Wick's normal ordering which implies a formal subtraction of the zero-point energy. However, as every form of energy gravitates, the absolute value of the vacuum energy is, in principle, a measurable quantity and cannot be correctly defined by normal ordering [51].

Rather a meaningful definition of the physical vacuum energy must take into account that free quantum fields are not physical and that physical fields are in general subject to external constraints such as interactions with other fields. One can obtain an idealised description of such circumstances by forcing the fields to satisfy certain boundary conditions. Therefore the physical vacuum energy - the Casimir energy - should depend on these boundary conditions. In particular in the case of extra-dimensional scenarios it should depend on global properties of the spacetime such as the topology and boundary conditions of the compactification.

Motivated by this observation the Casimir energy is generally defined as the difference between the zero-point energy corresponding to the vacuum configuration where the fields have to fulfil certain boundary conditions and the free vacuum configuration, respectively. Since the computation of the Casimir energy is plagued with divergences, this formal definition must be supplemented with a regularisation prescription in order to obtain a finite energy difference. A convenient regularisation scheme which we will employ in the following calculations is known under the name zeta function regularisation [52,53]. For a review and applications of zeta function regularisation see e.g. [54]. In the framework of this thesis, we are mainly interested in the Casimir energy on toroidal orbifolds. Casimir energies for various theories compactified on two internal dimensions have been studied by quite a number of groups [55–57].

In the next chapter we will consider an $SO(10)$ gauge theory compactified on the orbifold $T^2/\left(\mathbb{Z}_2 \times \mathbb{Z}_2^{\text{PS}} \times \mathbb{Z}_2^{\text{GG}}\right)$. The field content is quite complicated and will be discussed in detail later. For the discussion of the Casimir energy we will concentrate on one basic ingredient which we already discussed in the last chapter, namely the $SO(10)$ vector multiplet which resides in the bulk of the six-dimensional space. The goal of this chapter is to study the generation of a non-trivial potential for the volume modulus induced by quantum effects of massless and massive components of this vector multiplet, which can potentially lead to a stabilisation of the extra-dimensional volume [13, 14]. To see if a stabilisation can be achieved, we will calculate the one-loop quantum effective potential around a constant flat background. It is obvious that the outcome of this calculation depends on the field content and the boundary conditions of the theory. To see the effect of gauge symmetry breaking on the modulus potential, we will start off with the simpler example of $T^2/\mathbb{Z}_2$ where the full gauge group survives the compactification and compare it with $T^2/\left(\mathbb{Z}_2 \times \mathbb{Z}_2^{\text{PS}} \times \mathbb{Z}_2^{\text{GG}}\right)$ where also the gauge symmetries are broken.

2. The Casimir Energy on $\mathbf{T^2/\mathbb{Z}_2}$

Let us start with the Casimir energy for a six-dimensional vector multiplet in the adjoint representation of $SO(10)$ compactified on the orbifold $T^2/\mathbb{Z}_2$. As long as supersymmetry is unbroken, the Casimir energy will be identically zero [55], provided the fields all share the same boundary conditions. Therefore we have to specify the supersymmetry breaking mechanism, before we can start the calculation of the Casimir energy.

A supersymmetry breaking mechanism which naturally fits into the framework of orbifolded theories is gaugino mediation. We will postpone the detailed discussion of this mechanism to the next chapter and only use the fact here that this leads to a brane-localised soft supersymmetry breaking mass term for the gauginos. In general, brane localised terms lead to a distortion of the Kaluza-Klein spectrum which also effects the Casimir energy. However, we assume the supersymmetry breaking brane masses to be small such that we can neglect the distortion they induce. We will place the supersymmetry breaking field at the brane $O = (0, 0)$, so only fields with positive parity can couple to it. In our setup only the gauginos λ_1 can obtain a supersymmetry breaking mass, whereas λ_2 does not couple to the brane and remains massless. Therefore it is sufficient to concentrate on the massless $\mathcal{N} = 1$ four-dimensional vector multiplet $V = (A_\mu, \lambda_1)$ in the following discussion.

We can express the Casimir energy of gauge fields and gauginos in terms of the Casimir energy of a real scalar field. This can be seen after appropriate gauge fixing and essentially amounts to a counting of the corresponding degrees of freedom [55]. To be explicit, the Casimir energy for our four-dimensional fields A_μ and λ_1 in the adjoint representation of $SO(10)$ is simply given by

$$V_{A_\mu} = +90 V_s \,, \tag{III.1a}$$
$$V_{\lambda_1} = -90 V_s \,, \tag{III.1b}$$

where V_s is the Casimir energy of the real scalar field obeying the same boundary conditions. Thus, it is enough to perform the vacuum energy calculation for this single scalar field.

2.1. Casimir Energy due to a Scalar Field

The exact vacuum state of a quantum field theory, including all effects of quantum corrections, can be obtained by minimizing the effective potential, which can be extracted from the one-particle irreducible (1PI) effective action. The definition of the 1PI effective action in terms of functional integrals can be found in almost any quantum field theory textbook, see e.g. [58]. The corresponding effective potential agrees with the classical potential to lowest order in perturbation theory, but is modified in higher orders by quantum corrections. We will be interested in exactly these modifications, because they lift the flatness of the classical modulus potential.

In the following we will calculate the effective potential for the compactification moduli due to the scalar Kaluza-Klein modes around a constant flat background. We emphasize that we do not attempt to understand how nature chooses a particular compactification scheme. Rather we simply assume that the topology in which physics takes place is $\mathcal{M} \times T^2/\mathbb{Z}_2$, and within this framework we study a contribution to the potential of the extra-dimensional radii. We start from the classical action of the four-dimensional Kaluza-Klein modes of a scalar bulk field which one obtains by dimensional reduction.

Schematically this action can be written as

$$S = \frac{1}{2}\int \mathrm{d}^4x \sum_{m,n} \left\{ \partial^\mu \phi^{(m,n)} \partial_\mu \phi^{(m,n)} - \left(\mathcal{M}_{m,n}^2 + M^2\right) (\phi^{(m,n)})^2 \right\} \ , \tag{III.2}$$

with $\mathcal{M}_{m,n}$ the Kaluza-Klein masses and M a brane-localised supersymmetry breaking mass. Here we have neglected small distortions of the Kaluza-Klein spectrum induced by the brane-localised mass term. Starting from its functional integral definition, the one-loop contribution to the effective potential as a function of the classical fields $\varphi = \langle\phi\rangle, R_y, R_z$ can be written as [58]

$$\begin{aligned} -\int \mathrm{d}^4x \; V_{\text{eff}}[\varphi, R_y, R_z] &= -\frac{i}{2} \log\det \left[\frac{\delta^2 S}{\delta\phi\delta\phi}\right]_{\phi=\varphi} \\ &= +\frac{i}{2} \log\det \left[\sum_{m,n} \left(\partial^2 + \mathcal{M}_{m,n}^2 + M^2\right)\right] \\ &= +\frac{i}{2} \operatorname{Tr}\log \left[\sum_{m,n} \left(\partial^2 + \mathcal{M}_{m,n}^2 + M^2\right)\right] \ , \end{aligned} \tag{III.3}$$

where the dependence on the extra-dimensional radii is induced by the Kaluza-Klein masses $\mathcal{M}_{m,n}^2$. Note that for the action given above, this effective potential is independent of φ and therefore already corresponds to its minimum, which is equivalent to the vacuum energy as a function of the extra-dimensional moduli.

Let us now come to the specific case of $T^2/\mathbb{Z}_2$ and calculate the contribution of the even scalar bulk field Φ_+. Using the explicit form of the mode expansion (II.10), performing the trace and Wick rotating to Euclidean space we obtain for the Casimir energy

$$V_{\text{s}} = \frac{1}{2}\left[\delta_{0,m}\sum_{n\geq 0} + \sum_{m>0}\sum_{n=-\infty}^{\infty}\right] \int \frac{\mathrm{d}^4k_E}{(2\pi)^4} \log\left(k_E^2 + \mathcal{M}_{m,n}^2 + M^2\right) \ . \tag{III.4}$$

Here the Kaluza-Klein masses are given by

$$\begin{aligned} \mathcal{M}_{m,n}^2 &= \frac{m^2}{R_y^2} + \frac{n^2}{R_z^2} \\ &= \frac{1}{R_z^2}\left[e^2 m^2 + n^2\right] \ , \end{aligned} \tag{III.5}$$

where we defined $e^2 = R_z^2/R_y^2$ for convenience. As mentioned above we will use zeta function regularisation to define the divergent expression,

$$V_{\text{s}} = -\frac{\mathrm{d}}{\mathrm{d}s}\zeta(s)\Big|_{s=0} \tag{III.6}$$

with

$$\begin{aligned}\zeta(s) &\equiv \frac{1}{2}\left[\sum\right]_{m,n}\int\frac{\mathrm{d}^4k_E}{(2\pi)^4}\left(k_E^2+\frac{1}{R_z^2}\left[e^2m^2+n^2)\right]+M^2\right)^{-s}\\ &= \frac{1}{2}\frac{1}{(2\pi)^4}\pi^2\frac{\Gamma(s-2)}{\Gamma(s)}\left[\sum\right]_{m,n}\left(\frac{1}{R_z^2}\left[e^2m^2+n^2\right]+M^2\right)^{2-s}\\ &= \frac{1}{32\pi^2R_z^{4-2s}}\frac{1}{(s-2)(s-1)}\left[\sum\right]_{m,n}\left(\left[e^2m^2+n^2\right]+R_z^2M^2\right)^{2-s}\ , \end{aligned}\tag{III.7}$$

where $[\sum]_{m,n}$ is shorthand for the sum given above. We defer the evaluation of the sum in (III.7) to the Appendix. Performing the sum, differentiating with respect to s and setting $s=0$ the Casimir energy of the massive scalar field can be written as

$$\begin{aligned}V_s^M =& -\frac{1}{64\pi^2R_z^4}\Bigg\{\frac{\pi M^6R_yR_z^5}{36}\left(-11+12\log[M]\right)\\ &+\frac{4}{\pi^2}\frac{R_z^5}{R_y^2}M^3\sum_{p=1}^{\infty}\frac{1}{p^3}K_3(2\pi pMR_y)\\ &+\frac{8}{\pi^2}\left(\frac{R_z}{R_y}\right)^{5/2}\sum_{p=1}^{+\infty}\frac{1}{p^{5/2}}\sum_{m=0}^{\infty}\left(m^2+M^2R_y^2\right)^{\frac{5}{4}}K_{5/2}\left(2\pi\,p\,\tfrac{R_z}{R_y}\sqrt{m^2+M^2R_y^2}\right)\\ &+M^4R_z^4\left[\frac{3}{4}-\log(M)\right]\\ &-\frac{4}{\pi^2}(MR_z)^{5/2}\sum_{p=1}^{+\infty}\frac{1}{p^{5/2}}K_{5/2}\left(2\pi pMR_z\right)\Bigg\}\ . \end{aligned}\tag{III.8}$$

Here $K_a(x)$ are modified Bessel functions of the second kind. Although it is not obvious from this expression, the Casimir energy is symmetric under the interchange of R_y and R_z. We can now use this result to obtain the Casimir energy of the vector multiplet on $T^2/\mathbb{Z}_2$.

2.2. Casimir Energy due to the Vector Multiplet

With the result of the last section, the Casimir energy of the vector multiplet can now simply be written as

$$V_V = 90\cdot\left(V_s^0-V_s^M\right)\ . \tag{III.9}$$

Here M is the supersymmetry breaking mass of the gauginos. Clearly, as long as supersymmetry is unbroken, the Casimir energy will vanish. To see the effect of supersymmetry breaking, it will be convenient to expand the Casimir energy in a power series in $x = M\sqrt{R_yR_z} \ll 1$. Remember that our calculation is valid only for brane masses which are considerably smaller than the compactification scale in order not to distort

the Kaluza-Klein spectrum, hence this expansion is justified.[1] The leading contribution is obtained for $M = 0$. Here the gauge fields contribute an attractive potential while the potential due to the gauginos is repulsive. However, this term will cancel between fermions and bosons and therefore it is the next-to-leading term which gives the main contribution to the Casimir energy. We defer the explicit calculation of the power series to the Appendix again and only state the final result here,

$$\begin{aligned} V_V = &- \frac{1}{32\pi R_y^4} M^2 R_y R_z \\ &- \frac{45M^2}{32\pi^4 R_z^2} \sum_{p=1}^{+\infty} \frac{1}{p^3} \left\{ \frac{R_z}{R_y} \frac{\pi p}{\sinh^2(\pi p R_z/R_y)} + \coth(\pi p R_z/R_y) \right\} . \end{aligned} \tag{III.10}$$

We see that the presence of the vector multiplet leads to an attractive force. Note however that unlike the massless case the attractive force is due to the gauginos. This contribution clearly tends to contract the extra-dimensional volume and does not lead to a stabilisation on its own. However, before we come to a more detailed discussion about possible stabilisation mechanisms, let us perform the corresponding calculation for the orbifold we will be mainly concerned with in this thesis.

3. The Casimir Energy on $\mathbf{T}^2/\left(\mathbb{Z}_2 \times \mathbb{Z}_2^{\mathrm{PS}} \times \mathbb{Z}_2^{\mathrm{GG}}\right)$

In this section we repeat the calculation of the Casimir energy for the modified setup of $T^2/\left(\mathbb{Z}_2 \times \mathbb{Z}_2^{\mathrm{PS}} \times \mathbb{Z}_2^{\mathrm{GG}}\right)$. We assume again a non-vanishing F-term vacuum expectation value localised at the fixed point $O = (0,0)$ to be responsible for the breakdown of supersymmetry. Then only fields which couple to this brane can obtain a supersymmetry breaking mass term. The corresponding mode expansions are given in (II.16). Let us again calculate the Casimir energy of scalar bulk fields, this time with several different boundary conditions.

3.1. Casimir Energy due to a Scalar Field

As before the Casimir energy can be written as

$$V_{\mathrm{s}} = \frac{1}{2} \left[\sum\right]_{m,n} \int \frac{\mathrm{d}^4 k_E}{(2\pi)^4} \log\left(k_E^2 + \mathcal{M}_{m,n}^2 + M^2\right) , \tag{III.11}$$

with $[\sum]_{m,n}$ shorthand for the double sum and $\mathcal{M}_{m,n}^2$ denoting the Kaluza-Klein masses. However, unlike the case considered before, we have to take into account several different Kaluza-Klein masses and also two different sums, as can be seen from the mode expansion

[1] Actually, the mass term can also be interpreted as a bulk mass term. In this case our result is correct irrespectable of the size of the mass term.

(II.16). The explicit form of the Kaluza-Klein masses $\mathcal{M}_{m,n}^2$ for the different boundary conditions can be found in Table II.1. Generically they can be written as

$$\begin{aligned}\mathcal{M}_{m,n}^2 &= 4\left[\frac{(m+\alpha)^2}{R_y^2} + \frac{(n+\beta)^2)}{R_z^2}\right] \\ &= \frac{4}{R_z^2}\left[e^2(m+\alpha)^2 + (n+\beta)^2)\right] \ , \end{aligned} \tag{III.12}$$

where $\alpha, \beta \in \{0, \frac{1}{2}\}$ and we introduced $e^2 = R_z^2/R_y^2$ for convenience. Using again zeta function regularisation the Casimir energy can now be written as

$$V_{\mathrm{s}} = -\left.\frac{\mathrm{d}\zeta(s)}{\mathrm{d}s}\right|_{s=0} , \tag{III.13}$$

with

$$\begin{aligned}\zeta(s) &\equiv \frac{1}{2}\left[\sum\right]_{m,n} \int \frac{\mathrm{d}^4 k_E}{(2\pi)^4}\left(k_E^2 + \frac{4}{R_z^2}\left[e^2(m+\alpha)^2 + (n+\beta)^2)\right] + M^2\right)^{-s} \\ &= \frac{1}{2}\frac{1}{(2\pi)^4}\pi^2\frac{\Gamma(s-2)}{\Gamma(s)}\left[\sum\right]_{m,n}\left(\frac{4}{R_z^2}\left[e^2(m+\alpha)^2 + (n+\beta)^2)\right] + M^2\right)^{2-s} \\ &= \frac{4^{2-s}}{32\pi^2 R_z^{4-2s}}\frac{1}{(s-2)(s-1)}\left[\sum\right]_{m,n}\left(\left[e^2(m+\alpha)^2 + (n+\beta)^2)\right] + \frac{R_z^2}{4}M^2\right)^{2-s} . \end{aligned} \tag{III.14}$$

We again defer the evaluation of the Casimir sum to the Appendix. For the fields with mode expansion Φ_{+-+} and Φ_{+--} the sum is given by

$$\left[\sum\right]_{m,n} = \sum_{m=0}^{\infty}\sum_{n=-\infty}^{\infty} \ . \tag{III.15}$$

We denote the corresponding Casimir energy by $V_{s,\mathrm{I}}^{\alpha,\beta,M}$. It can be written as

$$\begin{aligned}V_{s,\mathrm{I}}^{\alpha,\beta,M} = &-\frac{1}{4\pi^2 R_z^4}\Bigg\{-\frac{16\pi}{15}\frac{M^5 R_z^5}{32}\zeta_H(0,\alpha) \\ &+ \pi\frac{R_y R_z^5 M^6}{2304}\left[-11 + 12\log(M)\right] \\ &+ \frac{4}{\pi^2}\frac{R_z^5 M^3}{8R_y^2}\sum_{p=1}^{\infty}\frac{\cos(2\pi p\alpha)}{p^3}K_3(\pi p M R_y) \\ &+ \frac{8}{\pi^2}\left(\frac{R_z}{R_y}\right)^{5/2}\sum_{p=1}^{+\infty}\frac{\cos(2\pi p\beta)}{p^{5/2}}\sum_{m=0}^{\infty}\left((m+\alpha)^2 + \tfrac{M^2 R_y^2}{4}\right)^{\frac{5}{4}} \\ &\qquad K_{5/2}\left(2\pi\, p\, \tfrac{R_z}{R_y}\sqrt{(m+\alpha)^2 + M^2 R_y^2/4}\right)\Bigg\} . \end{aligned} \tag{III.16}$$

Here $\zeta_H(x)$ is the Hurwitz zeta function. Although $\alpha = 1/2$ for both fields, we kept it general at this stage, because we will also need the expression for $\alpha = 0$ in the following.

Coming to the contribution to the Casimir energy of the remaining two fields which couple to the supersymmetry breaking brane, namely Φ_{+++} and Φ_{++-}, we have to use the sum

$$\Big[\sum\Big]_{m,n} = \left[\delta_{0,m}\sum_{n=0}^{\infty} + \sum_{m=1}^{\infty}\sum_{n=-\infty}^{\infty}\right] . \tag{III.17}$$

In the Appendix we show that the resulting Casimir energy, $V_{s,\mathrm{II}}^{\alpha,\beta,M}$, can be written as the sum of $V_{s,\mathrm{I}}^{\alpha,\beta,M}$ and an additional piece,

$$V_{s,\mathrm{II}}^{\alpha,\beta,M} = V_{s,\mathrm{I}}^{\alpha,\beta,M} + \widetilde{V}_s^{\alpha,\beta,M} , \tag{III.18}$$

with

$$\begin{aligned}\widetilde{V}_s^{\alpha,\beta,M} = &-\frac{1}{4\pi^2 R_z^4}\Bigg\{-\frac{R_z^4}{R_y^4}\left(\alpha^2+\frac{M^2R_y^2}{4}\right)^2\left[\frac{3}{2}-\log\left(\tfrac{4\alpha}{R_y^2}+M^2\right)\zeta_H(0,1-\beta)\right.\\ &+\frac{8\pi}{15}\frac{R_z^5}{R_y^5}\left(\alpha^2+\frac{M^2R_y^2}{4}\right)^{5/2}\\ &-\frac{4}{\pi^2}\left(\frac{R_z}{R_y}\right)^{5/2}\left(\alpha^2+\tfrac{M^2R_y^2}{4}\right)^{5/4}\sum_{p=1}^{\infty}\frac{\cos(2\pi p(1-\beta))}{p^{5/2}}\\ &\left.K_{5/2}\left(2\pi p\tfrac{R_z}{R_y}\sqrt{\alpha^2+M^2R_y^2/4}\right)\right\} .\end{aligned} \tag{III.19}$$

3.2. Casimir Energy due to the Vector Multiplet

From Table II.1 and the mode decomposition we can read off the total Casimir energy of the vector multiplet on $T^2/\left(\mathbb{Z}_2\times\mathbb{Z}_2^{\mathrm{PS}}\times\mathbb{Z}_2^{\mathrm{GG}}\right)$. The gauge bosons remain massless and have the same sign as the real scalar while the gauginos acquire a supersymmetry breaking mass M and have opposite signs,

$$\begin{aligned}V_V = \quad & 26\cdot\left(V_{s,\mathrm{II}}^{(0,0)}-V_{s,\mathrm{II}}^{(0,0,M)}\right)+24\cdot\left(V_{s,\mathrm{II}}^{(0,1/2)}-V_{s,\mathrm{II}}^{(0,1/2,M)}\right)\\ &+16\cdot\left(V_{s,\mathrm{I}}^{(1/2,0)}-V_{s,\mathrm{I}}^{(1/2,0,M)}\right)+24\cdot\left(V_{s,\mathrm{I}}^{(1/2,1/2)}-V_{s,\mathrm{I}}^{(1/2,1/2,M)}\right) .\end{aligned} \tag{III.20}$$

To see the effect of supersymmetry breaking, we will again expand the Casimir energy in a power series in $x = M\sqrt{R_yR_z} \ll 1$. The corresponding calculations can be found in the Appendix. Keeping only the terms which are $\mathcal{O}(x^2)$ we finally obtain for the Casimir

energy due to the vector multiplet on $T^2/\left(\mathbb{Z}_2 \times \mathbb{Z}_2^{\mathrm{PS}} \times \mathbb{Z}_2^{\mathrm{GG}}\right)$

$$\begin{aligned} V_V = &- \frac{1}{48\pi R_y^4} M^2 R_y R_z - \frac{3}{8\pi^4 R_z^2} M^2 \zeta(3) \\ &- \frac{M^2}{8\pi^4 R_z^2} \sum_{p=1}^{\infty} \frac{1}{p^3} \Bigg\{ \left[13 + 8\cos(\pi p)\right] \coth(\pi p R_z/R_y) \\ &+ 12[1+\cos(\pi p)] \left(1 + \pi \tfrac{R_z}{R_y} \coth(\pi p R_z/R_y)\right) \frac{1}{\sinh(\pi p R_z/R_y)} \\ &+ \pi \tfrac{R_z}{R_y} \left(13 + 8\cos(\pi p)\right) \frac{1}{\sinh^2(\pi p R_z/R_y)} \Bigg\} . \end{aligned} \tag{III.21}$$

We see that this potential again leads to an attractive force.[2] Therefore the Casimir energy tends to contract the size of the extra dimensions down to the Planck length. However, at this stage one should note that in addition to the one-loop contributions from bulk fields, there will also be a tree-level contribution of the higher-dimensional cosmological constant to the four-dimensional effective action. The presence of this term is required as a zero-derivative counterterm for divergences which arise in the calculation of the one-loop effective potential [55]. This term changes the shape of the potential and can potentially generate a minimum at larger values of the radii.

Furthermore a realistic theory requires additional fields which will also contribute to the Casimir energy. With the help of (III.16) and (III.19) their effect can be easily incorporated. A detailed study of the modulus potential (III.21) including the effect of additional fields as well as of the higher-dimensional cosmological constant is left for future work.

Summary and Concluding Remarks

In this chapter we have calculated the Casimir energy due to a vector multiplet in the adjoint representation of $SO(10)$ on the orbifolds $T^2/\mathbb{Z}_2$ and $T^2/\left(\mathbb{Z}_2 \times \mathbb{Z}_2^{\mathrm{PS}} \times \mathbb{Z}_2^{\mathrm{GG}}\right)$. To see the effect of supersymmetry breaking, we expanded the result in a power series, where the leading massless terms cancelled within one supermultiplet. We found that, for the given boundary conditions, the Casimir energy leads to an attractive force. To avoid a contraction of the extra-dimensional space down to the Planck length, additional contributions to the effective potential have to be taken into account. Our result for the Casimir energy will be essential in a detailed study of the modulus potential.

[2] The repulsive terms which are proportional to $\cos(\pi p)$ are always dominated by the attractive ones. However, it should be noted that this is not generically the case and only valid for the specific setup we consider here, since there are also repulsive contributions which could dominate over the attractive ones if we had chosen different boundary conditions. For example, the field Φ_{++-} leads to a repulsive force and if it were not for the (over-) compensation from fields with other boundary conditions, the extra dimensions would expand rather than contract. Therefore one cannot make general statements about the behaviour of the modulus potential when only knowing the field content.

IV. Gaugino Mediation in a Supersymmetric Orbifold GUT

Supersymmetric orbifold GUTs [6–12] are attractive candidates for unified theories explaining the masses and mixings of fermions. Features such as the doublet-triplet splitting and the absence of dimension-five operators for proton decay, which are difficult to realise in four-dimensional grand unified theories, are easily obtained. Furthermore – with the start of the LHC a few months ahead - there is an increasing interest in specific predictions for the superparticle mass spectrum, which results from the interplay between fermion mass models and models for supersymmetry breaking. Following this rationale, we consider an $SO(10)$ theory in six dimensions, proposed in [11, 20], in combination with gaugino-mediated supersymmetry breaking [16, 17].

In the next section, we briefly describe the relevant properties of the orbifold model, further details can be found in [11, 18–20]. Having outlined the basic ideas, we will combine the orbifold model with gaugino mediation, a supersymmetry breaking mechanism which can naturally be embedded into the orbifold framework. Here we are in particular interested in the supersymmetry breaking couplings needed to calculate the mass spectrum of the superpartners. Moving on to Section 3, we demonstrate that the presence of extra matter fields in the bulk leads to severe problems with flavour-changing neutral currents (FCNCs) unless the couplings of these fields to the supersymmetry breaking field are suppressed. Using naïve dimensional analysis (NDA) in Section 4, we derive upper bounds on the unknown couplings of the theory and thus on the non-vanishing soft masses as well as supersymmetric Higgs mass parameter μ and the soft bilinear coupling $B\mu$ at high energy. Finally, we calculate the low-energy superparticle mass spectrum in Section 5.

1. The Orbifold GUT Model

The symmetries and the particle content of the standard model as well as the apparent unification of gauge couplings at $M_{\rm GUT} \sim 10^{16}\,{\rm GeV}$ [59] hint towards grand unified theories. With the increasing evidence for neutrino masses, implying the existence of a right-handed neutrino, there is also an increasing motivation for $SO(10)$ as the GUT gauge group[1]. This is because $SO(10)$ allows for the unification of all quarks and leptons into one irreducible spinor representation, including the right-handed neutrino.

Guided by these preliminary thoughts, we consider an $\mathcal{N} = 1$ supersymmetric $SO(10)$ gauge theory in six dimensions compactified on the orbifold $T^2/\left(\mathbb{Z}_2 \times \mathbb{Z}_2^{\rm PS} \times \mathbb{Z}_2^{\rm GG}\right)$ [11].

[1] Of course larger gauge groups which have $SO(10)$ as a subgroup are well motivated too.

We already discussed some features of this model in Sections II.2 and II.3, in particular how symmetry breaking is achieved by the compactification. Recall that the extended supersymmetry is broken by the first $\mathbb{Z}_2$ reflection, such that the zero modes of the six-dimensional vector multiplet form a massless four-dimensional $\mathcal{N} = 1$ vector multiplet in the adjoint representation of $SO(10)$. Local breaking of $SO(10)$ to the Pati-Salam group $G_{\text{PS}} = SU(4) \times SU(2) \times SU(2)$ and to the extended Georgi-Glashow group $G_{\text{GG}} = SU(5) \times U(1)_X$ is achieved by acting with the other two $\mathbb{Z}_2$-symmetries on the gauge fields, leading to the following pattern of remaining gauge symmetries: At O the full $SO(10)$ survives, whereas at the other fixed points, O_{PS}, O_{GG} and O_{fl}, $SO(10)$ is broken to its three GUT subgroups G_{PS}, G_{GG} and flipped $SU(5)$, G_{fl}, respectively. The intersection of these GUT groups yields the standard model group with an additional $U(1)$ factor, $G_{\text{SM}'} = SU(3)_C \times SU(2)_L \times U(1)_Y \times U(1)_X$, as unbroken gauge symmetry below the compactification scale. In this setup it is natural to identify the compactification scale with the GUT scale.

The field content of the theory is strongly constrained by requiring the cancellation of bulk and brane anomalies [19]: The vector multiplet V is a **45**-plet of $SO(10)$, which has an irreducible anomaly in six dimensions. In order to cancel this anomaly, two additional bulk hypermultiplets $H_{1,2}$ in the fundamental representation of $SO(10)$ have to be introduced. A bulk hypermultiplet corresponds to a chiral and antichiral superfield from the four-dimensional perspective, $H = (H, H')$, but the antichiral part will always be projected out by a condition similar to (II.12a):

$$\begin{aligned} \mathbb{Z}_2: &\quad PH(x,-y,-z) = +H(x,y,z) \\ \mathbb{Z}_2: &\quad PH'(x,-y,-z) = -H'(x,y,z)\ . \end{aligned} \tag{IV.1}$$

Therefore H will always refer to the $\mathcal{N} = 1$ chiral multiplet from now on. Coming back to the field content, the breaking of the gauge symmetry $U(1)_X$ can be achieved by adding two **16**-plets Φ, Φ^c together with two **10**-plets $H_{3,4}$ to cancel the reintroduced anomalies. Vacuum expectation values of Φ and Φ^c break the surviving $U(1)_X$ while the electroweak gauge group is broken by expectation values of the doublets contained in H_1 and H_2. Note that the symmetry related to the difference of baryon and lepton number, $U(1)_{B-L}$, is a subgroup of the local symmetry $U(1)_Y \times U(1)_X$ and is of course broken simultaneously.

The fields present in the theory so far cannot account for quarks and leptons. As a guideline for the introduction of matter we use - in addition to the condition of anomaly cancellation – the embedding of quantum numbers into the adjoint representation of E_8.[2] This implies that only two more bulk **16**-plets ϕ and ϕ^c together with two **10**-plets $H_{5,6}$ are allowed [20] and therefore the three quark lepton generations have to be brane fields. We denote the three corresponding **16**-plets as ψ_i, $i = 1, 2, 3$.

To summarise, the bulk contains six **10**-plets, $H_1, \ldots, H_6$, and four **16**-plets, $\Phi, \Phi^c, \phi, \phi^c$, as hypermultiplets. We choose the parities of ϕ, ϕ^c and H_5, H_6 such that their zero modes

[2] Maybe our six-dimensional $SO(10)$ model can be understood as a part of a higher-dimensional theory with gauge group E_8, as it emerges in string theory.

are

$$L = l_4 = \begin{pmatrix} \nu_4 \\ e_4 \end{pmatrix} , \quad L^c = l_4^c = \begin{pmatrix} n_4^c \\ e_4^c \end{pmatrix} , \quad G_5^c = d_4^c , \quad G_6 = d_4 . \tag{IV.2}$$

These zero modes act as a fourth generation of down (s)quarks and (s)leptons and mix with the three generations of brane fields. We allocate the three sequential **16**-plets to the three branes where $SO(10)$ is broken to its three GUT subgroups, placing ψ_1 at O_{GG}, ψ_2 at O_{fl} and ψ_3 at O_{PS}. The three "families" are then separated by distances large compared to the cutoff scale Λ. Hence, they can only have diagonal Yukawa couplings with the bulk Higgs fields. The brane fields, however, can mix with the bulk zero modes without suppression. As these mixings take place only among left-handed leptons and right-handed down-quarks, a characteristic pattern of mass matrices consistent with experimental data can be obtained [20].

Having successfully incorporated the masses and mixings of fermions, the next logical step would be to calculate the corresponding quantities for the superpartners. As with all supersymmetric quantities, they cannot be evaluated unambiguously and depend crucially on the way supersymmetry is broken. Therefore, before we can start our calculation, we should think about a suitable mechanism leading to the breakdown of supersymmetry. Given the higher-dimensional setup with various branes, this mechanism involves in general bulk as well as brane fields. A supersymmetry breaking mechanism, which naturally fits into the context of orbifold GUTs goes under the name gaugino mediation and we will show how to combine it with our model in the next section.

2. Implementing Gaugino Mediated Supersymmetry Breaking

The underlying assumption of gaugino mediation [16, 17] is that gauge fields live in the bulk whereas matter fields – at least in the original proposal – are confined to branes. In this scenario supersymmetry is broken by some dynamical mechanism on an additional, spatially separated brane. In general, the corresponding source brane Lagrangian involves all the fields required to break supersymmetry dynamically as well as couplings to the bulk gauge fields. However, not all these terms are necessary in order to compute the MSSM gaugino and scalar masses. In contrast, if we assume that the leading supersymmetry breaking vacuum expectation value is acquired by the F-term component of a gauge singlet chiral superfield, we only need terms of the effective action which couple this singlet to the bulk gauge fields. The leading superpotential term results in non-vanishing masses for the gauginos at the compactification scale, whereas all other supersymmetry breaking terms are negligible. So how do squarks and sleptons obtain their masses? Below the compactification scale the theory is effectively four-dimensional and masses at the compactification scale have to be evolved using renormalisation group techniques. This evolution then yields masses for all other superpartners at the weak scale and these are the masses which can be determined experimentally, e.g. at the LHC. A very nice feature of the simplest version of gaugino mediation with only gauge fields

in the bulk is that the problem of flavour changing neutral currents is under control, since gauge interactions are flavour universal and we start from vanishing (and hence diagonal) soft mass matrices at the compactification scale. In a more general setup with various bulk fields, the situation is more complicated: In principle all fields living in the bulk can have direct couplings to the supersymmetry breaking source and the problem of FCNCs has to be re-addressed. However, we postpone this discussion to Section 3 and start off with implementing a suitable version of gaugino mediation into our orbifold model.

The orbifold model has the minimal amount of supersymmetry in six dimensions, corresponding to $\mathcal{N} = 2$ extended supersymmetry in four dimensions. As explained in the last section, the breaking to $\mathcal{N} = 1$ supersymmetry is achieved by appropriate boundary conditions acting on the bulk hypermultiplets and on the chiral adjoint superfield Ψ contained in the six-dimensional vector multiplet. To fully break supersymmetry we place the gauge-singlet chiral superfield of gaugino mediation at the fixed point O. We want the corresponding brane Lagrangian to yield gaugino masses, since they cannot be generated radiatively when starting from a vanishing mass at the compactification scale. Therefore, the source brane Lagrangian coupling the zero modes of the gauge fields to the chiral field on the source brane should include a term

$$\mathscr{L}_S \supset \frac{g_4^2 h}{4\Lambda} \int \mathrm{d}^2\theta \, S \, W^\alpha W_\alpha + \mathrm{h.c.} \,, \tag{IV.3}$$

where g_4 is the four-dimensional gauge coupling, h is a dimensionless coupling and Λ is the cutoff of the theory. The gauge singlet S as well as the field strength superfield W^α are four-dimensional $\mathcal{N} = 1$ superfields[3]. When the chiral superfield S acquires a vacuum expectation value F_S, supersymmetry is broken and the gaugino obtains a mass

$$m_{1/2} = \frac{g_4^2 h F_S}{2\Lambda} \tag{IV.4}$$

at the compactification scale. Other bulk fields including the fourth generation of squarks and sleptons can also couple directly to the supersymmetry breaking source. All the remaining squarks and sleptons live on branes and can obtain soft supersymmetry breaking masses only via loop contributions, which are negligible here, and via renormalisation group running, as noted before. To study the resulting scalar masses and mixings we first have to discuss all couplings which can lead to mass terms.

2.1. The Superpotential

The superpotential determines the supersymmetry conserving mass terms and Yukawa couplings. In addition to gauge invariance the allowed terms are restricted by R-invariance and an additional $U(1)_{\tilde{X}}$ symmetry with the charge assignments given in Table IV.1.

[3] Starting from the six-dimensional theory, the effective four-dimensional fields are obtained by integrating out the two extra dimensions. This leads to a volume factor between the original six-dimensional fields and the properly normalised fields we use here, $\Phi = \sqrt{V}\Phi_6$.

	H_1	H_2	Φ^c	H_3	Φ	H_4	ψ_i	ϕ^c	ϕ	H_5	H_6	S
R	0	0	0	2	0	2	1	1	1	1	1	0
$\tilde{X}$	-2a	-2a	-a	2a	a	-2a	a	-a	a	2a	-2a	0

Table IV.1.: Charge assignments for the symmetries $U(1)_R$ and $U(1)_{\tilde{X}}$

The most general brane superpotential without the singlet field S is given in [20]. All zero modes can be found in Table IV.2. Since the fields ψ_i and ϕ have the same quantum numbers, they can be combined to the quartet $\psi_\alpha = (\psi_i, \phi)$. When the bulk fields are replaced by their zero modes, only 9 of the 23 terms appearing in the superpotential remain. They are given by

$$W = M^d H_5 H_6 + M^l_\alpha \psi_\alpha \phi^c + \frac{1}{2} h^{(1)}_{\alpha\beta} \psi_\alpha \psi_\beta H_1 + \frac{1}{2} h^{(2)}_{\alpha\beta} \psi_\alpha \psi_\beta H_2 + f_\alpha \Phi \psi_\alpha H_6 + \frac{h^N_{\alpha\beta}}{2\Lambda} \psi_\alpha \psi_\beta \Phi^c \Phi^c + \frac{g^d_\alpha}{\Lambda} \Phi^c \psi_\alpha H_5 H_1 + f^D \Phi^c \Phi^c H_3 + f^G \Phi \Phi H_4 \, . \tag{IV.5}$$

As discussed in [18], after the breaking of $U(1)_X \times U(1)_{\tilde{X}}$ to a global $U(1)$ subgroup, the superpotential (IV.5) yields masses of order M_{GUT} for unwanted colour triplets contained in Φ, Φ^c, H_3 and H_4. In this way, there are no additional contributions to the running of the gauge couplings below that scale and gauge coupling unification is maintained.

Consider now terms which involve the supersymmetry breaking singlet field S. From (IV.3) and the ordinary kinetic term

$$\frac{1}{4} \int \mathrm{d}^2\theta \, W^\alpha W_\alpha + \mathrm{h.c.}$$

for the gauge fields W^α we conclude that S must have $U(1)_{\tilde{X}}$- and R-charge 0 to leave the Lagrangian invariant. Therefore, terms respecting all the symmetries including $U(1)_{\tilde{X}}$ are simply given by

$$\mathscr{L}_S \propto \int \mathrm{d}^2\theta \, \frac{S}{\Lambda} W + \mathrm{h.c.} \, , \tag{IV.6}$$

where W is the superpotential given above and where we only keep those terms of W which are at most cubic in the fields. Note that in addition ψ_α has to be replaced by ϕ, since the matter fields ψ_i cannot have direct couplings to the source brane. Moreover, we are interested only in terms which are non-zero when replacing the fields by their zero modes. To see which terms remain in the low energy theory, it is helpful to have a look at the parity assignments and branching rules of the fundamental and spinor representation of $SO(10)$ [18, 60]. They can be found in Table IV.2.

A brief explanation of our conventions is in order. Generically superfields in the bulk are denoted by a capital letter, with the exception being the bulk fields which belong to the fourth generation (cf. Eq. (IV.2)). In contrast, the brane fields ψ_i are denoted by small letters, such that the MSSM chiral superfields are written as

$$\psi = (q, u^c, e^c, l, d^c, n^c) \, . \tag{IV.7}$$

$SO(10)$	**10**							
SM′	$(\mathbf{1},\mathbf{2};-\frac{1}{2},-2)$		$(\mathbf{1},\mathbf{2};\frac{1}{2},2)$		$(\bar{\mathbf{3}},\mathbf{1};\frac{1}{3},-2)$		$(\mathbf{3},\mathbf{1};-\frac{1}{3},2)$	
	H^c		H		G^c		G	
	$\mathbb{Z}_2^{\mathrm{PS}}$	$\mathbb{Z}_2^{\mathrm{GG}}$	$\mathbb{Z}_2^{\mathrm{PS}}$	$\mathbb{Z}_2^{\mathrm{GG}}$	$\mathbb{Z}_2^{\mathrm{PS}}$	$\mathbb{Z}_2^{\mathrm{GG}}$	$\mathbb{Z}_2^{\mathrm{PS}}$	$\mathbb{Z}_2^{\mathrm{GG}}$
H_1	$+$	$+$	$+$	$-$	$-$	$+$	$-$	$-$
H_2	$+$	$-$	$+$	$+$	$-$	$-$	$-$	$+$
H_3	$-$	$+$	$-$	$+$	$+$	$+$	$+$	$-$
H_4	$-$	$-$	$-$	$+$	$+$	$-$	$+$	$+$
H_5	$-$	$+$	$-$	$-$	$+$	$+$	$+$	$-$
H_6	$-$	$-$	$-$	$+$	$+$	$-$	$+$	$+$

$SO(10)$	**16**							
SM′	$(\mathbf{3},\mathbf{2};\frac{1}{6},-1)$		$(\mathbf{1},\mathbf{2};-\frac{1}{2},3)$		$(\bar{\mathbf{3}},\mathbf{1};-\frac{2}{3},-1)$ $(\mathbf{1},\mathbf{1};1,-1)$		$(\bar{\mathbf{3}},\mathbf{1},\frac{1}{3},3)$ $(\mathbf{1},\mathbf{1};0,-5)$	
	Q		L		U^c, E^c		D^c, N^c	
	$\mathbb{Z}_2^{\mathrm{PS}}$	$\mathbb{Z}_2^{\mathrm{GG}}$	$\mathbb{Z}_2^{\mathrm{PS}}$	$\mathbb{Z}_2^{\mathrm{GG}}$	$\mathbb{Z}_2^{\mathrm{PS}}$	$\mathbb{Z}_2^{\mathrm{GG}}$	$\mathbb{Z}_2^{\mathrm{PS}}$	$\mathbb{Z}_2^{\mathrm{GG}}$
Φ	$-$	$-$	$-$	$+$	$+$	$-$	$+$	$+$
ϕ	$+$	$-$	$+$	$+$	$-$	$-$	$-$	$+$

Table IV.2.: Decomposition and parity assignments for the bulk **16**- and **10**-plets of $SO(10)$. The $\overline{\mathbf{16}}$-plets Φ^c, ϕ^c have the same parities as Φ and ϕ and of course conjugate quantum numbers with respect to the extended standard model gauge group. Only fields which have all parities $+$ remain in the low energy theory.

Here we follow a standard convention, that all chiral supermultiplets are defined in terms of left-handed Weyl spinors, so that the conjugates of the right-handed quarks and leptons appear in the decomposition. However, the c's on these fields are part of the name and do not denote any kind of conjugation. Rather, e.g. $e = e_L$ contained in the $SU(2)_L$ doublet l is the left-handed piece of a Dirac spinor, while $e^c = C\bar{e}_R^T$ is the name given to the conjugate of the right-handed piece of the Dirac spinor with C the charge conjugation matrix.

Coming back to the remaining terms of the zero mode source brane Lagrangian, we note that when the **16**-plets Φ, Φ^c acquire a vev $\langle\Phi\rangle = \langle\Phi^c\rangle = v_N \sim M_{\mathrm{GUT}}$ leading to the spontaneous breakdown of $U(1)_{B-L}$ we obtain (cf. Eq. (IV.2))

$$\mathscr{L}_S \supset -\int \mathrm{d}^2\theta\, \frac{S}{\Lambda}\left(\tilde{M}^d d_4^c d_4 + \tilde{M}_4^l l_4 l_4^c\right) + \mathrm{h.c.} \tag{IV.8}$$

Additional terms involving the heavy fields Φ, Φ^c have been dropped. When setting the chiral field S to its vev F_S, the scalar components of the superfields remain, whereas the fermionic components are projected out.

2.2. The Kähler Potential

In addition, soft mass terms can arise from the Kähler potential. We assume the global $U(1)_{\tilde{X}}$ symmetry to be only approximate and allow for explicit breaking here. This is necessary in order to obtain a μ-term, which is not allowed in the superpotential, since the combination $H_1 H_2$ is not invariant under $U(1)_{\tilde{X}}$ (cf. Table IV.1). Besides, an explicit breaking of $U(1)_{\tilde{X}}$ is in fact required in order to avoid Goldstone bosons. Kähler potential terms which result in non-negligible effects have to involve fields which acquire a large vev in order to compensate for the suppression by the cutoff scale Λ. In our case, large vevs are acquired by Φ, Φ^c and S. We find that all terms without the singlet field S do not contribute to any soft masses but merely give corrections to the kinetic terms. Concentrating on the terms involving S, we do not consider terms with heavy fields that have no influence on low-energy physics. In terms of the zero modes, the relevant part of the Kähler potential is

$$\begin{aligned}\mathscr{L}_S \supset &-\int \mathrm{d}^4\theta \left\{ \frac{S^\dagger}{\Lambda}\left(a H_2 H_1^c + b_1 H_1^{c\dagger} H_1^c + b_2 H_2^\dagger H_2\right) + \mathrm{h.c.} \right. \\ &\qquad \left. + \frac{1}{\Lambda^2} S^\dagger S \left[c_1 H_1^{c\dagger} H_1^c + c_2 H_2^\dagger H_2 + (d H_2 H_1^c + \mathrm{h.c.})\right] \right\} \\ &-\int \mathrm{d}^4\theta \left\{ \frac{e_i}{\Lambda} S^\dagger B_i^\dagger B_i + \mathrm{h.c.} + \frac{e_i'}{\Lambda^2} S^\dagger S\, B_i^\dagger B_i \right\},\end{aligned} \tag{IV.9}$$

yielding an effective μ-term, soft Higgs masses, a $B\mu$-term and soft masses for all other bulk fields. B_i $(i = 1, \dots)$ stands for any bulk matter field except $H_{1,2}$. Although the μ-term itself is not a soft term, it is generated only after the breaking of supersymmetry via the Giudice-Masiero mechanism [61]. Note that there would be no electroweak symmetry

breaking without the breaking of supersymmetry and hence no massive (s)particles at the electroweak scale.

To see the contributions to the soft masses explicitly, we express the Lagrangian by component fields, plugging in the F-term vev F_S and the scalar vev v_N. Furthermore, we employ the equations of motion for the auxiliary fields and assume real couplings for simplicity. Concentrating on the fourth generation and on the Higgs fields, this results in the following scalar mass terms:

$$\begin{aligned}\mathscr{L}_S \supset & -\frac{F_S^\dagger F_S}{\Lambda^2}\Big[\left(a^2+b_1^2+c_1\right)\tilde{h}_1^{c\dagger}\tilde{h}_1^c+\left(a^2+b_2^2+c_2\right)\tilde{h}_2^\dagger\tilde{h}_2 \\ & \qquad +\left(a\left(b_1+b_2\right)+d\right)\tilde{h}_1^c\tilde{h}_2+\text{h.c.}\Big] \\ & -\frac{F_S^\dagger F_S}{\Lambda^2}\Big[\left(e_d^2+e_d'\right)\tilde{d}_4^\dagger\tilde{d}_4+\left(e_{d^c}^2+e_{d^c}'\right)\tilde{d}_4^{c\dagger}\tilde{d}_4^c+\left(e_l^2+e_l'\right)\tilde{l}_4^\dagger\tilde{l}_4+\left(e_{l^c}^2+e_{l^c}'\right)\tilde{l}_4^{c\dagger}\tilde{l}_4^c\Big] \\ & -\frac{F_S}{\Lambda}\Big[\tilde{M}^d\tilde{d}_4^c\tilde{d}_4+\tilde{M}_4^l\tilde{l}_4\tilde{l}_4^c\Big]+\text{h.c.}\,, \end{aligned} \tag{IV.10}$$

where we have included the contribution from Eq. (IV.8) in the last line. We denote the components of a chiral multiplet by $(\tilde{\phi},\phi,F_\Phi)$, with $\Phi = H_1^c, H_2, d_4, d_4^c, l_4, l_4^c$. Note that the Higgs mass contribution proportional to a^2 is supersymmetric and hence the soft Higgs masses are given by the terms proportional to $(b_{1,2}^2+c_{1,2})$.

In writing down (IV.10) we assume that there are no sizable contributions to the scalar masses from D-terms, which can arise when a gauged $U(1)$ symmetry is broken or when there are soft supersymmetry breaking terms which lift a D-flat direction in the scalar potential [62, 63]. Having analysed all terms in the super- and Kähler potential which can induce gaugino and scalar masses, we are now in a position to re-address the question of flavour changing neutral currents in our model.

3. The Scalar Mass Matrices and FCNCs

Flavour changing processes such as $\mu \to e\gamma$ are known to be strongly constrained experimentally [64]. To avoid inducing such processes at the one-loop level, the squark and slepton mass matrices have to be approximately diagonal in a basis where quark and lepton mass matrices are diagonal[4]. Furthermore we should keep in mind that all the parameters we read off from our super- and Kähler potential are valid at the compactification scale and have to be translated to quantities at the electroweak scale via renormalisation group running. This means that the mass matrices which are diagonal at the high scale do not necessarily remain so. However, as we will see in Section 5,

[4] Another possible source for the suppression of flavour changing neutral currents are extremely heavy scalar superpartners, but this seems discrepant with the motivation for supersymmetry as a cure for the hierarchy problem (see Introduction). Nevertheless there have been some attempts – usually referred to as 'split supersymmetry' – which try to solve the supersymmetric flavour problem exactly this way, see e.g. [65]

the dominant renormalisation group corrections are due to gauge interactions and will respect the flavour conserving properties. Only RG corrections originating from Yukawa interactions can induce some flavour mixing, but these contributions are negligible.

In the following, we shall analyse the structure of squark and slepton mass matrices in our orbifold GUT model. We have seen in the previous section that only the scalars of the fourth generation, which are very heavy, obtain soft masses, since they are bulk fields. We will demonstrate now that this leads to soft masses for the light scalars, too. At the compactification scale, we integrate out the heavy degrees of freedom to obtain an effective theory with three generations. This requires diagonalising the mass matrices, and the corresponding transformations transmit supersymmetry breaking effects from the fourth to the light generations.

We start our analysis of FCNCs with the diagonalisation of the fermionic mass matrices [20]. This is achieved by a change of basis for the fermions. Transforming the scalar fields in the same way, we can see if there are sizeable off-diagonal terms in the scalar mass matrices leading to flavour changing neutral currents. From the zero mode superpotential (IV.5) and the decomposition (IV.7), we find that the superpotential relevant for particle masses is given by

$$W \supset d_\alpha m^d_{\alpha\beta} d^c_\beta + e^c_\alpha m^e_{\alpha\beta} e_\beta + n^c_\alpha m^D_{\alpha\beta} \nu_\beta + u^c_i m^u_{ij} u_j + \frac{1}{2} n^c_i M_{ij} n^c_j \,, \tag{IV.11}$$

where m^d, m^e and m^D are 4×4 mass matrices

$$m^d = \begin{pmatrix} h^d_{11} v_d & 0 & 0 & g^d_1 \frac{v_N}{\Lambda} v_d \\ 0 & h^d_{22} v_d & 0 & g^d_2 \frac{v_N}{\Lambda} v_d \\ 0 & 0 & h^d_{33} v_d & g^d_3 \frac{v_N}{\Lambda} v_d \\ f_1 v_N & f_2 v_N & f_3 v_N & M^d \end{pmatrix} , \tag{IV.12}$$

$$m^e = \begin{pmatrix} h^d_{11} v_d & 0 & 0 & h^e_{14} v_d \\ 0 & h^e_{22} v_d & 0 & h^e_{24} v_d \\ 0 & 0 & h^d_{33} v_d & h^e_{34} v_d \\ M^l_1 & M^l_2 & M^l_3 & M^l_4 \end{pmatrix} , \tag{IV.13}$$

$$m^D = \begin{pmatrix} h^D_{11} v_u & 0 & 0 & h^D_{14} v_u \\ 0 & h^u_{22} v_u & 0 & h^D_{24} v_u \\ 0 & 0 & h^u_{33} v_u & h^D_{34} v_u \\ M^l_1 & M^l_2 & M^l_3 & M^l_4 \end{pmatrix} , \tag{IV.14}$$

whereas m^u and M are diagonal 3×3 matrices,

$$m^u = \begin{pmatrix} h^u_{11} v_u & 0 & 0 \\ 0 & h^u_{22} v_u & 0 \\ 0 & 0 & h^u_{33} v_u \end{pmatrix} , \qquad M = \begin{pmatrix} h^N_{11} \frac{v_N^2}{\Lambda} & 0 & 0 \\ 0 & h^N_{22} \frac{v_N^2}{\Lambda} & 0 \\ 0 & 0 & h^N_{33} \frac{v_N^2}{\Lambda} \end{pmatrix} . \tag{IV.15}$$

The m^d, m^e and m^D mass matrices are all of the form

$$m = \begin{pmatrix} \mu_1 & 0 & 0 & \widetilde{\mu}_1 \\ 0 & \mu_2 & 0 & \widetilde{\mu}_2 \\ 0 & 0 & \mu_3 & \widetilde{\mu}_3 \\ \widetilde{M}_1 & \widetilde{M}_2 & \widetilde{M}_3 & \widetilde{M}_4 \end{pmatrix} . \tag{IV.16}$$

Here $\mu_i, \widetilde{\mu}_i \sim v$ and $\widetilde{M}_i \sim M_{\rm GUT}$. While μ_i and $\widetilde{\mu}_i$ have to be hierarchical to account for the observed particle masses, we assume no hierarchy between the $\widetilde{M}_i$. We have neglected corrections of order $\mathcal{O}(v_N/\Lambda)$. For simplicity, we assume all matrices to be real. The up-type quark and Majorana mass matrices m^u and M are diagonal 3×3 matrices, since the corresponding fields do not have partners in the bulk.

The 4×4 mass matrices m can be brought to the block-diagonal form (which is sufficient to integrate out the heavy mass eigenstate)

$$m' = U_4^\dagger m V_4 = \begin{pmatrix} \widehat{m} & 0 \\ 0 & \widetilde{M} \end{pmatrix} + \mathcal{O}\left(\frac{v^2}{\widetilde{M}}\right) \tag{IV.17}$$

by the transformation

$$e \to e' = V_4^\dagger e \quad , \quad e^c \to e^{c\prime} = e^c\, U_4 \, , \tag{IV.18}$$

where we have chosen the charged leptons for concreteness. Here U_4 and V_4 are the unitary matrices

$$U_4 = \begin{pmatrix} 1 & 0 & 0 & \frac{\mu_1 \widetilde{M}_1 + \widetilde{\mu}_1 \widetilde{M}_4}{\widetilde{M}^2} \\ 0 & 1 & 0 & \frac{\mu_2 \widetilde{M}_2 + \widetilde{\mu}_2 \widetilde{M}_4}{\widetilde{M}^2} \\ 0 & 0 & 1 & \frac{\mu_3 \widetilde{M}_3 + \widetilde{\mu}_3 \widetilde{M}_4}{\widetilde{M}^2} \\ -\frac{\mu_1 \widetilde{M}_1 + \widetilde{\mu}_1 \widetilde{M}_4}{\widetilde{M}^2} & -\frac{\mu_2 \widetilde{M}_2 + \widetilde{\mu}_2 \widetilde{M}_4}{\widetilde{M}^2} & -\frac{\mu_3 \widetilde{M}_3 + \widetilde{\mu}_3 \widetilde{M}_4}{\widetilde{M}^2} & 1 \end{pmatrix} + \mathcal{O}\left(\frac{v^2}{\widetilde{M}^2}\right) , \tag{IV.19a}$$

$$V_4 = \begin{pmatrix} \frac{\widetilde{M}_4}{\widetilde{M}_{14}} & 0 & -\frac{\widetilde{M}_1 \widetilde{M}_{23}}{\widetilde{M}\, \widetilde{M}_{14}} & \frac{\widetilde{M}_1}{\widetilde{M}} \\ 0 & \frac{\widetilde{M}_3}{\widetilde{M}_{23}} & \frac{\widetilde{M}_2 \widetilde{M}_{14}}{\widetilde{M}\, \widetilde{M}_{23}} & \frac{\widetilde{M}_2}{\widetilde{M}} \\ 0 & -\frac{\widetilde{M}_2}{\widetilde{M}_{23}} & \frac{\widetilde{M}_3 \widetilde{M}_{14}}{\widetilde{M}\, \widetilde{M}_{23}} & \frac{\widetilde{M}_3}{\widetilde{M}} \\ -\frac{\widetilde{M}_1}{\widetilde{M}_{14}} & 0 & -\frac{\widetilde{M}_4 \widetilde{M}_{23}}{\widetilde{M}\, \widetilde{M}_{14}} & \frac{\widetilde{M}_4}{\widetilde{M}} \end{pmatrix} \tag{IV.19b}$$

with $\widetilde{M} = \sqrt{\sum_\alpha \widetilde{M}_\alpha^2}$ and $\widetilde{M}_{\alpha\beta} = \sqrt{\widetilde{M}_\alpha^2 + \widetilde{M}_\beta^2}$ [66]. The mass matrix of the three light generations is clearly given by (cf. (IV.17))

$$\widehat{m} = \begin{pmatrix} \mu_1 (V_4)_{1j} + \widetilde{\mu}_1 (V_4)_{4j} \\ \mu_2 (V_4)_{2j} + \widetilde{\mu}_2 (V_4)_{4j} \\ \mu_3 (V_4)_{3j} + \widetilde{\mu}_3 (V_4)_{4j} \end{pmatrix} . \tag{IV.20}$$

The transformation V_4 contributes to the desired large mixing between the left-handed leptons. U_4, on the other hand, is close to the unit matrix, so that there is only small mixing among the right-handed fields. Note that the situation is reversed in the down-quark sector, where the right-handed fields are strongly mixed while the left-handed ones are not.

As long as supersymmetry is unbroken, fermion and scalar mass matrices are directly related. The supersymmetry conserving charged slepton mass matrices are $m^2_{e_\mathrm{L}} = m^{e\dagger} m^e$ and $m^2_{e_\mathrm{R}} = m^e m^{e\dagger}$. In addition, there are the soft masses $m^2_{\tilde{e}_\mathrm{L}}$ etc. with non-zero 44-element. Among them is the matrix $m^2_{\tilde{e}_\mathrm{LR}}$, which arises from Eq. (IV.8) and mixes $\tilde{l}_4$ and $\tilde{l}^c_4$, but it can be neglected for our purposes. For the complete mass matrices we use the notation $m^2_{\tilde{e}_\mathrm{L},\mathrm{tot}} = m^2_{e_\mathrm{L}} + m^2_{\tilde{e}_\mathrm{L}}$ etc. Under the transformation (IV.18), they change to

$$\begin{aligned} m'^2_{\tilde{e}_\mathrm{L},\mathrm{tot}} &= V_4^\dagger\, m^2_{e_\mathrm{L}}\, V_4 + V_4^\dagger\, m^2_{\tilde{e}_\mathrm{L}}\, V_4 \\ &= \begin{pmatrix} \widehat{m}^\dagger \widehat{m} & 0 \\ 0 & \widetilde{M}^2 \end{pmatrix} + V_4^\dagger \begin{pmatrix} 0 & 0 \\ 0 & m^2_{\tilde{l}_\mathrm{4L}} \end{pmatrix} V_4 + \mathcal{O}(v^2) \begin{pmatrix} \frac{v^2}{\widetilde{M}^2} & 1 \\ 1 & 1 \end{pmatrix}, \qquad \text{(IV.21a)} \\ m'^2_{\tilde{e}_\mathrm{R},\mathrm{tot}} &= U_4^\dagger\, m^2_{e_\mathrm{R}}\, U_4 + U_4^\dagger\, m^2_{\tilde{e}_\mathrm{R}}\, U_4 \\ &= \begin{pmatrix} \widehat{m}\widehat{m}^\dagger & 0 \\ 0 & \widetilde{M}^2 + m^2_{\tilde{l}_\mathrm{4R}} \end{pmatrix} + \mathcal{O}\left(\frac{v^3}{\widetilde{M}}, \frac{v\, m^2_{\tilde{l}_\mathrm{4R}}}{\widetilde{M}} \right), \qquad \text{(IV.21b)} \end{aligned}$$

where the fourth-generation soft masses are denoted by $m^2_{\tilde{l}_\mathrm{4L}}$ and $m^2_{\tilde{l}_\mathrm{4R}}$, in analogy to those of the first three generations, although both l_4 and l^c_4 are $SU(2)_\mathrm{L}$ doublets. The matrices are block-diagonal up to rotations by angles of order $v^2/\widetilde{M}^2$ or smaller, which can safely be neglected. Hence the heavy mass eigenstate can be integrated out, leaving only the 3×3 mass matrices of the light generations. From (IV.21b) we see that the soft masses of the light "right-handed" sleptons are highly suppressed. This is not true however for their "left-handed" counterparts (IV.21a), whose 3×3 mass matrix is given by

$$(m'^2_{\tilde{e}_\mathrm{L},\mathrm{tot}})_{ij} = (\widehat{m}^\dagger \widehat{m})_{ij} + (V_4)_{4i} (V_4)_{4j}\, m^2_{\tilde{l}_\mathrm{4L}} = (\widehat{m}^\dagger \widehat{m})_{ij} + (\widehat{m}^2_{\tilde{e}_\mathrm{L}})_{ij}\ . \qquad \text{(IV.22)}$$

To see the implications of the term $(\widehat{m}^2_{\tilde{e}_\mathrm{L}})_{ij}$, we first diagonalise the light fermion mass matrix $\widehat{m}$ by a second change of basis,

$$m_\mathrm{diag} = V_\mathrm{CKM}\, \widehat{m}\, \widehat{V}\ . \qquad \text{(IV.23)}$$

In the approximation $\mu_1 = \mu_2 = 0$, where the mass matrix $\widehat{m}$ has one zero eigenvalue, the transformation matrix $\widehat{V}$ is known explicitly [66],

$$\widehat{V} = \begin{pmatrix} -\frac{\widetilde{M}_2 \widetilde{M}_4}{\widetilde{M}_{12} \widetilde{M}_{14}} & \frac{\widetilde{M}_1 \left(\bar{\mu}_3 \widetilde{M}_3 \widetilde{M}_4 - \mu_3 \widetilde{M}^2_{124} \right)}{\bar{\mu}_3 \widetilde{M} \widetilde{M}_{12} \widetilde{M}_{14}} & -\frac{\bar{\mu}_3}{\bar{\mu}_3} \frac{\widetilde{M}_1}{\widetilde{M}_{14}} \\ \frac{\widetilde{M}_1 \widetilde{M}_3}{\widetilde{M}_{12} \widetilde{M}_{23}} & \frac{\widetilde{M}_2 \left(\bar{\mu}_3 \widetilde{M}^2_{123} - \mu_3 \widetilde{M}_3 \widetilde{M}_4 \right)}{\bar{\mu}_3 \widetilde{M} \widetilde{M}_{12} \widetilde{M}_{23}} & -\frac{\mu_3}{\bar{\mu}_3} \frac{\widetilde{M}_2}{\widetilde{M}_{23}} \\ \frac{\widetilde{M}_1 \widetilde{M}_2 \widetilde{M}}{\widetilde{M}_{12} \widetilde{M}_{14} \widetilde{M}_{23}} & -\frac{\bar{\mu}_3 \widetilde{M}^2_1 \widetilde{M}_3 + \mu_3 \widetilde{M}^2_2 \widetilde{M}_4}{\bar{\mu}_3 \widetilde{M}_{12} \widetilde{M}_{14} \widetilde{M}_{23}} & -\frac{\bar{\mu}_3}{\bar{\mu}_3} \frac{\widetilde{M}_4 \widetilde{M}_{23}}{\widetilde{M} \widetilde{M}_{14}} + \frac{\mu_3}{\bar{\mu}_3} \frac{\widetilde{M}_3 \widetilde{M}_{14}}{\widetilde{M} \widetilde{M}_{23}} \end{pmatrix} \qquad \text{(IV.24)}$$

up to a rotation of the second and third generation by a small angle Θ_R given by the ratio of the 23- and 33-elements of $\widehat{V}^\dagger\,\widehat{m}^\dagger\widehat{m}\,\widehat{V}$,

$$\Theta_R \simeq (\widetilde{\mu}_1^2+\widetilde{\mu}_2^2)/\bar{\mu}_3^2 \ll 1\ .$$

In Eq. (IV.24), we have defined $\widetilde{M}^2_{\alpha\beta\gamma} = \widetilde{M}^2_\alpha + \widetilde{M}^2_\beta + \widetilde{M}^2_\gamma$ and

$$\bar{\mu}_3^2 = \widetilde{\mu}_3^2\left(1-\frac{\widetilde{M}_4^2}{\widetilde{M^2}}\right)+\mu_3^2\left(1-\frac{\widetilde{M}_3^2}{\widetilde{M^2}}\right)-2\mu_3\widetilde{\mu}_3\frac{\widetilde{M}_3\widetilde{M}_4}{\widetilde{M^2}}\ . \tag{IV.25}$$

Using this matrix, we finally obtain for the charged slepton mass matrix in the basis where the charged fermion mass matrix is diagonal

$$\widehat{V}^\dagger\,(\widehat{m}^\dagger\widehat{m}+\widehat{m}^2_{\tilde{e}_{\rm L}})\,\widehat{V} =$$
$$\begin{pmatrix} 0 & 0 & 0 \\ 0 & \frac{\mu_3^2\widetilde{M}^2_{12}}{\bar{\mu}_3^2\widetilde{M^2}}\left(\widetilde{\mu}_1^2+\widetilde{\mu}_2^2+m^2_{\tilde{l}_{4\rm L}}\right) & \frac{\mu_3\widetilde{M}_{12}\left(\widetilde{\mu}_3\widetilde{M}^2_{123}-\mu_3\widetilde{M}_3\widetilde{M}_4\right)}{\bar{\mu}_3^2\widetilde{M}^3}\left(\widetilde{\mu}_1^2+\widetilde{\mu}_2^2+m^2_{\tilde{l}_{4\rm L}}\right) \\ 0 & \frac{\mu_3\widetilde{M}_{12}\left(\widetilde{\mu}_3\widetilde{M}^2_{123}-\mu_3\widetilde{M}_3\widetilde{M}_4\right)}{\bar{\mu}_3^2\widetilde{M}^3}\left(\widetilde{\mu}_1^2+\widetilde{\mu}_2^2+m^2_{\tilde{l}_{4\rm L}}\right) & \bar{\mu}_3^2+\frac{\left(\widetilde{\mu}_3\widetilde{M}^2_{123}-\mu_3\widetilde{M}_3\widetilde{M}_4\right)^2}{\bar{\mu}_3^2\widetilde{M}^4}m^2_{\tilde{l}_{4\rm L}}+\mathcal{O}\big(\frac{\widetilde{\mu}_1^2+\widetilde{\mu}_2^2}{\bar{\mu}_3^2}\big) \end{pmatrix}.$$

The non-zero off-diagonal elements are of similar size as the diagonal elements, unless $m_{\tilde{l}_{4\rm L}} \ll \bar{\mu}_3 \sim m_\tau$. Numerically, we find that the same is true for the 12- and 13-entries, if μ_1 and μ_2 are non-zero. This leads to unacceptably large FCNCs in the lepton sector. The situation in the down quark sector is analogous.

Unfortunately we have to conclude that the solution of the FCNC problem in the simplest gaugino mediation scenario does not carry over to the more general case. We expect this problem to be generic in higher-dimensional theories with mixing between bulk and brane matter fields as long as the bulk fields can couple to the hidden sector (cf. e.g. [67]). In the following, we shall assume that soft masses for bulk matter fields, contrary to the bulk Higgs fields, are strongly suppressed, i.e. $m_{\tilde{l}_{4\rm L,R}} \simeq m_{\tilde{d}_{4\rm L,R}} \simeq 0$. Within the present framework of orbifold GUTs, the coupling of brane and bulk fields cannot be understood dynamically. One might hope that when constructing such a model from a top down perspective, e.g. starting from the heterotic string, such couplings turn out to be negligible.

At this point we want to remind the reader that the aim of this chapter is to evaluate the superparticle mass spectrum. We have learned by now that this has to be done with the help of RG equations, which translate the high scale parameters into parameters accessible by experiment. However, in principle these high scale parameters are free parameters of the theory and cannot be calculated from first principles – at least not in our effective field theory setup. This means that even after we specified the supersymmetry breaking mechanism, we will not be able to obtain a specific prediction for the mass spectrum. Instead we have to scan over the corresponding parameter space and see what kind of spectra are typical for our scenario. Therefore it would be helpful to know if the values of the parameters we scan over are constrained in any way. Fortunately it

turns out that indeed the parameters must not exceed certain bounds in order for the effective theory to be valid up to the cutoff scale. A very useful technique, which allows to estimate these bounds is 'naïve dimensional analysis' [21]. Following this line of thinking, we derive upper bounds on the size of the corresponding operator coefficients, before we come to the resulting mass spectrum at the electroweak scale.

4. Constraints from Naïve Dimensional Analysis

The main idea of naïve dimensional analysis (NDA) is that the effective theory should remain valid up to the cutoff scale Λ, implying upper bounds for the unknown coefficients of effective field theory operators[5]. For a strongly coupled theory one usually assumes that all loops are equally important ('loop democracy'). For a theory which remains calculable up to the cutoff scale the loops should contribute accordingly less. Unlike the naïve expectation, the condition of loop democracy does not imply that all couplings in the effective theory should be $\lesssim \mathcal{O}(1)$ in units of Λ. This is because loop integrals are kinematically suppressed by a geometrical factor of order

$$\ell_D = 2^D \pi^{D/2} \Gamma(D/2) \tag{IV.26}$$

which rapidly grows with the number of dimensions. This can result in large deviations from the naïve expectation.

So how does NDA work in practice? In order to derive bounds on the soft parameters, we have to constrain the couplings of the brane field $S(x)$ to bulk fields $B(x,y)$. For this purpose, we rewrite the relevant part of the six-dimensional Lagrangian

$$\mathscr{L}_{B,S} = \mathscr{L}_{\text{bulk}}(B(x,y)) + \delta^2(y - y_S)\, \mathscr{L}_S(B(x,y), S(x)) \tag{IV.27}$$

in terms of dimensionless fields $\hat{B}(x,y)$ and $\hat{S}(x)$, and the cutoff Λ, up to which the theory should be valid,

$$\mathscr{L}_{B,S} = \frac{\Lambda^6}{\ell_6/C}\, \hat{\mathscr{L}}_{\text{bulk}}(\hat{B}(x,y)) + \delta^2(y - y_S)\, \frac{\Lambda^4}{\ell_4/C}\, \hat{\mathscr{L}}_S(\hat{B}(x,y), \hat{S}(x)) \,. \tag{IV.28}$$

Here $\ell_6 = 128\pi^3$, $\ell_4 = 16\pi^2$ and y_S corresponds to the extra-dimensional coordinates of the brane where the singlet field $S(x)$ resides, $y_S = (0,0)$. The factor C accounts for the multiplicity of fields in loop diagrams for a non-Abelian gauge group. If the kinetic

[5] Originally the authors of [21] assumed all couplings of the theory to become strong at the scale Λ. They argue that this is attractive from a string theory point of view, because it is extremely difficult to find phenomenologically viable vacua near a weak coupling regime because the theory then generally runs away to zero couplings [68]. The strong coupling assumption in turn yields an estimate for the parameter in question. However, we don't want to base our calculation on this strong coupling assumption and hence only derive upper bounds on the couplings.

terms of the original Lagrangian (IV.27) are canonical, the rescaling of chiral bulk and brane superfields reads

$$B(x,y) = \left(\frac{\Lambda^4 V}{\ell_6/C}\right)^{1/2} \hat{B}(x,y) \quad , \quad S(x) = \left(\frac{\Lambda^2}{\ell_4/C}\right)^{1/2} \hat{S}(x) \; . \tag{IV.29}$$

Note the additional factor of $\sqrt{V}$ for the bulk field due to the proper normalisation (see footnote 3). The combination C/ℓ_D gives the typical geometrical suppression of loop diagrams. This suppression is cancelled by enhancement factors which result from the pre-factors ℓ_6/C and ℓ_4/C in front of the Lagrangians $\hat{\mathscr{L}}$ in Eq. (IV.28). Consequently, all loops will be of the same order of magnitude, provided that all couplings are $\mathcal{O}(1)$. Thus, according to the NDA recipe the effective six-dimensional theory remains weakly coupled up to the cutoff Λ, if the dimensionless couplings in Eq. (IV.28) are smaller than one.

Let us apply NDA to the part of the brane Lagrangian giving rise to Higgs and Higgsino masses, which corresponds to the first two lines of Eq. (IV.9). Since $\mathrm{d}\theta$ has mass dimension $1/2$, it also has to be divided by the corresponding power of the cutoff to obtain a dimensionless expression. Using Eq. (IV.29), we obtain

$$\begin{aligned}\mathscr{L}_S \supset -\frac{\Lambda^4}{\ell_4/C} \int \frac{\mathrm{d}^4\theta}{\Lambda^2} \Bigg\{ & \frac{V\Lambda^2\sqrt{\ell_4 C}}{\ell_6} \left(a\hat{S}^\dagger \hat{H}_2 \hat{H}_1^c + b_1 \hat{S}^\dagger \hat{H}_1^{c\dagger} \hat{H}_1^c + b_2 \hat{S}^\dagger \hat{H}_2^\dagger \hat{H}_2 + \mathrm{h.c.} \right) \\ & + \frac{V\Lambda^2 C}{\ell_6} \hat{S}^\dagger \hat{S} \left[c_1 \hat{H}_1^{c\dagger} \hat{H}_1^c + c_2 \hat{H}_2^\dagger \hat{H}_2 + \left(d\hat{H}_2 \hat{H}_1^c + \mathrm{h.c.} \right) \right] \Bigg\} \; . \end{aligned} \tag{IV.30}$$

The NDA requirement that all couplings be smaller than one implies the following constraints on $a, b_{1,2}, c_{1,2}, d$:

$$\frac{V\Lambda^2\sqrt{\ell_4 C}}{\ell_6} (a, b_1, b_2) < 1 \; , \tag{IV.31a}$$

$$(c_1, c_2, d) \frac{V\Lambda^2 C}{\ell_6} < 1 \; . \tag{IV.31b}$$

Using $\ell_4 = 16\pi^2$ and $\ell_6 = 128\pi^3$, one then obtains upper bounds on the couplings at the compactification scale,

$$(a, b_1, b_2) < \frac{32\pi^2}{V\Lambda^2\sqrt{C}} \; , \tag{IV.32a}$$

$$(c_1, c_2, d) < \frac{128\pi^3}{V\Lambda^2 C} \; . \tag{IV.32b}$$

These inequalities translate into upper bounds on the μ- and $B\mu$-terms and on the soft

Higgs masses,

$$\mu = \frac{aF_S^\dagger}{\Lambda} < \frac{32\pi^2 F_S^\dagger}{V\sqrt{C}\Lambda^3} , \tag{IV.33a}$$

$$B\mu = \frac{\left(a\,(b_1+b_2)+d\right) F_S^\dagger F_S}{\Lambda^2} < \left(1+\frac{16\pi}{V\Lambda^2}\right)\frac{128\pi^3 F_S^\dagger F_S}{VC\Lambda^4} , \tag{IV.33b}$$

$$(m_{\tilde{h}_2}^2, m_{\tilde{h}_1}^2) = \frac{(c_2+b_2^2, c_1+b_1^2)\, F_S^\dagger F_S}{\Lambda^2} < \left(1+\frac{8\pi}{V\Lambda^2}\right)\frac{128\pi^3 F_S^\dagger F_S}{VC\Lambda^4} . \tag{IV.33c}$$

Applying the NDA recipe to those terms of Eqs. (IV.8) and (IV.9) giving rise to soft superparticle masses we obtain

$$\begin{aligned}\mathscr{L}_S \supset -\frac{\Lambda^4}{\ell_4/C}\Bigg[&\int \frac{\mathrm{d}^2\theta}{\Lambda}\,\frac{\sqrt{\ell_4/C}}{\ell_6/C}\Lambda^2 V\left(\frac{\tilde{M}^d}{\Lambda}\hat{S}\hat{H}_5\hat{H}_6 + \frac{\tilde{M}_4^l}{\Lambda}\hat{S}\hat{\phi}\hat{\phi}^c\right) + \text{h.c.}\\ &+ \int \frac{\mathrm{d}^4\theta}{\Lambda^2}\,\frac{\sqrt{\ell_4/C}}{\ell_6/C}\Lambda^2 V\left\{e_i\hat{S}^\dagger\hat{B}_i^\dagger\hat{B}_i + \text{h.c.} + \frac{e_i'}{\sqrt{\ell_4/C}}\hat{S}^\dagger\hat{S}\,\hat{B}_i^\dagger\hat{B}_i\right\}\Bigg] .\end{aligned} \tag{IV.34}$$

The resulting upper bounds on the masses can be found in Table IV.3. A similar analysis for the gaugino mass resulting from (IV.3) has been performed in [22]. We have included this bound in Table IV.3. Furthermore we have included the gravitino mass $m_{3/2}$. When the gaugino mass $m_{1/2}$ is fixed, this leads to a lower bound on the gravitino mass. This will become important in the next chapter, where we will discuss supersymmetric dark matter candidates.

To be more explicit, we make assumptions about the values of the parameters involved. The compactification scale is assumed to be of order the unification scale, $V^{-1/2} = M_{\text{GUT}} = 2.5\cdot 10^{16}\,\text{GeV}$. The cutoff Λ is given by the six-dimensional Planck scale, $\Lambda = M_6 = M_4^{1/2}V^{-1/4} = 2.4\cdot 10^{17}\,\text{GeV}$. We choose the group theory factor to be the quadratic Casimir operator, which gives $C = C_2(G) = 8$ for the gauge group $G = SO(10)$. This leads to the numerical values for the NDA bounds shown in the last column of Table IV.3.

Equipped with this knowledge of possible parameter values, we now turn to the spectrum of superpartners at low energies.

5. The Low-Energy Sparticle Spectrum

In order to find the spectrum at low energy, we have to take into account the running of the parameters. Given the high scale boundary conditions as input, the corresponding renormalisation group equations (RGEs) are solved numerically, where electroweak precision data as well as successful radiative electroweak symmetry breaking are taken into account. We employ SOFTSUSY [69] for this purpose, a program which calculates the spectrum of superpartners in the MSSM.

$m_{1/2}$	$= \frac{g_4^2 h F_S}{2\Lambda}$	$< \frac{16\pi^2 F_S}{\sqrt{C}V\Lambda^3}$	$< 1\,\mathrm{TeV}$
$m^2_{\tilde{d}_{4\mathrm{RL}}}$	$= \frac{F_S}{\Lambda}\tilde{M}^d$	$< \frac{32\pi^2 F_S}{\sqrt{C}V\Lambda^2}$	$< (2\cdot 10^7\,\mathrm{TeV})^2$
$m^2_{\tilde{l}_{4\mathrm{LR}}}$	$= \frac{F_S}{\Lambda}\tilde{M}^l_4$	$< \frac{32\pi^2 F_S}{\sqrt{C}V\Lambda^2}$	$< (2\cdot 10^7\,\mathrm{TeV})^2$
$m^2_{\tilde{d}_{4\mathrm{L}}}$	$= (e_d^2 + e_d')\frac{F_S^\dagger F_S}{\Lambda^2}$	$< (1+\frac{8\pi}{V\Lambda^2})\frac{128\pi^3 F_S^\dagger F_S}{CV\Lambda^4}$	$< (4\,\mathrm{TeV})^2$
$m^2_{\tilde{l}_{4\mathrm{L}}}$	$= (e_l^2 + e_l')\frac{F_S^\dagger F_S}{\Lambda^2}$	$< (1+\frac{8\pi}{V\Lambda^2})\frac{128\pi^3 F_S^\dagger F_S}{CV\Lambda^4}$	$< (4\,\mathrm{TeV})^2$
μ	$= a\frac{F_S^\dagger}{\Lambda}$	$< \frac{32\pi^2 F_S^\dagger}{\sqrt{C}V\Lambda^3}$	$< 2\,\mathrm{TeV}$
$(m^2_{\tilde{h}_2}, m^2_{\tilde{h}_1})$	$= (c_2 + b_2^2, c_1 + b_1^2)\frac{F_S^\dagger F_S}{\Lambda^2}$	$< (1+\frac{8\pi}{V\Lambda^2})\frac{128\pi^3 F_S^\dagger F_S}{CV\Lambda^4}$	$< (4\,\mathrm{TeV})^2$
$B\mu$	$= \big(a\,(b_1+b_2)+d\big)\frac{F_S^\dagger F_S}{\Lambda^2}$	$< (1+\frac{16\pi}{V\Lambda^2})\frac{128\pi^3 F_S^\dagger F_S}{CV\Lambda^4}$	$< (5\,\mathrm{TeV})^2$
$m_{3/2}$	$= \frac{F_S}{\sqrt{3}M_4}$		$= 100\,\mathrm{GeV}$

Table IV.3.: NDA constraints on mass parameters. The numerical values are valid for $F_S = 4\cdot 10^{20}\,\mathrm{GeV}^2$, which is a typical scale for the F-term vev in our scenario yielding a gravitino mass of $m_{3/2} = 100\,\mathrm{GeV}$. The masses for the fields l_4^c, d_4^c are analogous to those of l_4, d_4.

Imposing $m_{\tilde{l}_{4\mathrm{L,R}}} = m_{\tilde{d}_{4\mathrm{L,R}}} = 0$ in order to avoid unacceptably large flavour changing neutral currents (cf. Section 3), the boundary conditions at the compactification scale $V^{-1/2} = M_{\mathrm{GUT}}$ are given by

$$M_1 = M_2 = M_3 = m_{1/2} \neq 0\,, \tag{IV.35a}$$

$$m^2_{\tilde{\phi}_\mathrm{L}} = m^2_{\tilde{\phi}_\mathrm{R}} = 0 \quad \text{for all squarks and sleptons } \tilde{\phi}\,, \tag{IV.35b}$$

$$A_{\tilde{\phi}} = 0 \quad \text{for all squarks and sleptons } \tilde{\phi}\,, \tag{IV.35c}$$

$$\mu, B\mu, m^2_{\tilde{h}_i} \neq 0 \quad (i = 1,2)\,. \tag{IV.35d}$$

Here $M_{1,2,3}$ are the soft gaugino masses, $m_{\tilde{\phi}}$ are the soft scalar masses and $A_{\tilde{\phi}}$ is the scalar trilinear coupling. Since we are considering an $SO(10)$ GUT, the gaugino masses $M_{1,2,3}$ as well as the corresponding gauge couplings

$$g_1 = g_2 = g_3 = g \simeq \frac{1}{\sqrt{2}}\,, \tag{IV.36}$$

are unified at M_{GUT}. These gauge couplings are written in GUT charge normalisation, which means that in terms of the conventional electroweak gauge couplings g and g' one has $g_2 = g$ and $g_1 = \sqrt{5/3}g'$.

With these boundary conditions the scalar mass matrices remain almost diagonal, since only very small renormalisation group corrections originating from the Yukawa

couplings induce some flavour mixing. Therefore flavour changing neutral currents are suppressed. In writing down the boundary conditions (IV.35) we have neglected small corrections to the scalar masses from gaugino loops [16] as well as corrections to the gauge couplings from brane-localised terms breaking the unified gauge symmetry (see e.g. [70]). Upper limits on the non-vanishing parameters are summarised in Table IV.3. Note that although the boundary conditions (IV.35) were derived from our specific model, they could also arise from other theoretical frameworks. Therefore the results from our renormalisation group analysis are not restricted to our specific theoretical construction and can also be applied to other scenarios. Actually the boundary conditions (IV.35) agree with those of the usual gaugino mediation scenario with bulk Higgs fields [17]. Furthermore, for $m^2_{\tilde{h}_i} = 0$, these boundary conditions have previously been considered in different contexts such as no-scale models [71, 72]. Nevertheless, no comprehensive analysis of nearly vanishing soft scalar masses $m_{\tilde{\phi}}$ with un-suppressed soft Higgs masses has been performed so far.

For phenomenological considerations it is often useful to introduce the quantity $\tan\beta \equiv v_u/v_d$, which is the ratio of the two Higgs vacuum expectation values. The conditions for successful electroweak symmetry breaking then allow us to eliminate two of the Lagrangian parameters, $|\mu|$ and $B\mu$, in favour of $\tan\beta$ (see e.g. [2]). The phase of μ remains undetermined however, and we have to specify the sign of μ. This leads to the following non-vanishing input parameters at the compactification scale

$$m_{1/2}\,, \quad m^2_{\tilde{h}_1}\,, \quad m^2_{\tilde{h}_2}\,, \quad \tan\beta \quad \text{and} \quad \text{sign}(\mu)\,. \tag{IV.37}$$

If we choose a certain value for the universal gaugino mass $m_{1/2}$, this implies a lower bound on the vev F_S according to the first row of Table IV.3. The choice is constrained by the lower bound on the Higgs mass from LEP, $m_h > 114.4\,\text{GeV}$, because lighter gauginos imply a lighter Higgs[6]. As a benchmark point for our discussion which leads to Higgs masses above the LEP bound, we choose

$$m_{1/2} = 500\,\text{GeV}\,, \quad \tan\beta = 10 \qquad \text{and} \qquad \text{sign}(\mu) = +1\,. \tag{IV.38}$$

This leads to a lower bound on F_S,

$$F_S > 2 \cdot 10^{20}\,\text{GeV}^2\,, \tag{IV.39}$$

resulting directly in a lower bound on the gravitino mass

$$m_{3/2} > 50\,\text{GeV}\,. \tag{IV.40}$$

We use the current best-fit value $m_t = 172.7\,\text{GeV}$ [73] for the top mass. As noted above, for given $\tan\beta$ and $\text{sign}(\mu)$ the values of μ and $B\mu$ are determined by the conditions for

[6] There is a small region in parameterspace where the experimental constraints on the supersymmetric Higgs bosons are weaker. In this "light Higgs window" the two lightest Higgs bosons h^0 and A^0 can be both around $90 - 100\,\text{GeV}$. However, the LEP bound on the Standard Model Higgs also applies to much of the MSSM parameterspace and hence we use it here.

electroweak symmetry breaking. We find that their numerical values at the compactification scale are well below their NDA bounds. Hence our benchmark point is viable and the only parameters left undetermined are the two soft Higgs masses $m^2_{\tilde{h}_1}$ and $m^2_{\tilde{h}_2}$.

In the following we will analyse the impact of the high-scale parameters on the superparticle spectrum and determine the regions in parameterspace which result in a viable phenomenology. In this section we will mostly be concerned with experimental constraints from collider physics and field theoretic consistency (no tachyonic states). Additional constraints which arise from cosmological considerations will be discussed in the next chapter. We use SOFTSUSY to scan over the two soft Higgs masses. The allowed parameter range is shown in Figure IV.1, whereas the resulting spectrum is given in Figure IV.3. In addition to the numerical treatment, we will discuss some features of the spectrum which can be understood analytically.

5.1. Renormalisation Group Equations

To obtain an analytical understanding of the results, let us consider the one-loop renormalisation group equations (RGEs) for the soft masses at the compactification scale [74, 75],

$$16\pi^2 \frac{\mathrm{d}M_i^2}{\mathrm{d}t} = 4 b_i g^2 m_{1/2}^2 \,, \tag{IV.41a}$$

$$16\pi^2 \frac{\mathrm{d}m^2_{\tilde{q}_{3\mathrm{L}}}}{\mathrm{d}t} = -\frac{84}{5} g^2 m_{1/2}^2 + \frac{1}{5} g^2 \,\mathrm{Tr}(Y m^2) + X_t + X_b \,, \tag{IV.41b}$$

$$16\pi^2 \frac{\mathrm{d}m^2_{\tilde{t}_{\mathrm{R}}}}{\mathrm{d}t} = -\frac{64}{5} g^2 m_{1/2}^2 - \frac{4}{5} g^2 \,\mathrm{Tr}(Y m^2) + 2X_t \,, \tag{IV.41c}$$

$$16\pi^2 \frac{\mathrm{d}m^2_{\tilde{b}_{\mathrm{R}}}}{\mathrm{d}t} = -\frac{56}{5} g^2 m_{1/2}^2 + \frac{2}{5} g^2 \,\mathrm{Tr}(Y m^2) + 2X_b \,, \tag{IV.41d}$$

$$16\pi^2 \frac{\mathrm{d}m^2_{\tilde{\tau}_{\mathrm{L}}}}{\mathrm{d}t} = -\frac{36}{5} g^2 m_{1/2}^2 - \frac{3}{5} g^2 \,\mathrm{Tr}(Y m^2) + X_\tau \,, \tag{IV.41e}$$

$$16\pi^2 \frac{\mathrm{d}m^2_{\tilde{\tau}_{\mathrm{R}}}}{\mathrm{d}t} = -\frac{24}{5} g^2 m_{1/2}^2 + \frac{6}{5} g^2 \,\mathrm{Tr}(Y m^2) + 2X_\tau \,, \tag{IV.41f}$$

$$16\pi^2 \frac{\mathrm{d}m^2_{\tilde{h}_1}}{\mathrm{d}t} = -\frac{36}{5} g^2 m_{1/2}^2 - \frac{3}{5} g^2 \,\mathrm{Tr}(Y m^2) + 3X_b + X_\tau \,, \tag{IV.41g}$$

$$16\pi^2 \frac{\mathrm{d}m^2_{\tilde{h}_2}}{\mathrm{d}t} = -\frac{36}{5} g^2 m_{1/2}^2 + \frac{3}{5} g^2 \,\mathrm{Tr}(Y m^2) + 3X_t \,, \tag{IV.41h}$$

where $t = \ln \frac{\mu}{\mu_0}$ with the renormalisation scale μ, $b_i = (\frac{33}{5}, 1, -3)$ are the coefficients in the RGEs of the gauge couplings,

$$16\pi^2 \frac{\mathrm{d}g_i^2}{\mathrm{d}t} = 2 b_i g^4 \,, \tag{IV.42}$$

and

$$X_t = 2y_t^2 m_{\tilde{h}_2}^2 \simeq \frac{1}{2}\left(1+\cot^2\beta\right) m_{\tilde{h}_2}^2 \ , \tag{IV.43a}$$

$$X_b = 2y_b^2\, m_{\tilde{h}_1}^2 \simeq 5\cdot 10^{-5}\left(1+\tan^2\beta\right) m_{\tilde{h}_1}^2 \ , \tag{IV.43b}$$

$$X_\tau = 2y_\tau^2\, m_{\tilde{h}_1}^2 \simeq 10^{-4}\left(1+\tan^2\beta\right) m_{\tilde{h}_1}^2 \ . \tag{IV.43c}$$

The numerical values in the previous equations represent the typical orders of magnitude of the top, bottom and tau Yukawa couplings at high energy. We assume a not too large $\tan\beta$, so that X_b and X_τ are negligible at the GUT scale. However, we will see that X_τ can become relevant at lower energies. The term $\mathrm{Tr}(Ym^2)$, often abbreviated by S, vanishes for universal scalar masses but plays an important role in our case, if one of the soft Higgs masses is sufficiently large. At M_{GUT}, it is given by

$$\mathrm{Tr}(Ym^2) = m_{\tilde{h}_2}^2 - m_{\tilde{h}_1}^2 \ . \tag{IV.44}$$

The RGEs for the first and second generation scalar masses are obtained from the above equations by omitting X_t, X_b and X_τ. We do not list the RGEs for μ, $B\mu$ and the A-terms, since they are not relevant for our discussion. We will also use

$$16\pi^2 \frac{\mathrm{d}(g_i^2 M_i^2)}{\mathrm{d}t} = 6 b_i g^4 m_{1/2}^2 \ , \tag{IV.45a}$$

$$16\pi^2 \frac{\mathrm{d}\,\mathrm{Tr}(Ym^2)}{\mathrm{d}t} = \frac{66}{5} g^2\,\mathrm{Tr}(Ym^2) \ . \tag{IV.45b}$$

5.2. Gaugino Masses

The 1-loop RGEs (IV.41a) for the gaugino masses do not depend on the scalar masses, so that their low-energy values remain virtually the same in all cases as long as we do not change $m_{1/2}$. Numerically, we find

$$M_1(M_Z) \simeq 200\,\mathrm{GeV} \ , \tag{IV.46a}$$

$$M_2(M_Z) \simeq 380\,\mathrm{GeV} \ , \tag{IV.46b}$$

$$M_3(M_Z) \simeq 1200\,\mathrm{GeV} \ . \tag{IV.46c}$$

To good approximation, the lightest neutralino is the bino and the second-lightest one is the wino, unless $m_{\tilde{h}_2}^2$ is sizable. In the latter case, the electroweak symmetry breaking conditions lead to a rather small μ, so that there is significant mixing between the neutralinos.

5.3. Allowed Parameter Space for the Soft Higgs Masses

In addition to the constraints from NDA, there are phenomenological limits on the soft masses $m_{\tilde{h}_i}^2$ at the compactification scale, which turn out to be more restrictive. The resulting allowed region in parameter space is shown in Figure IV.1.

One constraint is that the running of the parameters down to the weak scale must not produce tachyons. For scalar masses which vanish at the compactification scale this means that their β-function must not be positive there.[7] The one-loop RGE (IV.41e) for the left-handed sleptons gives the most restrictive constraint on $m^2_{\tilde{h}_1}$,

$$m^2_{\tilde{h}_1} < 12\, m^2_{1/2} + m^2_{\tilde{h}_2} \,. \tag{IV.47}$$

The upper bounds on $m^2_{\tilde{h}_2}$ are due to the experimental limits on the superparticle masses [24]. If the initial value of $m^2_{\tilde{h}_2}$ is too large, this mass squared crosses zero at a rather low energy, so that its absolute value at the electroweak scale is small. Consequently, the μ parameter is also small, leading to a Higgsino-like chargino with a mass below the current limit of 94 GeV. If we increased $m^2_{\tilde{h}_2}$ further, there would be no successful electroweak symmetry breaking. This limit on $m^2_{\tilde{h}_2}$ is the relevant one for almost all values of $m^2_{\tilde{h}_1}$. Only for very small $m^2_{\tilde{h}_1}$, the experimental requirement that the lighter stau be heavier than 86 GeV becomes more restrictive.

For simplicity we only consider positive soft Higgs masses at the compactification scale.[8] With negative soft masses, it is possible to end up in the "light Higgs window" at the electroweak scale, though only in a very narrow parameter range. In this window with both m_{h^0} and m_{A^0} around 90 – 100 GeV we can decrease $m_{1/2}$ significantly down to at least 250 GeV.

5.4. Dependence of the Spectrum on the Higgs Masses

Due to the large effects of the strong interaction, the squark masses experience the fastest running and end up around a TeV. The lighter stop mass runs more slowly due to X_t, which is always sizable at lower energies, and reaches a value of about 800 GeV. If all scalar soft masses vanish at the GUT scale, the left-handed slepton masses change significantly in the beginning, but afterwards the evolution flattens as $g_1^2 M_1^2$ and $g_2^2 M_2^2$ decrease (cf. Eq. (IV.45a)). Hence, they reach intermediate values between 300 and 400 GeV at low energies. The flattening of the evolution is even more pronounced for the right-handed slepton masses, since here it depends only on $g_1^2 M_1^2$, which decreases faster than $g_2^2 M_2^2$. As a consequence, these scalars remain lighter than the lightest neutralino [16], which is approximately the bino: $m_{\tilde{e}_\mathrm{R}}(M_Z) \simeq 180\,\mathrm{GeV}$, $m_{\chi_1^0} \simeq 200\,\mathrm{GeV}$. For both slepton "chiralities", the third generation is slightly lighter than the first two due to X_τ.

For $m^2_{\tilde{h}_1} \neq m^2_{\tilde{h}_2}$, the term involving $\mathrm{Tr}(Y m^2)$ is non-vanishing and can lead to important changes [17,77–79]. We shall first consider the case where it is negative ($m^2_{\tilde{h}_1} > m^2_{\tilde{h}_2}$)

[7] Strictly speaking, a scalar mass squared may arrive at a positive value at low energies even if its β-function is positive at the compactification scale. We do not take this possibility into account, so that the constraints are conservative.

[8] After the publication of [36] a similar work [76] appeared, were a more detailed study of the negative soft Higgs masses can be found.

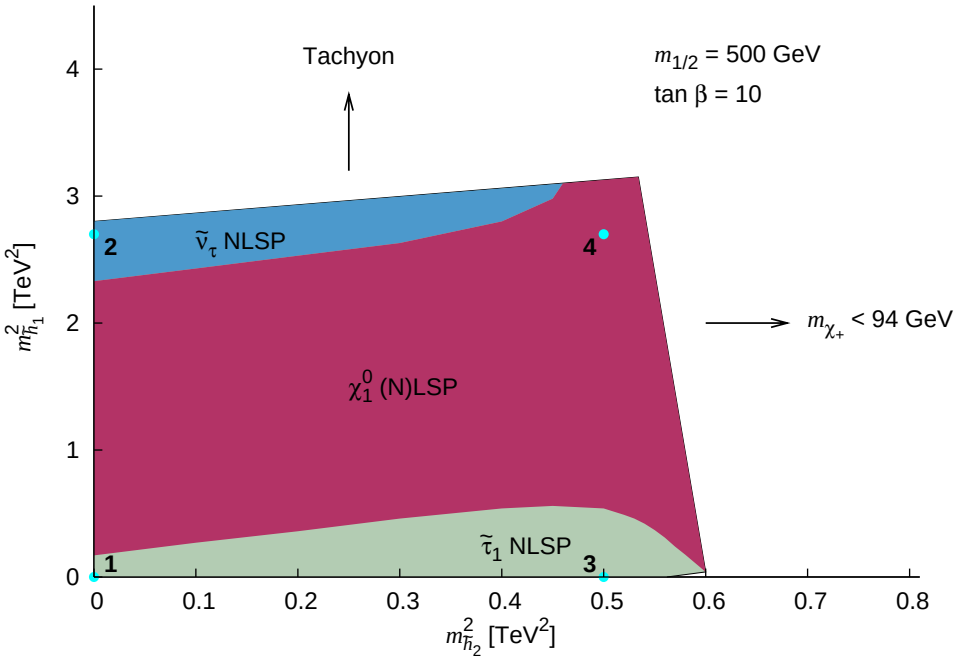

Figure IV.1.: Allowed region for the soft Higgs masses for $m_{1/2} = 500\,\mathrm{GeV}$ and $\tan\beta = 10$. In the magenta coloured area, a neutralino is lighter than all sleptons, whereas in the green region a stau and in the blue region a sneutrino is the lightest MSSM sparticles. In the case of a slepton being the lightest MSSM sparticle, we demand the gravitino to be even lighter for cosmological reasons. This is consistent with (IV.40). For the points marked by the coloured dots, the resulting superparticle mass spectrum is shown in Figure IV.3.

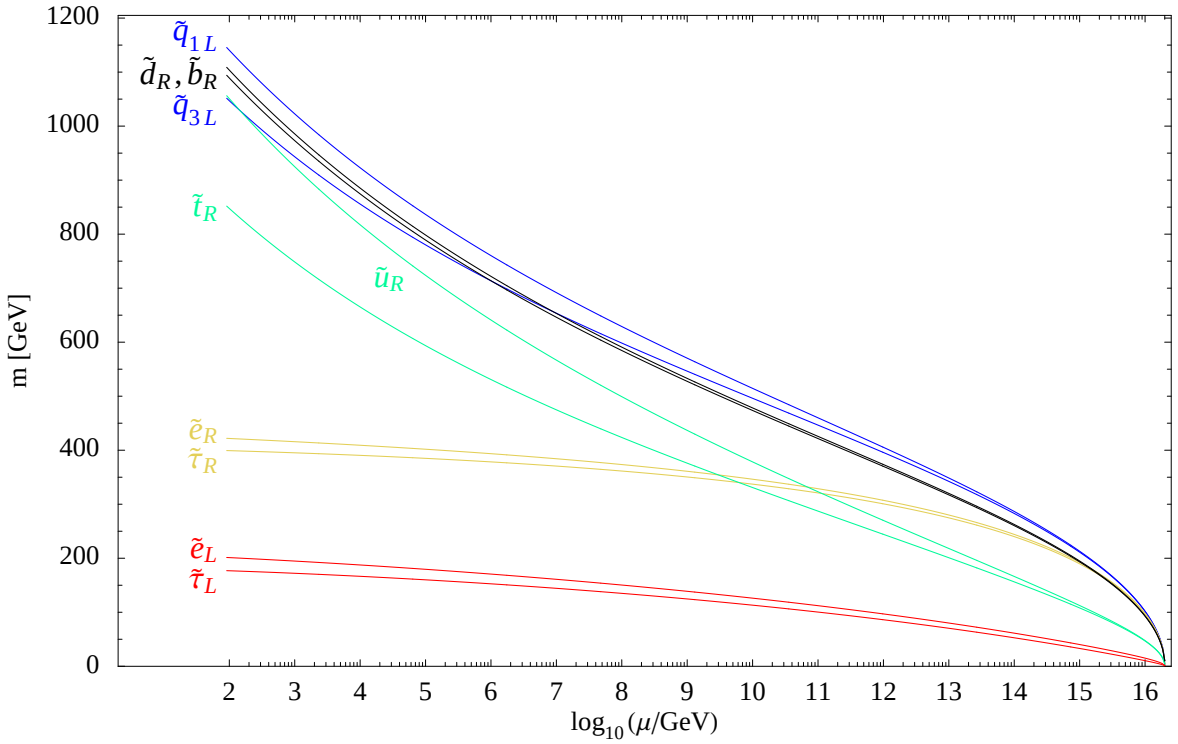

Figure IV.2.: Evolution of the scalar soft masses for $m^2_{\tilde{h}_1} = 2.7\,\mathrm{TeV}^2$, $m^2_{\tilde{h}_2} = 0$ (point 2 in Figure IV.1), $m_{1/2} = 500\,\mathrm{GeV}$, $\tan\beta = 10$ and $\mathrm{sign}(\mu) = +1$ at M_{GUT}.

and saturates the bound from Eq. (IV.47) (numerically, we find a slightly stronger bound of $m^2_{\tilde{h}_1} - m^2_{\tilde{h}_2} < 2.7\,\mathrm{TeV}^2$, which we use here). Then $|\,\mathrm{Tr}(Ym^2)/m^2_{1/2}| \sim 10$, so that the first and second terms on the r.h.s. of the RGEs (IV.41b) – (IV.41f) can be of the same order of magnitude. An example for the running of the scalar masses is shown in Figure IV.2.

The most drastic change occurs in the slepton spectrum. For the largest possible value of $\mathrm{Tr}(Ym^2)$, the r.h.s. of Eq. (IV.41e) vanishes exactly at the GUT scale. It turns negative only at lower energies due to the fast decrease of $|\,\mathrm{Tr}(Ym^2)|$ (cf. Eq. (IV.45b)). As a result, the left-handed sleptons remain relatively light, with a low-energy mass below 200 GeV. Contrary to that, both terms in the RGE for the right-handed slepton masses are of the same sign, leading to an unusually fast running near the GUT scale. At lower energies, the evolution slows down quickly due to the fast decrease of both $g_1^2 M_1^2$ and $|\,\mathrm{Tr}(Ym^2)|$. The resulting masses are close to 400 GeV. The NLSP is a left-handed sneutrino in this case [78], with a slightly heavier stau $\tilde{\tau}_1$ due to the $SU(2)_\mathrm{L}$ and $U(1)_\mathrm{Y}$ D-terms.

In the squark sector, large masses are generated again due to the strong interaction. At high energies, there is a significant cancellation in the RGE (IV.41c) for the right-handed up-type squark masses, while the contributions to the other squark mass RGEs add up. Consequently, $m_{\tilde{u}_\mathrm{R}}$ and $m_{\tilde{t}_\mathrm{R}}$ run quite slowly until $|\,\mathrm{Tr}(Ym^2)|$ has decreased sufficiently.

Afterwards, $m_{\tilde{u}_{\mathrm{R}}}$ runs faster and comes close to the masses of the left-handed and right-handed down-type squarks at the electroweak scale.

If $m^2_{\tilde{h}_1}$ is neither close to zero nor to its upper bound, the running of the right-handed slepton masses is sufficiently enhanced to lift them above the lightest neutralino mass. At the same time, the running of the left-handed slepton masses is damped weakly enough, so that they are heavier than the lightest neutralino, too [17, 78]. A neutralino NLSP together with a gravitino LSP heavier than a GeV is excluded by cosmology [32–34, 80, 81]. Therefore, this case is only viable if the neutralino is the LSP and the gravitino is heavier. This is possible, because we only have a lower bound on the gravitino mass. The corresponding region in parameter space is marked by the magenta coloured area in Figure IV.1. It grows for large values of $m^2_{\tilde{h}_2}$, since then mixing additionally decreases the lightest neutralino mass. A neutralino LSP is also often obtained if the compactification scale is larger than the unification scale. In this case, the running above M_{GUT} tends to make the sleptons heavier than the lightest neutralino [79, 82].

For $m^2_{\tilde{h}_2} > m^2_{\tilde{h}_1}$, $\mathrm{Tr}(Ym^2)$ is positive. Now the evolution of the right-handed slepton masses is slowed down by the $\mathrm{Tr}(Ym^2)$-term, while that of the left-handed masses is enhanced. Consequently, the NLSP is the predominantly right-handed $\tilde{\tau}_1$, with a mass of about 100 GeV for $m^2_{\tilde{h}_2} = 0.5\,\mathrm{TeV}^2$ and $m^2_{\tilde{h}_1} = 0$. For these values, the masses of the left-handed sleptons are roughly 350 GeV.

Since $m^2_{\tilde{h}_2}$ cannot be much larger than $0.5\,\mathrm{TeV}^2$, the RGEs for the squark masses are always dominated by the term proportional to $g_3^2 M_3^2$. Consequently, the low-energy masses are almost unchanged compared to the case of vanishing soft scalar masses at the compactification scale, except for $m_{\tilde{q}_{3\mathrm{L}}}$ and $m_{\tilde{t}_{\mathrm{R}}}$, which decrease by up to 60 GeV due to the larger X_t.

As the dominant parts of the RGEs depend only on the difference $m^2_{\tilde{h}_1} - m^2_{\tilde{h}_2}$, the same is true for the spectrum to a good approximation. The sum is only relevant for those third-generation masses whose evolution is sensitive to the X_i, most notably $m_{\tilde{t}_{\mathrm{R}}}$. In Figure IV.3, we show the superparticle spectra that we obtain at the four points in parameter space marked by the coloured dots in Figure IV.1.

5.5. Dependence on the Gaugino Masses

To a first approximation, varying the high-energy gaugino mass simply leads to a rescaling of the scalar spectrum. If $m_{1/2}$ is increased while keeping the other soft masses fixed, the relative sizes of $\mathrm{Tr}(Ym^2)$ and the X_i decrease. Hence, they become less important and the spectrum comes closer to the one obtained in the minimal case of vanishing scalar masses.

As mentioned before, the LEP bound on the lightest Higgs mass leads to a lower bound on $m_{1/2}$. Actually, with our benchmark value $m_{1/2} = 500$ GeV we obtain a Higgs mass slightly below 114 GeV for small soft masses. However, the mass can easily be

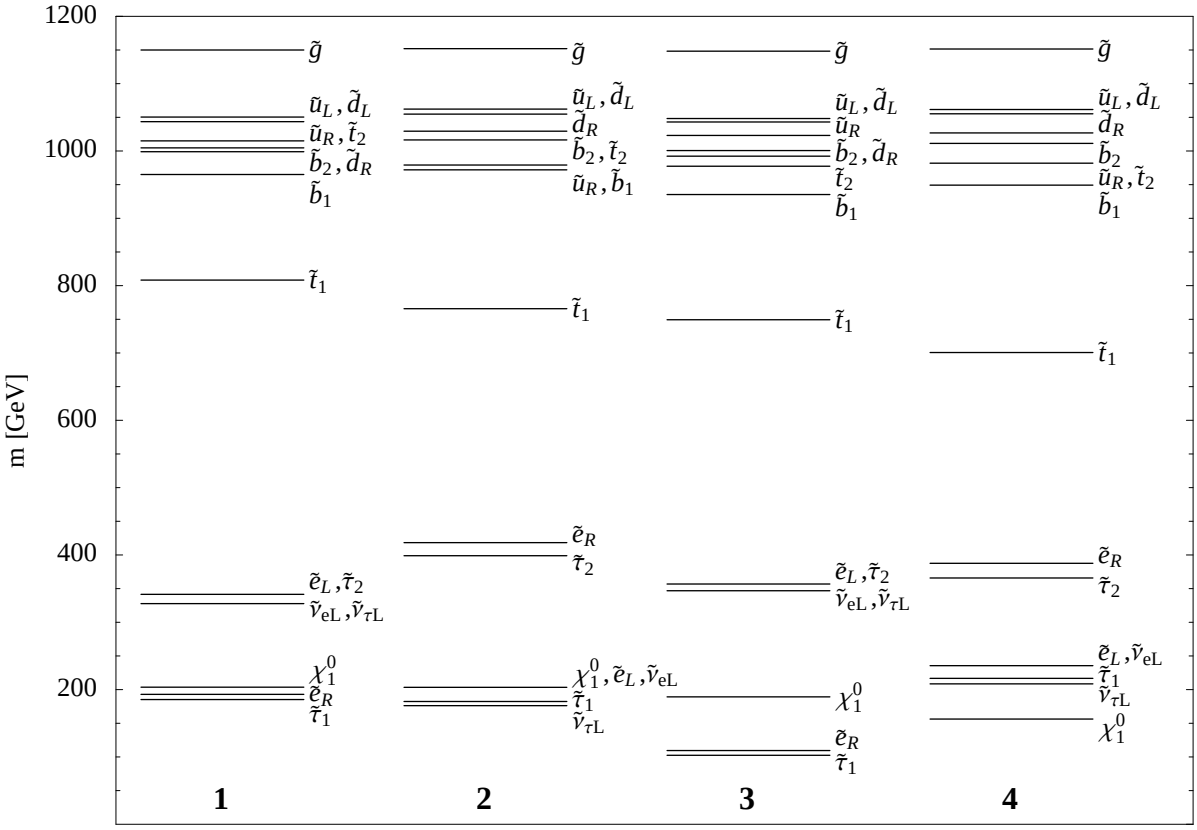

Figure IV.3.: Spectra of superparticle pole masses. The numbers at the bottom correspond to the points in parameter space marked by the coloured dots in Figure IV.1. The high-energy boundary conditions for the soft Higgs masses were $m_{\tilde{h}_1}^2 = m_{\tilde{h}_2}^2 = 0$ (point 1), $m_{\tilde{h}_1}^2 = 2.7\,\mathrm{TeV}^2$, $m_{\tilde{h}_2}^2 = 0$ (point 2), $m_{\tilde{h}_1}^2 = 0$, $m_{\tilde{h}_2}^2 = 0.5\,\mathrm{TeV}^2$ (point 3), and $m_{\tilde{h}_1}^2 = 2.7\,\mathrm{TeV}^2$, $m_{\tilde{h}_2}^2 = 0.5\,\mathrm{TeV}^2$ (point 4), respectively. In all cases, we used $m_{1/2} = 500\,\mathrm{GeV}$, $\tan\beta = 10$ and $\mathrm{sign}(\mu) = +1$. As the first and second generation scalars are degenerate, only the first generation is listed in the figure. Particles with a mass difference of less than about 3 GeV are represented by a single line. The heavier neutralinos and the charginos have been omitted for better readability.

pushed beyond the bound by raising the top mass by about 1.5 GeV above its present best-fit value of 172.7 GeV. Furthermore, a non-zero mass $m^2_{\tilde{h}_1}$ also causes an increase of the Higgs mass. If $m^2_{\tilde{h}_1}$ takes the maximal value allowed by Eq. (IV.47), a unified gaugino mass of slightly less than 400 GeV is compatible with the LEP bound (for $m_t = 172.7\,\text{GeV}$).

5.6. Dependence on $\tan\beta$

The influence of $\tan\beta$ on the results is also rather straightforward to understand. As to the RGEs, it only enters in the parameters X_t, X_b and X_τ, which play a role in the evolution of the third-generation soft masses. Hence, a change of $\tan\beta$ leads to a change of the mass splitting between this generation and the first two.

If $\tan\beta$ is significantly smaller than 10, the value used in our benchmark scenario, X_t increases. Consequently, $\tilde{t}_\text{R}$ and $\tilde{q}_{3\text{L}}$ become slightly lighter. On the other hand, X_b and X_τ are negligible now, so that the inter-generation mass splitting in the slepton and right-handed down-type squark sector becomes tiny. The Higgs mass bound leads to severer restrictions now. If $\tan\beta < 8$, raising the top mass to the maximal value of 175.6 GeV allowed by experiment no longer yields $m_{h^0} > 114.4\,\text{GeV}$ for $m^2_{\tilde{h}_1} = 0$. If $\tan\beta < 6$, the bound is violated even for maximal m_t and $m^2_{\tilde{h}_1}$, i.e. a gaugino mass larger than 500 GeV is required.

For larger values of $\tan\beta$, X_b and X_τ become more important. Nevertheless, the impact of the former parameter on the RG evolution remains subdominant compared to that of the strong interaction. Hence, its increase only causes a larger splitting between $m_{\tilde{d}_\text{R}}$ and $m_{\tilde{b}_\text{R}}$, but does not lead to any new restrictions. In contrast, the lighter stau mass decreases a lot faster at lower energies due to the larger X_τ. On the one hand, this increases the parameter space region where the $\tilde{\tau}_1$ is lighter than the neutralinos, as shown in Figure IV.4 for $\tan\beta = 20$. On the other hand, the soft scalar masses have to satisfy severer upper bounds in order to avoid tachyons and a too light stau. As $\tan\beta$ increases beyond 20, mixing causes an additional decrease of $m_{\tilde{\tau}_1}$, as the off-diagonal term in the mass matrix, $(m^2_{\tilde{\tau}})_{12} \simeq -v\mu y_\tau$, becomes comparable to the diagonal entries. For $\tan\beta = 25$, the region of parameter space where the neutralino is lighter than the $\tilde{\tau}_1$ almost vanishes. For $\tan\beta = 35$, the model is only viable if all soft scalar masses vanish at the GUT scale, and for $\tan\beta > 35$ the lighter stau mass always lies below its experimental limit.[9]

These problems are alleviated for heavier gauginos. In order to obtain a viable model with $\tan\beta = 50$, one requires $m_{1/2} \gtrsim 850\,\text{GeV}$, if all other soft masses vanish. If they are non-zero, the gaugino mass has to be even larger. In the resulting spectrum, only one stau is relatively light, while the remaining superparticle masses lie above 300 GeV.

[9] Valid points in parameter space may exist for negative soft Higgs masses, but even in this case the allowed region is rather small.

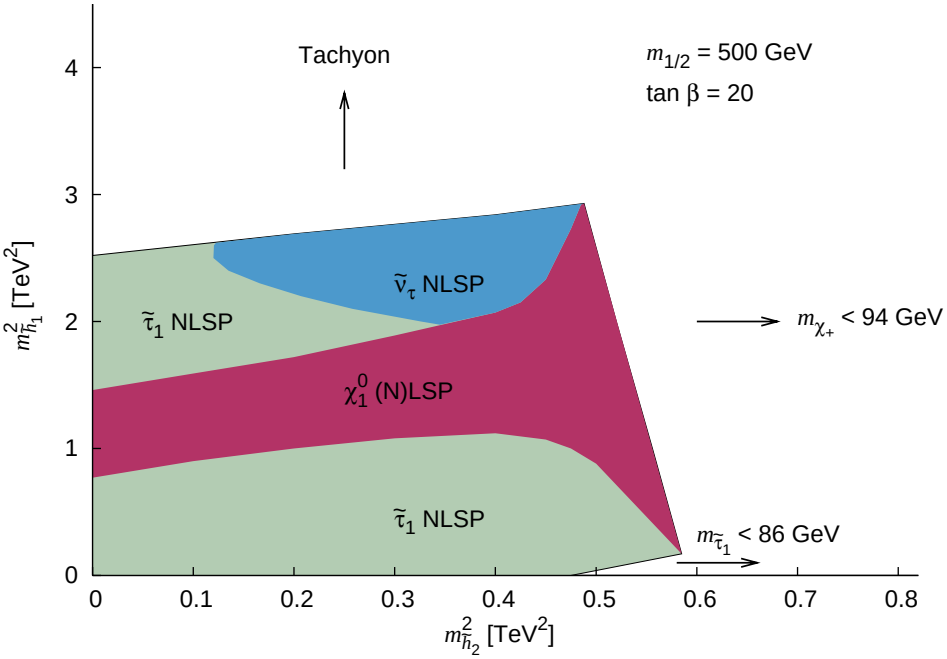

Figure IV.4.: Allowed region for the soft Higgs masses for $\tan\beta = 20$. Comparing this with Fig IV.1 we see that the region in parameterspace resulting in a slepton NLSP grows with $\tan\beta$, while the total allowed area shrinks.

As the lower bound on the gravitino mass rises with $m_{1/2}$, the gravitino may become heavier than the stau, which is excluded by cosmology[10].

We conclude that the model favours $10 \lesssim \tan\beta \lesssim 25$. For values far outside this range, the phenomenological bounds on the soft masses are much more restrictive than the NDA limits, which appears unnatural.

Summary and Concluding Remarks

In this chapter we have discussed the superparticle mass spectrum resulting from the interplay of gaugino mediated supersymmetry breaking and an $SO(10)$ orbifold GUT model. We found that the couplings of bulk matter fields to the supersymmetry breaking gauge singlet brane field have to be suppressed in order to avoid large FCNCs. We have also determined bounds on the supersymmetry breaking parameters by naïve dimensional analysis, which turn out not to restrict the phenomenologically allowed parameter regions. The parameters relevant for the superparticle mass spectrum are the universal gaugino mass, the soft Higgs masses, $\tan\beta$ and the sign of μ. We have analysed their impact on the spectrum and determined the region in parameter space that results

[10] This will be discussed in more detail in the next chapter. Like with most 'no go' situations in physics, there is a loophole: If there exists an additional exotic superparticle (e.g. the axino) which plays the role of the LSP, this scenario is still viable.

in a viable phenomenology. Either the right-handed or the left-handed sleptons can be lighter than all neutralinos. The corresponding parameter region grows with $\tan\beta$.

So far we were mainly concerned with the MSSM particle content of the theory. Nevertheless we know that supersymmetry is likely to be a local symmetry if it is realised in nature and that we necessarily have to include the gravitino in this case. We already included the gravitino mass in Table IV.3 and found that at our benchmark point the lower bound is given by (IV.40). This admits the possibility that the gravitino is the lightest superparticle in the parameter regions where sleptons are lighter than all neutralinos. This is desirable from a cosmological point of view, since in this case the gravitino could make up the dark matter.

However, the question remains if such a scenario leads to a viable phenomenology. This is because in addition to the constraints from collider searches there are cosmological constraints which we have not considered so far. Such cosmological constraints come from the observed dark matter density, the observed abundance of light elements and from distortions in the cosmic microwave background. In the next chapter we therefore study the impact of these constraints on the different possible scenarios in gaugino mediation.

V. Dark Matter from Gaugino Mediation

The evidence for the existence of non-baryonic cold dark matter is compelling at all observed astrophysical scales.[1] Indirect observation of dark matter ranges from rotation curves of galaxies over signatures in the cosmic microwave background (CMB) to N body structure formation simulations. The cold dark matter density is known to lie in the $3\,\sigma$ range [84][2]

$$0.106 < \Omega_{\rm DM} h^2 < 0.123\ . \tag{V.1}$$

Here $\Omega_{\rm DM}$ is the average energy density in non-baryonic dark matter divided by the total critical density that would lead to a spatially flat universe, while h is the Hubble constant in units of 100 km sec^{-1} Mpc^{-1}. The observed value is $h^2 \sim 0.5$ with an error of order 10%. In addition, the distribution of dark matter can be inferred from weak gravitational lensing [85].

Despite the detailed knowledge about the distribution and amount of dark matter in our universe, the basic fact of being dark does not supply much information, and the nature of dark matter is still unknown. The fact, however, that it has a large non-baryonic component suggests that dark matter consists of elementary particles which do not belong to the field content of the Standard Model. Furthermore, the notion 'cold' means that during the time of structure formation these particles were non-relativistic, which implies that they cannot be too light. So what is dark matter most likely made of? The constraint 'cold non-baryonic' turns out not to be overly restrictive, so that there is no shortage of dark matter candidates. A particularly well motivated dark matter candidate, however, arises in R parity conserving supersymmetric theories. In such theories the lightest supersymmetric particle (LSP) is stable and cannot decay into Standard Model particles. Hence an electrically neutral LSP might account for cold dark matter.[3] In supersymmetric theories there are three obvious candidates: the lightest neutralino, the lightest sneutrino and the gravitino. However, the possibility of a sneutrino LSP making up the dark matter has been largely ruled out by direct searches [23, 24].

[1] There are alternative approaches trying to explain the observed phenomena which are usually interpreted as evidence for dark matter. The most prominent one assumes a deviation from the known laws of gravitation ('modified gravity'). However, a study of colliding galaxy clusters showed that even in a modified gravity setup, the majority of the mass must be some form of dark matter [83].

[2] The analysis (labeled "All Data − LYA") used the measurements of the CMB power spectrum (temperature and polarisation) by WMAP (3-year data) and other experiments, the SDSS and 2dF galaxy clustering analyses, the SDSS luminous red galaxy constraints on the acoustic peak, as well as the Gold and the SNLS supernovae samples.

[3] Even if the theory contains non-vanishing R parity violating couplings, the LSP can still account for dark matter if it is sufficiently long-lived (see e.g. [86]).

In the last chapter we found that varying the boundary conditions for the bulk Higgs fields at the GUT scale, several particles could potentially be the LSP. In addition to the gravitino, these candidates are the lightest neutralino and a scalar lepton, $\widetilde{\tau}$ or $\widetilde{\nu}$. Since a scalar lepton is excluded as LSP [23, 24], it can only be the next-to-lightest superparticle (NLSP) with the gravitino as LSP. This is consistent with the superparticle spectrum (cf. Figure IV.5) and the lower bound on the gravitino mass in gaugino mediation (cf. (IV.40)). With the constraints from Chapter 3 and from direct searches in mind, gaugino mediation seems to allow for four possible different scenarios: On the one hand we have the $\widetilde{G}$-$\widetilde{\tau}$ and the $\widetilde{G}$-$\widetilde{\nu}$ scenarios with $\widetilde{\tau}$ and $\widetilde{\nu}$ as NLSP, respectively. On the other hand we have the standard neutralino LSP scenario and in addition the $\widetilde{G}$-χ scenario with the neutralino being the NLSP. However, in Figures IV.1 and IV.4 we have not included cosmological constraints yet. Therefore, not all of the afore mentioned scenarios necessarily lead to a viable phenomenology. The most important cosmological constraints arise from the observed cold dark matter density as well as from the observed abundances of primordial light elements. The implementation of these constraints will be the main subject of this chapter.

Both, for the constraints from BBN as well as for those from the observed cold dark matter density, the abundance $Y_{\text{(N)LSP}}$ of the (N)LSP is essential. In the next section we will therefore briefly discuss how and under which assumptions the abundance can be calculated. This also gives the opportunity to familiarise the reader with some notation we will use in the remainder of this chapter.

1. The Thermal Relic Density

In the early universe, sparticles existed in thermal equilibrium with the ordinary Standard Model particles.[4] As the universe expanded and the temperature dropped, heavier sparticles could no longer be produced. They eventually annihilated or decayed into lighter supersymmetric particles. The lightest supersymmetric particles were stable and could only annihilate into Standard Model particles. However, these annihilation processes were efficient only, as long as the particle density was high enough. As the density decreased, the annihilation rate became smaller than the expansion rate of the universe. At this point, the interactions which maintained thermal equilibrium 'froze out' and the thermal relic density 'froze in'.

To understand the corresponding processes more quantitatively, one must follow the evolution of the particle's phase space distribution function $f(x,p)$.[5] This distribution function is governed by the Boltzmann equations (for details of the formalism see

[4] The only exception is the gravitino, which only reaches thermal equilibrium when the Goldstino component is sufficiently large, i.e. for very small masses. As there is a sizeable lower bound on the gravitino mass in gaugino mediation, the corresponding coupling is too small and the gravitino will reach thermal equilibrium only for ridiculously high temperatures.

[5] The particle number density n is obtained by integrating the phase space distribution function $f(x,p)$ over the momenta and summing the spin.

e.g. [87]). In general, the Boltzmann equations are a coupled set of partial differential equations for the phase space distributions of all species present. Fortunately, for many problems, this set reduces to one differential equation for the species of interest, while all other species will have equilibrium phase space distributions. In the following we will especially be interested in the number density of a species which is long-lived compared to the age of the universe when its interactions freeze out. In our scenario, this species can be the neutralino, the stau or the sneutrino, respectively. Note that the sleptons are sufficiently long-lived, because of the lower bound on the gravitino mass (cf. (V.18)). Before we write down the corresponding Boltzmann equation, we should note that the masses of the sleptons from different generations are almost degenerate in gaugino mediation. Furthermore, the lightest neutralino can also be quite close in mass. If the mass difference is of order T_f or smaller,[6] the heavier particles are thermally accessible and the heavier particles will be nearly as abundant as the relic species. This means that the relic abundance of e.g. the $\widetilde{\tau}_1$ is determined by not only its annihilation processes, but also by 'coannihilation' processes such as $\widetilde{\tau}_1\tilde{\mu}_1 \to \tau_1\mu_1$ [88].

Since all the heavier sparticles will finally decay into the LSP, the relevant quantity is the total number density of the i coannihilating particles, $n = \sum_i n_i$. For example, in the case that the lighter stau is the LSP, the sum is over all three coannihilating sleptons, $\widetilde{\tau}_1, \tilde{\mu}_1, \tilde{e}_1$ [89]. After some simplifying assumptions such as assuming a homogeneous and isotropic Friedmann-Robertson-Walker (FRW) universe, CP invariance and Maxwell-Boltzmann statistics, the Boltzmann equations can be brought into a simplified form, describing the time evolution of the particle number density n

$$\frac{dn}{dt} + 3Hn = -\sum_{i,j} \langle \sigma_{ij} v \rangle \left(n_i n_j - n_i^{\mathrm{eq}} n_j^{\mathrm{eq}} \right) , \tag{V.2}$$

where H is the Hubble parameter and $\langle \sigma_{ij} v \rangle$ is the thermally averaged annihilation cross section times the relative velocity v of particles i and j. More precisely σ_{ij} is the total annihilation cross section of $i + j \to X + X'$,

$$\sigma_{ij} = \sum_{X,X'} \sigma(i + j \to X + X') , \tag{V.3}$$

where X, X' denote the possible standard model particles. Furthermore, n_i^{eq} is the number density of species i at thermal equilibrium. The $3Hn$-term governs the expansion of the universe diluting the number density, while the right-hand side of (V.2) accounts for number changing processes. The dependence of the annihilation cross section on the temperature can be quite complicated, especially in the vicinity of a resonance [90].

In the absence of interactions, the number density evolves inversely proportional to the spatial volume, $n \sim R^{-3}$, where R is the scale factor. In order to scale out the effect of an expanding universe, one usually considers the evolution of the number of

[6] For particles which may potentially play the role of cold dark matter, the corresponding freeze out temperature is approximately $T_f \sim m/25$, with m the mass of the cold relic. The mass difference where coannihilations become important therefore corresponds to $\Delta m/m \lesssim 5\%$.

particles in a comoving volume. This can be realised by dividing the number density n by a quantity which is also constant per comoving volume. We will follow a standard convention[7] and use the entropy density $s = 2\pi^2 g_* T^3/45$ for this purpose, with g_* the relativistic degrees of freedom and T the temperature. The resulting variable

$$Y \equiv \frac{n}{s} \tag{V.4}$$

is called the abundance.

In general, the evolution equation (V.2) has to be solved numerically, since no closed-form solutions are known in the general case. We use micrOMEGAs 1.3.6 [91, 92] to calculate the abundance and the energy density of the (N)LSP. The code includes all possible coannihilation processes and care is taken to handle poles and thresholds. The input parameters are the soft supersymmetry breaking terms of the MSSM. As before we determine the superpartner spectrum with the help of SOFTSUSY 2.0.6 [69].[8]

Now that we know how to obtain the abundances of the (N)LSPs, we can turn to the cosmological constraints which result from the observed cold dark matter density and from primordial nucleosynthesis. Since the BBN constraints are rather complicated, and in part also a bit more ambiguous than the dark matter density constraint, we will briefly discuss the current status in the following.

2. BBN Constraints on the Abundance of NLSPs

Big Bang Nucleosynthesis (BBN) offers the deepest reliable probe of the early universe, as it is based on well-understood Standard Model physics. Given the baryon density of the universe, the reaction rates can be calculated in the standard cosmological setup. Predictions of the abundances of light elements synthesised during the BBN epoch are in good overall agreement with the abundances inferred from data. Therefore, the standard hot big bang cosmology is validated and any new physics is highly constrained, because the predicted abundances are highly sensitive to the cosmological scenario. Nevertheless it should be noted that at least for some of the observed abundances there are still sizeable uncertainties. This is because the abundances observed are not primordial, since stellar processes alter the ratios of the light elements. Therefore, systematic errors are an important and often dominant limitation to the precision with which primordial abundances can be inferred. Also it should be noted, that even in the standard BBN scenario there is some discrepancy between the BBN prediction and the observed abundance of

[7] Some authors also normalise with respect to the background photon number density $n_\gamma = 2\zeta(3)T^3/\pi^2$ with ζ the Riemann zeta function. In the era of interest, the two normalisations are related by $s \simeq 7 n_\gamma$.

[8] For the top quark pole mass, we use the latest best-fit value of 172.5 GeV [93]. In addition, we use $m_b(m_b) = 4.25\,\text{GeV}$ and $\alpha_s^{\text{SM }\overline{\text{MS}}}(M_Z) = 0.1187$, the default values of SOFTSUSY. Some other SM parameters are hard-coded in micrOMEGAs, $\alpha_{\text{em}}^{-1\,\text{SM }\overline{\text{MS}}}(M_Z) = 127.90896$, $G_F = 1.16637 \cdot 10^{-5}\,\text{GeV}^{-2}$, and $m_\tau = 1.777\,\text{GeV}$.

^{7}Li [94]. This might actually be a hint at some deviation from the concordance cosmology and despite considerable astrophysical uncertainties, there are many proposals to resolve this discrepancy by new physics.

Primordial nucleosynthesis starts about 1 s after the big bang at a temperature of about 0.7 MeV with the freeze out of neutrons from the thermal bath. Subsequently, all light elements are synthesised during the 'first three minutes'. In gaugino mediation it turns out that for gravitino dark matter the NLSP decays considerably after the start of big bang nucleosynthesis (cf. (V.18)). Since the decay products of these long-lived particles can alter the primordial light element abundances [80, 95, 96], this leads to constraints on the released energy in such NLSP decays. The effects of both electromagnetic and hadronic showers can be important, depending on the lifetime of the NLSP. To a good approximation the constraints can be quantified by upper bounds on the product

$$\xi_{\mathrm{em,had}} \equiv \epsilon_{\mathrm{em,had}} \cdot Y_{\mathrm{NLSP}} \,. \tag{V.5}$$

Here $\epsilon_{\mathrm{em,had}}$ is the average electromagnetic or hadronic energy emitted in a single NLSP decay and the abundance Y_{NLSP} is given as in (V.4) by the NLSP number density prior to decay divided by the total entropy density.

The calculations of the bounds on electromagnetic and hadronic energy release are rather involved and we will resort to existing results in the literature. The strength of these bounds strongly depends on the lifetime of the NLSP.

Lets first have a look at the effects of hadronic energy release. At early times ($t \lesssim 100$s) energetic hadrons lose their energy quite rapidly through electromagnetic interactions, so that the direct destruction of light elements is subdominant. They can, however, change the neutron to proton ratio via interconversion effects, which obviously also leads to a change of the light element abundances. At later times ($10^2\mathrm{s} \lesssim t \lesssim 10^7\mathrm{s}$), as the hadrons are not stopped efficiently anymore and mesons decay before they interact with the background nucleons, hadrodissociation processes become dominant.

We now turn to the effects of electromagnetic energy release. At early times high energy leptons and photons emitted by late-decaying particles are thermalised quickly through interactions with background particles. They initiate electromagnetic cascades and the initial energy is quickly converted into soft photons. The energy distribution of the resulting photons is highly suppressed for energies above the threshold for electron positron pair production, $E_\gamma \lesssim E_{\mathrm{max}}$. This maximal energy is inversely proportional to the background photon temperature [97]. Therefore constraints on electromagnetic energy release are negligible for early times ($t \lesssim 10^4$s) as the maximal photon energy is too small to destroy any light elements. At times around ($10^4\mathrm{s} \lesssim t \lesssim 10^6\mathrm{s}$) the maximal photon energy slightly increases and elements with very low binding energies can be destroyed. Here the main constraint is from the over-destruction of Deuterium. For later times ($t \gtrsim 10^7$s) the photon energy becomes large enough to photo-dissociate ^{4}He and even a small destruction rate becomes a significant production mechanism for D and ^{3}He. As can be seen in Figure V.1 there is a time between 10^6s and 10^7s where the overproduction and over-destruction of Deuterium cancels. Finally we should note

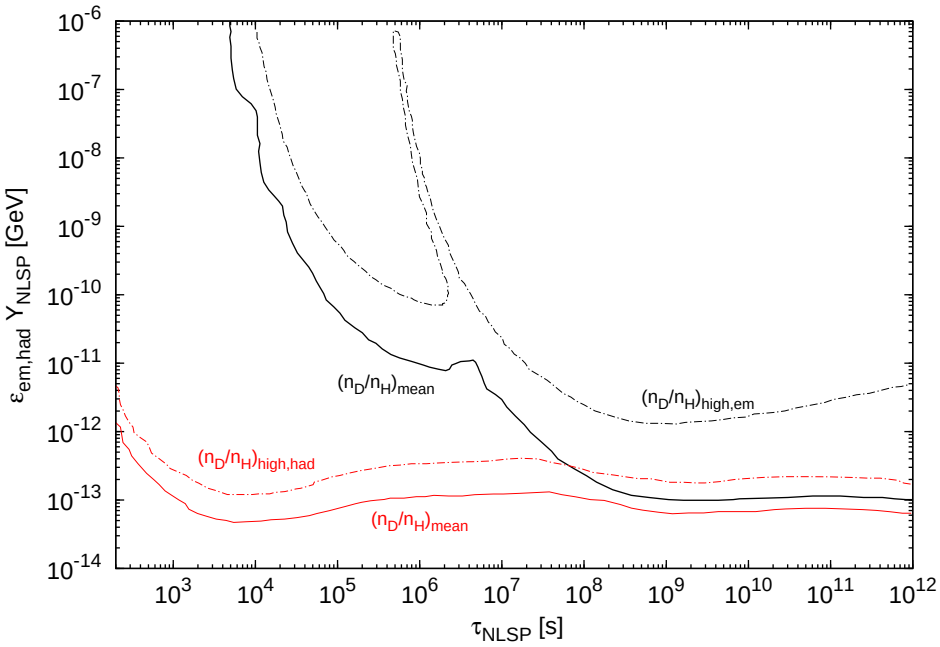

Figure V.1.: Upper limits on electromagnetic and hadronic energy release as a function of the NLSP lifetime, adapted from Figure 9 of [98]. The solid black and red lines give the severe electromagnetic and hadronic constraints resulting from the severe Deuterium bound (V.6). The corresponding dash-dotted lines result from the conservative constraints.

that the branching ratios for a charged NLSP decaying into photons or leptons is usually much larger than for the corresponding hadronic channels and therefore the constraint on electromagnetic energy release becomes dominant for late times.

For our analysis we use the bounds compiled in Figure V.1, which is adapted from Figure 9 of [98]. The bounds were computed in the earlier studies [80, 95]. As there is still considerable uncertainty in the measurements of the primordial element abundances, the author of [98] used two different data sets, giving "severe" and "conservative" limits. The observed abundances of ^{3}He, ^{6}Li and ^{7}Li are not used, since they still suffer from large systematic uncertainties. This leaves the observed abundances of D and ^{4}He as the only source for constraints from primordial nucleosynthesis. For our scenario with very long-lived NLSPs the bound from D is always stronger than the one from ^{4}He. Therefore we concentrate on bounds from Deuterium in the following. Figure V.1 shows the limits on electromagnetic and hadronic energy release as a function of the NLSP lifetime. All lines assume a baryon asymmetry of $\eta = 6.1 \cdot 10^{-10}$. The red solid and dash-dotted lines indicate the severe and conservative limits at the 95% confidence level (C.L.) for the electromagnetic energy release. The black solid and dash-dotted lines refer to severe and conservative constraints in the hadronic case. These bounds assume an NLSP mass of 1 TeV, but since they are quite insensitive to this mass, we will use them here, too. Furthermore, they assume that there is no entropy production between the decoupling of the NLSP and the start of BBN. Both the electromagnetic and hadronic severe limits

are derived from the 1σ interval [80]

$$2.40 \cdot 10^{-5} < (n_{\mathrm{D}}/n_{\mathrm{H}})_{\mathrm{mean}} < 3.22 \cdot 10^{-5} \,, \tag{V.6}$$

where n_{X} is a primordial number density. This range corresponds to the mean of the existing observations. The conservative limits were imported from two different analyses which use two different Deuterium bounds. In [80] the conservative limit for the hadronic case was derived from the highest value among these observations,

$$3.31 \cdot 10^{-5} < (n_{\mathrm{D}}/n_{\mathrm{H}})_{\mathrm{high,had}} < 4.57 \cdot 10^{-5} \qquad \text{had} \,, \tag{V.7}$$

whereas the conservative limit for the electromagnetic case used a more conservative observational bound, [95],

$$1.3 \cdot 10^{-5} < (n_{\mathrm{D}}/n_{\mathrm{H}})_{\mathrm{high,em}} < 5.3 \cdot 10^{-5} \qquad \text{em} \,, 2\sigma \tag{V.8}$$

Here the upper limit is considerably larger, because it is the 2σ upper bound of the highest value reliably observed. Note that although the upper bounds on the Deuterium abundance leading to the conservative and severe constraints differ by less than a factor of two, the resulting bounds on $\epsilon_{\mathrm{em}} Y_{\mathrm{NLSP}}$ differ by an order of magnitude. In general overproduction or destruction effects from electromagnetic and hadronic energy release can add constructively or destructively [99]. However, we assume the constraints on hadronic and electromagnetic energy release to be independent, since sizeable cancellations happen only in very special cases. We consider points in parameter space violating the conservative limits to be "excluded", but points violating only the severe limits to be "disfavoured".

We are now in a position to determine the cosmologically allowed, disfavoured and excluded regions of our parameter space. Note that the following discussion, though motivated by our six-dimensional orbifold model, again also applies to other theoretical setups which lead to the same boundary conditions at the GUT scale. Since moderate values of $\tan\beta$ are favoured in models with gaugino-mediated supersymmetry breaking, we consider the cases $\tan\beta = 10$ and $\tan\beta = 20$ as before. Furthermore, we use the same benchmark point as in Chapter IV given by $m_{1/2} = 500\,\mathrm{GeV}$ and sign $\mu > 0$. In the next section we will discuss neutralino dark matter and then turn to gravitino dark matter with slepton NLSPs in Section 4.

3. Neutralino Dark Matter

3.1. Calculation of the Abundance

We first consider the case where a neutralino is lighter than all sleptons and squarks, so that it is an LSP or NLSP candidate. In the corresponding parameter space region for

$\tan\beta = 20$, we find numerically

$$2.6 \cdot 10^{-13} \leq Y_\chi \leq 5.0 \cdot 10^{-12} \,, \tag{V.9a}$$
$$83.0\,\mathrm{GeV} \leq m_\chi \leq 204\,\mathrm{GeV} \,, \tag{V.9b}$$
$$8.15 \cdot 10^{-3} \leq \Omega_\chi h^2 \leq 0.273 \,. \tag{V.9c}$$

For $\tan\beta = 10$, the results are very similar, with a slightly larger maximal abundance of $8.7 \cdot 10^{-12}$. Here the relation between neutralino relic abundance Y_χ and energy density $\Omega_\chi h^2$ is given by

$$Y_\chi = \frac{\Omega_\chi \rho_c}{s\, m_\chi} \simeq 3.64 \cdot 10^{-11} \left(\frac{100\,\mathrm{GeV}}{m_\chi}\right) \Omega_\chi h^2 \,, \tag{V.10}$$

with ρ_c the critical density and s the entropy density of the universe. Note that in the region where the neutralino has its maximal abundance, the neutralino mass almost acquires its maximal value and hence the maximal energy density $\Omega_\chi^{\max} h^2$ is just slightly below $m_\chi^{\max} \cdot Y_\chi^{\max} \cdot s/\rho_c$. We now consider the cosmological constraints for the neutralino (N)LSP case. Let us first turn to the neutralino LSP scenario.

3.2. Neutralino LSP

Gaugino mediation provides only a lower bound on the mass of the gravitino. Therefore, it may well be quite heavy, and the lightest neutralino may be the LSP. In this case, decays of the long-lived gravitino threaten the success of BBN, which leads to an upper bound on the gravitino density and thus on the reheating temperature [80, 95]. Of course, this bound can be avoided if the gravitino is sufficiently heavy and therefore decays before the start of primordial nucleosynthesis. The other superparticles decay into the LSP before the start of BBN and do not cause problems, unless LSP and NLSP are nearly degenerate. For example, if the NLSP is a stau, BBN constraints become potentially important for $m_{\tilde\tau} - m_\chi \lesssim 100\,\mathrm{MeV}$ [100]. We neglect this possibility, since the corresponding region in the parameter space is tiny.

This leaves the observed cold dark matter density as the only constraint on the neutralino LSP scenario we have to consider. We use the 3σ range given in Equation (V.1). The upper limit excludes the white regions in Figure V.2. Since the dark matter could be made up of several components and since non-thermal production could be significant, we have two viable regions in parameter space. In the first one, the thermal neutralino relic density falls into the range (V.1) and hence this particle makes up all the dark matter. This region is shown in black in Figure V.2. There the bino contributes at least 75% (80%) to the lightest neutralino for $\tan\beta = 10$ ($\tan\beta = 20$). The missing 25% (20%) come from the two Higgsinos, while the wino component of $\sim 1\%$ is negligible. On the left edge the lightest neutralino is a pure bino. The second viable region is shown in magenta (dark-gray) in the figure. Here the thermal neutralino density is smaller than the lower bound in Eq. (V.1) and hence only constitutes a part of the dark

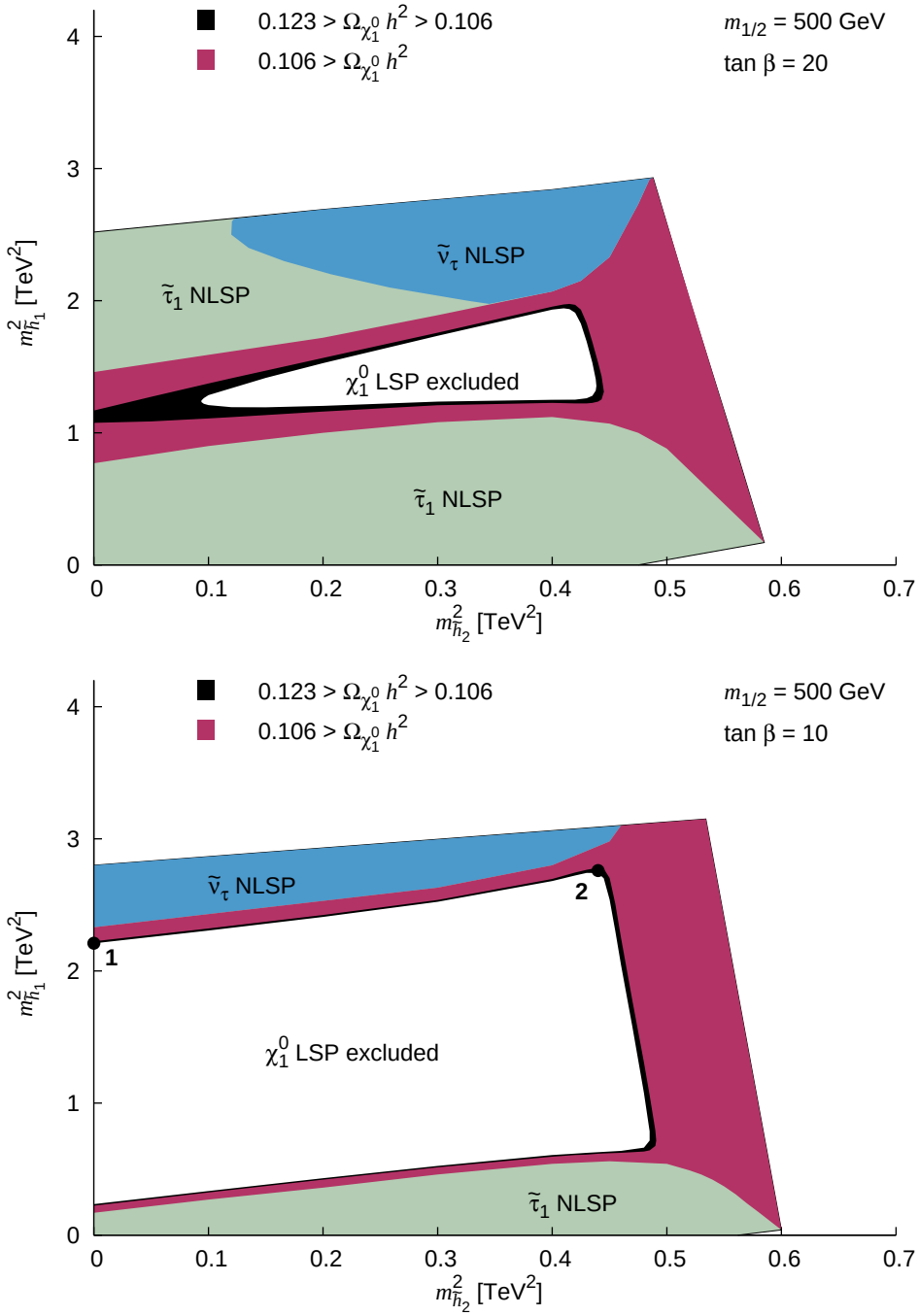

Figure V.2.: Allowed region for the soft Higgs masses for $m_{1/2} = 500\,\text{GeV}$ and $\tan\beta = 20$ ($\tan\beta = 10$). A neutralino is lighter than all sleptons in the white, black and magenta (dark-gray) area. The upper limit on $\Omega_\chi h^2$ excludes the white region, whereas in the magenta (dark-gray) area $\Omega_\chi h^2$ is smaller than the observed cold dark matter density. The correct dark matter density is obtained in the black region. In the green (light-gray) and blue (medium-gray) areas a slepton is the NLSP. For the points 1 and 2 the spin-independent cross-sections per nucleon are given in the text.

matter density. The lightest neutralino is almost a pure Higgsino at the right edge of the parameter space.

In most parts of the parameter space, some tuning is necessary if neutralinos are to make up all the dark matter. This is very similar to what has been found in other scenarios for SUSY breaking, for instance in mSUGRA (see for example [101–103]). In part, the reason is simply that the dark matter density has been measured rather accurately. For $\tan\beta = 20$ and small $m_{\tilde{h}_2}^2$, the situation looks somewhat better. Apparently, for $m_{\tilde{h}_2}^2 < 0.1\,\mathrm{TeV}^2$ the maximum of Ω_χ as a function of $m_{\tilde{h}_1}^2$ lies in the experimentally allowed region. Around the maximum, a change in $m_{\tilde{h}_1}^2$ leads only to a relatively small change in Ω_χ, so that the energy density remains in the favoured range in a rather broad strip of parameter space. For larger $m_{\tilde{h}_2}^2$, the maximum value of Ω_χ is too large. Consequently, it depends rather sensitively on $m_{\tilde{h}_1}^2$ in the allowed region, and thus this region is narrow.

Discovery Potential

Before we come to the case of a neutralino NLSP let us finally comment on the prospects of the detection of neutralino dark matter in our scenario. In direct detection experiments, the interactions of neutralinos with matter are searched for, e.g. by recording the recoil energy of nuclei, as neutralinos scatter off them when they pass through the earth. The necessary parameters for the calculation of the corresponding signal in the detector are the density and velocity distributions of the neutralinos as well as the neutralino-nucleon scattering cross-section. However, the halo of our galaxy is subject to considerable uncertainties in overall size, velocity and lumpiness, so that even if the Lagrangian parameters were known exactly, the signal rates would still be quite indefinite. Nevertheless, the knowledge of the neutralino-nucleon cross-section is very important to estimate the discovery potential for neutralinos. This cross-section also determines the rate at which neutralinos accrete into the earth and sun, which is important for indirect detection scenarios, where energetic neutrinos from neutralino annihilations are searched for [104].

At the parton level, the neutralino can interact with a quark by exchange of squarks in the s-channel, or Higgs scalars or a Z boson in the t-channel (see e.g. [104]). As in the general MSSM case, the detection cross-section is suppressed for a pure bino, since the Higgs and Z exchange require a Higgsino component. In fact, for $\tan\beta = 10$, $m_{\tilde{h}_1}^2 = 2.21\,\mathrm{TeV}^2$ and $m_{\tilde{h}_2}^2 = 0$ (point 1 in Figure V.2), one obtains $\sigma_{\chi p,n} = 9 \cdot 10^{-13}\,\mathrm{nb}$ for the spin-independent cross-section per nucleon [105], whereas the present bound on this cross-section is of the order of $10^{-9}\,\mathrm{nb}$ [106]. The cross-section is larger in the region with a larger Higgsino component, where for $\tan\beta = 10$, $m_{\tilde{h}_1}^2 = 2.76\,\mathrm{TeV}^2$, $m_{\tilde{h}_2}^2 = 0.44\,\mathrm{TeV}^2$ (point 2 in Figure V.2), one obtains $\sigma_{\chi p,n} = 4 \cdot 10^{-11}\,\mathrm{nb}$ [105]. Although the cross-section is at least one order of magnitude below the present bounds, it could be reached by the next generation of dark matter experiments [107].

3.3. Neutralino NLSP

With a light gravitino, a scenario with a gravitino LSP and a neutralino NLSP is possible, too. However, it turns out that this is ruled out by the BBN constraints in our scenario. We noticed in the last chapter that gaugino mediation gives a lower bound on the gravitino mass. In general this bound depends on $m_{1/2}$, the number of space-time dimensions and the compactification scale [22]. Motivated by our six-dimensional orbifold GUT, we chose $D = 6$ and $M_C = M_{\rm GUT}$ leading to $m_{3/2} \gtrsim 0.1 \cdot m_{1/2} \gtrsim 50\,\text{GeV}$. As the lower limit on $m_{3/2}$ was derived using naïve dimensional analysis, it can well be relaxed by a factor of order one. We therefore also consider $m_{3/2} = 10\,\text{GeV}$ as a conservative lower bound. Note that varying D between 5 and 10, the lower bound ranges between 20 GeV and 0.1 GeV.

The region where $m_\chi > m_{3/2} + m_Z$ is certainly excluded by the hadronic BBN constraints for all gravitino masses we consider, since the two-body decay $\chi_1^0 \to Z\widetilde{G}$ is possible and since the hadronic branching ratio of the Z is large, $B_{\rm had}^Z \sim 0.7$ [33, 81]. However, the situation is less clear for lighter neutralinos when the two-body decay into real Z bosons is kinematically forbidden. For $m_{3/2} = 50\,\text{GeV}$, this is the case for $m_\chi < 141\,\text{GeV}$. The corresponding parameter space region lies at the right end of the allowed region, where $m_{\tilde{h}_2}^2 \gtrsim 0.5\,\text{TeV}^2$. In this region, the μ parameter is rather small [36], so that there is significant mixing between the neutralinos. The Higgsino components of the lightest neutralino lead to a relatively large annihilation cross section and thus to a relatively small abundance. From Figure V.1 we can read off that the severe hadronic bound is never stronger than

$$\epsilon_{\rm had} Y_{\rm NLSP} \lesssim 5 \cdot 10^{-14}\,\text{GeV} \tag{V.11}$$

for any NLSP lifetime. The three-body decay $\chi_1^0 \to q\bar{q}\widetilde{G}$ through a virtual photon gives the leading contribution to the hadronic decay mode when the two-body decay is not allowed. With the estimate $\epsilon_{\rm had}^\chi \simeq \frac{2}{3}(m_\chi - m_{3/2}) \cdot 10^{-3}$ from [33], we find

$$1.0 \cdot 10^{-14}\,\text{GeV} \leq \epsilon_{\rm had}^\chi Y_\chi \leq 2.1 \cdot 10^{-14}\,\text{GeV}\ , \tag{V.12}$$

which is well below even the stringent hadronic bound (V.11). Ergo, there are no BBN constraints from hadronic energy release, but how does the situation look like in the electromagnetic case?

Considering the electromagnetic decay, the main contribution comes from the two-body decay $\chi_1^0 \to \gamma\widetilde{G}$. The corresponding average electromagnetic energy release is simply given by

$$\epsilon_{\rm em}^\chi \simeq \frac{m_\chi^2 - m_{3/2}^2}{2m_\chi} \tag{V.13}$$

and the width of the corresponding neutralino decay mode which fixes the neutralino NLSP lifetime can be written as [33]

$$\Gamma_\chi = \frac{|N_{11}\cos\theta_W + N_{12}\sin\theta_W|^2\, m_\chi^5}{48\pi\, m_{3/2}^2 M_{\rm P}^2} \left(1 - \frac{m_{3/2}^2}{m_\chi^2}\right)^3 \left(1 + 3\frac{m_{3/2}^2}{m_\chi^2}\right). \tag{V.14}$$

Here χ is a mixture of all different gauge eigenstates, $\chi \equiv N_{11}(-i\widetilde{B}) + N_{12}(-i\widetilde{W}) + N_{13}\widetilde{H}_d + N_{14}\widetilde{H}_u$, where the N_{1i} are elements of the neutralino mixing matrix, so that e.g. $|N_{11}|^2$ is the bino fraction. Applying these equations to our scenario we obtain

$$1.1 \cdot 10^{-11}\,\mathrm{GeV} \leq \epsilon_{\mathrm{em}}^{\chi} Y_{\chi} \leq 2.2 \cdot 10^{-11}\,\mathrm{GeV}\ , \tag{V.15}$$

$$3.3 \cdot 10^{8}\,\mathrm{s} \leq \tau_{\chi} \leq 4.1 \cdot 10^{10}\,\mathrm{s} \tag{V.16}$$

for both $\tan\beta = 10$ and $\tan\beta = 20$. The lifetimes here are rather long because we only consider neutralino masses below 141 GeV since otherwise the hadronic constraints are badly violated. As mentioned above in the region where the neutralino becomes this light it is predominantly a Higgsino and therefore gives only a small contribution to the neutralino width (V.14). Comparing with the electromagnetic limits in Figure V.1, we see that even the conservative BBN bound is violated. This result remains true for $m_{3/2} = 10\,\mathrm{GeV}$. Thus, we conclude that a neutralino NLSP with a mass below $m_Z + m_{3/2}$ is excluded by the BBN constraints on electromagnetic energy release. Consequently, the lightest neutralino is not a viable NLSP candidate in gaugino mediation.

4. Gravitino Dark Matter with Slepton NLSPs

4.1. Lifetime of Slepton NLSPs

The couplings between the gravitino and the MSSM particles are highly suppressed. Therefore, in the case of gravitino dark matter, the NLSP is typically long-lived. The mass eigenstates of the slepton NLSPs are in general a mixture of a left- and a right-handed part, $\tilde{\ell} = \cos\theta_\ell\,\tilde{\ell}_R + \sin\theta_\ell\,\tilde{\ell}_L$. The slepton decay rate however is dominated by the two-body decay into lepton and gravitino $\tilde{l}_{R,L} \to l_{R,L}\widetilde{G}$

$$\Gamma_{\tilde{l}}^{\text{2-body}} = \frac{m_{\tilde{l}}^5}{48\pi\, m_{3/2}^2\, M_{\mathrm{P}}^2}\left(1 - \frac{m_{3/2}^2}{m_{\tilde{l}}^2}\right)^4\ , \tag{V.17}$$

which is independent of the mixture. Here $m_{\tilde{l}}$ is the slepton mass, $M_{\mathrm{P}} = 2.4 \cdot 10^{18}\,\mathrm{GeV}$ is the reduced Planck mass, and the lepton mass has been neglected. With a typical largest slepton mass of around 200 GeV in the $\tilde{l}$ NLSP region and the smallest gravitino mass of 10 GeV this leads to a lower bound on the slepton lifetime of

$$\tau_{\tilde{l}} \gtrsim 1.8 \cdot 10^{5}\,\mathrm{s}\ , \tag{V.18}$$

which is a time where also the electromagnetic BBN constraints become stringent (cf. Figure V.1).

4.2. Stau NLSP

The $\widetilde{G}$-$\widetilde{\tau}$ scenario is particularly interesting, since it may allow to determine the gravitino mass and spin at colliders [25–30]. It is well known, however, to be strongly constrained

by primordial nucleosynthesis (BBN) [31–35]. In this section we therefore study the impact of such constraints on the $\widetilde{G}$-$\widetilde{\tau}$ scenario in gaugino mediation. As before the crucial quantity in calculating these constraints is the relic stau abundance.

Relic Stau Abundance

For both values of $\tan\beta$, imposing the lower bound from collider searches [24], we find that the stau mass varies between

$$86\,\mathrm{GeV} < m_{\widetilde{\tau}} \leq 203\,\mathrm{GeV} \tag{V.19}$$

in the $\widetilde{\tau}$ NLSP region. The upper limit on the stau mass within this region only depends on the mass of the lightest neutralino at the boundary between the two NLSP regions and is therefore almost independent of $\tan\beta$. With the gravitino masses $m_{3/2} = 50\,\mathrm{GeV}$and $m_{3/2} = 10\,\mathrm{GeV}$, this mass range corresponds to the range

$$\begin{aligned} 5.5 \cdot 10^6\,\mathrm{s} \leq \tau_{\widetilde{\tau}} \leq 1.6 \cdot 10^9\,\mathrm{s} \quad m_{3/2} = 50\,\mathrm{GeV} \\ 1.7 \cdot 10^5\,\mathrm{s} \leq \tau_{\widetilde{\tau}} \leq 1.3 \cdot 10^7\,\mathrm{s} \quad m_{3/2} = 10\,\mathrm{GeV} \end{aligned} \tag{V.20}$$

for the lifetimes. If we restrict ourselves to stau masses above $100\,\mathrm{GeV}$, the upper bound is lowered to $4.6 \cdot 10^8\,\mathrm{s}$ and $6.1 \cdot 10^6\,\mathrm{s}$ respectively.

The stau abundance in the $\widetilde{G}$-$\widetilde{\tau}$ scenario is shown in Figure V.3. For $\tan\beta = 20$ we find

$$1.3 \cdot 10^{-13} \leq Y_{\widetilde{\tau}} \leq 6.2 \cdot 10^{-13}\ . \tag{V.21}$$

The abundance is smallest in those parts of the parameter space where the lightest stau masses are reached. These are the lower right corner of the bottom region and the upper border of the upper region. Conversely, we find the largest values close to the neutralino NLSP region, where $m_{\widetilde{\tau}}$ is largest. Both qualitatively and quantitatively, the situation is very similar for $\tan\beta = 10$, except that in this case the top $\widetilde{\tau}$ NLSP region does not exist. The approximation

$$Y_{\widetilde{\tau}} \simeq 1.2 \cdot 10^{-13} \left(\frac{m_{\widetilde{\tau}}}{100\,\mathrm{GeV}}\right) \tag{V.22}$$

gives the stau abundance with a relative error of less than 10% for the largest part ($> 80\%$) of the parameter space, where coannihilation with the neutralino is less important (i.e. the part not too close to the neutralino LSP region). However, the first two generation sleptons are always close in mass to the stau, therefore we also have coannihilation with them. Although these coannihilation processes reduce the abundance of each lighter charged slepton species ($\tilde{e}, \tilde{\mu}$), the net abundance of staus becomes larger since each lighter selectron or smuon will finally decay into a stau NLSP. Therefore our approximation (V.22) gives a yield which is a factor two larger than the one given in [33]. For the left-handed sleptons this increase is even more pronounced. Usually

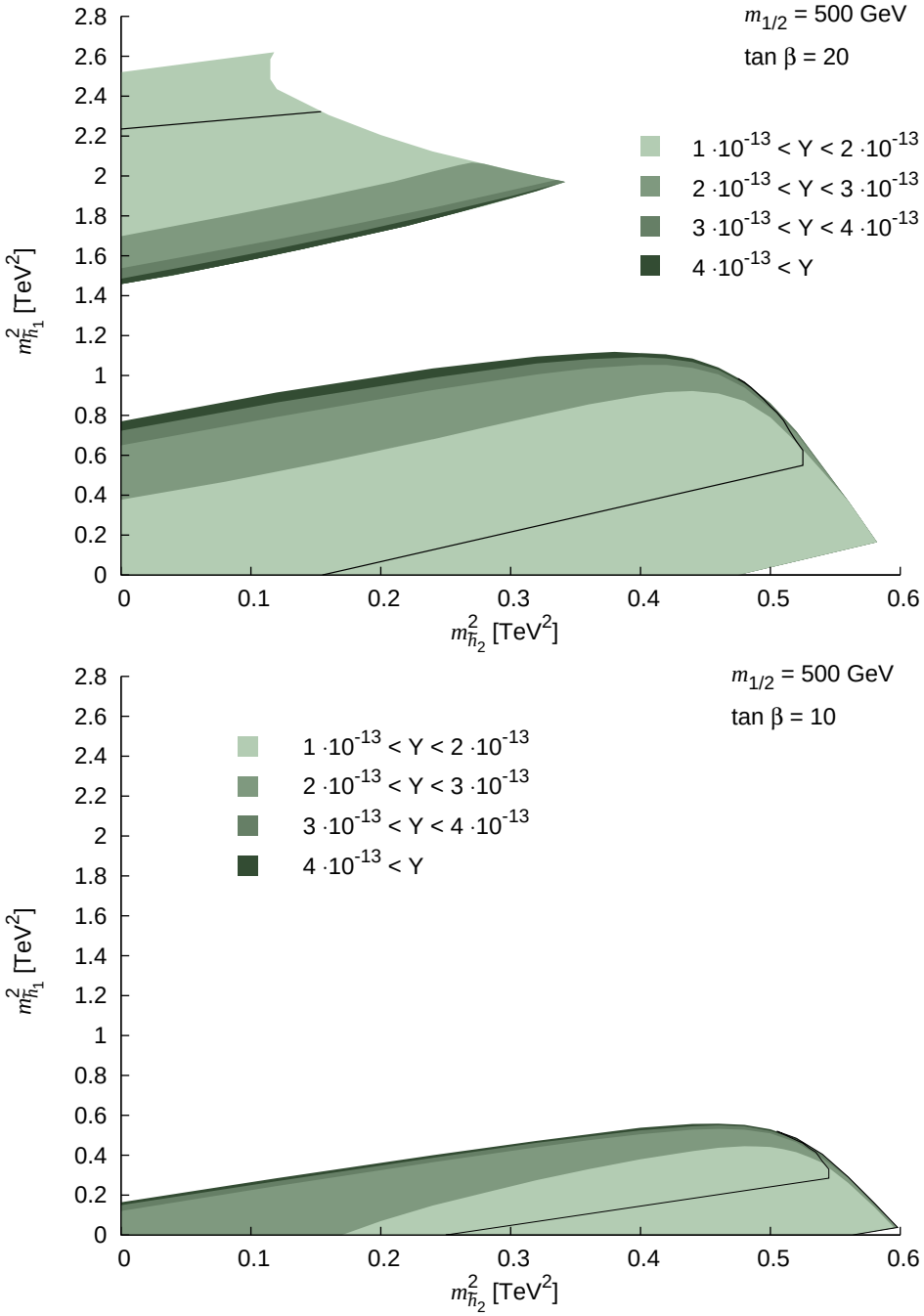

Figure V.3.: Stau abundance obtained numerically with micrOMEGAs in the $\widetilde{\tau}$ NLSP region. The area below (lower region) and above (upper region, in the case of $\tan\beta = 10$ non existing) the black line is excluded by the conservative electromagnetic BBN constraints for $m_{3/2} = 50\,\text{GeV}$ and $\epsilon_{\text{em}} = 0.5E_\tau$.

the abundance for left-handed sleptons is much less than for right-handed ones, because they have a larger annihilation cross-section. However, in our setup this turns out not to be the case and the abundance is as large as for the right-handed fields as can be seen in Figure V.3.

Constraints from BBN

We have seen in the last section that there are regions in parameterspace where the stau is extremely long-lived. Therefore these regions are subject to the very restrictive BBN constraints at late times.

Turning to the hadronic constraints first, we see that they are not overly restrictive in this case. The two-body decay $\widetilde{\tau} \to \tau \widetilde{G}$ gives no contribution to the hadronic energy release, although the emitted tau is unstable and decays partly into mesons. But since their electromagnetic interaction time is significantly shorter than their hadronic one, these mesons basically transfer all their kinetic energy into electromagnetic showers [108]. Furthermore, in our range of stau lifetimes, the stopped mesons finally decay before they induce interconversion effects. Therefore the leading hadronic constraints for late times are governed by three- and four-body decays. The three-body decays $\widetilde{\tau} \to \tau Z \widetilde{G},\ \nu W \widetilde{G}$ produce hadronic energy when the Z or W boson decays hadronically. When the three-body decay is kinematically forbidden, the four-body decay $\widetilde{\tau} \to \tau\, q\, \bar{q}\, \widetilde{G}$ may become important, although this radiative decay producing $q\bar{q}$ pairs via an intermediate gauge boson has only a small branching ratio. In order to obtain the hadronic energy release, the branching ratio as well as the energy spectrum of the emitted hadrons has to be calculated. The corresponding calculations for a right-handed stau with a bino as lightest neutralino have been performed in [98]. The result relevant for us is that the corresponding average hadronic energy release ϵ_{had} never exceeds $2 \cdot 10^{-3}\,\mathrm{GeV}$ for stau masses around $200\,\mathrm{GeV}$ [98]. Combining this bound with our result for the stau abundance we see that

$$\widetilde{\tau}_R: \quad \epsilon_{\mathrm{had}} Y_{\widetilde{\tau}} \lesssim 2 \cdot 10^{-15}\,\mathrm{GeV}\ , \tag{V.23}$$

so that even the stringent hadronic BBN bound (V.11) is easily satisfied in the case of the right-handed stau. We can directly apply this result to the case of $\tan\beta = 10$, where the stau is predominantly right-handed in the region where it is the NLSP and also to the lower region of the $\tan\beta = 20$ parameterspace (cf. Figures IV.1 and IV.4). However, in the upper region the stau is mainly left-handed, which generally leads to a larger hadronic branching ratio and therefore to stronger constraints. Unfortunately there is no calculation of the hadronic branching ratio for left-handed staus. This scenario is more complicated than the right-handed case, since also the W boson can be exchanged and more final states are possible. However, as we are a factor twenty below the severe hadronic constraint for the right-handed stau, we don't expect the bound to be violated even in the left-handed case. Furthermore, since the hadronic constraints are almost independent of the NLSP lifetime, the severe hadronic bound could be marginally

relevant only in the small region close to the neutralino LSP, where coannihilations lead to a much larger abundance of staus (cf. Figure V.3).

The electromagnetic bounds are significantly more constraining. In this case the two-body decay $\widetilde{\tau} \to \tau \widetilde{G}$ gives a large contribution. The energy of the τ produced in this decay is given by

$$E_\tau = \frac{m_{\widetilde{\tau}}^2 - m_{3/2}^2 + m_\tau^2}{2m_{\widetilde{\tau}}} \,. \tag{V.24}$$

Although the tau has a time-delated lifetime, it does not scatter off the background plasma before its decay and not the full initial tau energy ends up in an electromagnetic shower. This is because there will be always at least one neutrino emitted in the tau decay which carries away a sizable fraction of the energy [31]. To account for this energy loss, the electromagnetic energy release can be written as

$$\epsilon_{\mathrm{em}} = x E_\tau \,, \tag{V.25}$$

with $0.3 \leq x \leq 1$ the fraction of the initial tau energy which ends up in an electromagnetic shower. The precise value of x is in principle calculable, once the chirality and mass of the decaying stau as well as the gravitino mass is specified. However, as the variation in x is relatively small compared to other effects, we will simply assume $x = 0.5$ in the following. Combining again the average energy release ϵ_{em} with the abundance $Y_{\widetilde{\tau}}$ and scanning over the parameter space of gaugino mediation we find for $\tan\beta = 20$

$$1.9 \cdot 10^{-12}\,\mathrm{GeV} \leq \epsilon_{\mathrm{em}} Y_{\widetilde{\tau}} \leq 3.0 \cdot 10^{-11}\,\mathrm{GeV} \,. \tag{V.26}$$

The results for $\tan\beta = 10$ fall into the same range, but with a slightly smaller spread. In Figure V.4, we plot points from the $\widetilde{\tau}$ NLSP region for $\tan\beta = 10$ in the $\epsilon_{\mathrm{em}} Y_{\widetilde{\tau}} - \tau_{\widetilde{\tau}}$ plane. We also show the severe and conservative electromagnetic BBN constraints from Figure V.1. The red (dark-gray) points are the results for a gravitino mass of 50 GeV. We find that the severe constraints are always violated, while the conservative constraints can be satisfied. The same can be seen from Figure V.3 for the case of $\tan\beta = 20$, where the solid black lines mark the boundary between the parameter space regions allowed and excluded by the conservative BBN bounds. In the lower region, the area below and to the right of the line is excluded. In the upper region, this is the case for the area above the black line. Thus, it turns out that actually the largest part of the parameter space is allowed. The remaining part is typically excluded not because of an unusually large stau abundance but because of a too long lifetime due to a relatively small stau mass.

The severe BBN bounds can be satisfied, if the NLSP lifetime is shorter. This is the case for smaller gravitino masses. For $m_{3/2} = 10\,\mathrm{GeV}$, we see from the green (light-gray) points in Figure V.4 that large parts of the stau NLSP region are allowed by the severe constraints. The conservative constraints are always satisfied in this example.

The motivation for our benchmark gaugino mass of $m_{1/2} = 500\,\mathrm{GeV}$ was that this results in the lightest superparticle mass spectrum compatible with the LEP bound on

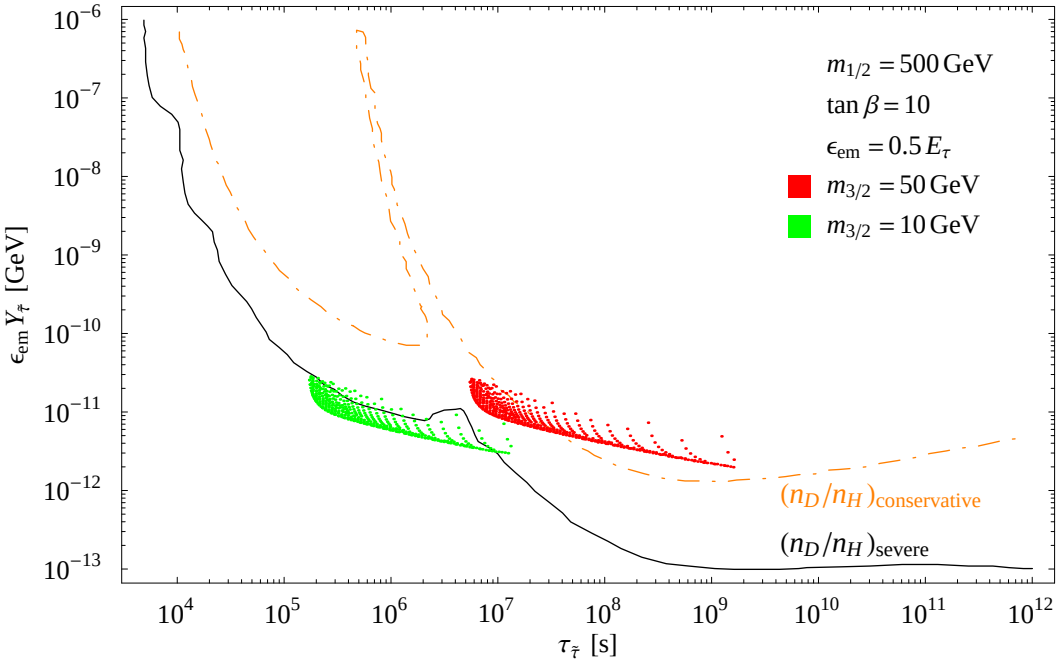

Figure V.4.: Points from the $\widetilde{\tau}$ NLSP region ($\tan\beta = 10$) in the $\epsilon_{\mathrm{em}} Y_{\widetilde{\tau}} - \tau_{\widetilde{\tau}}$ plane for $x = 0.5$ and $m_{1/2} = 500\,\mathrm{GeV}$, obtained by scanning over $m^2_{\tilde{h}_1}$ and $m^2_{\tilde{h}_2}$ with a step size of $5 \cdot 10^{-3}\,\mathrm{TeV}^2$ in both parameters. We show the results for two values of the gravitino mass, $m_{3/2} = 50\,\mathrm{GeV}$ (red or dark-gray) and $m_{3/2} = 10\,\mathrm{GeV}$ (green or light-gray). The solid black and dash-dotted orange lines show the severe and conservative electromagnetic BBN constraints from Figure 9 of [98]. (Only the constraints derived from the Deuterium abundance are shown, since those from the ^{4}He abundance are not relevant in the $\widetilde{\tau}$ NLSP region.)

the Higgs mass. Increasing the unified gaugino mass $m_{1/2}$ leads essentially to a rescaling of the superparticle spectrum. Since the NLSPs become heavier, their yield is larger. As an example, let us consider $m_{1/2} = 1\,\text{TeV}$ and $m_{3/2} = 100\,\text{GeV}$. Here the gravitino mass obviously corresponds to the NDA bound $m_{3/2} \gtrsim 0.1 \cdot m_{1/2}$ again. For $\tan\beta = 10$ this leads to

$$2.8 \cdot 10^{-13} < Y_{\widetilde{\tau}} \leq 1.1 \cdot 10^{-12} \,, \tag{V.27}$$

$$1.0 \cdot 10^{-11}\,\text{GeV} < \epsilon_{\text{em}} Y_{\widetilde{\tau}} < 1.1 \cdot 10^{-10}\,\text{GeV} \,. \tag{V.28}$$

As before, the estimate (V.22) works pretty well, so that $Y_{\widetilde{\tau}}$ and $\epsilon_{\text{em}} Y_{\widetilde{\tau}}$ grow by about a factor of two and four, respectively. On the other hand, the upper bound on the stau lifetime decreases significantly, since it depends on $m_{\tilde{l}}^{-5} m_{3/2}^2$,

$$5.5 \cdot 10^5\,\text{s} < \tau_{\widetilde{\tau}} < 5.7 \cdot 10^7\,\text{s} \,. \tag{V.29}$$

As a consequence, a larger part of the $\widetilde{\tau}$ NLSP region is compatible with the electromagnetic BBN constraints. However, the hadronic constraints become more severe, since the hadronic branching ratio of the NLSP strongly depends on the mass difference to the LSP. As the stau mass increases from 100 GeV to 1 TeV, also the branching ratio increases by an order of magnitude [98]. Nevertheless the hadronic constraints are still easily satisfied unless the stau mass is close to a TeV.

Catalysed BBN

Recently it has been argued that metastable charged particles might form bound states with positively charged nuclei [109–112]. This effect potentially modifies the nuclear reaction rates during the time of primordial nucleosynthesis. In particular the process $(^4\text{He}X^-) + \text{D} \rightarrow {}^6\text{Li} + X^-$ can lead to an enhanced production of ^{6}Li, which can be orders of magnitude above the observed value. Therefore this scenario could lead to significantly more restrictive constraints on the allowed relic abundance of these charged particles than those we considered here. In [113] bound-state effects in the CMSSM and mSUGRA are studied. The conclusion is reached that $\widetilde{\tau}$ NLSPs with lifetimes longer than $10^3 - 10^4$ s are excluded. If it turns out that this statement also holds in a more general framework than the CMSSM, the $\widetilde{G}$-$\widetilde{\tau}$ scenario will be ruled out for $m_{3/2} \gtrsim 10\,\text{GeV}$ unless there is sizeable entropy production between the decoupling of the staus from the thermal bath and the start of BBN [114]. Another possibility which leads to shorter stau lifetimes and therefore evades this constraint is to allow for small R-parity violating couplings [86].

4.3. Sneutrino NLSP

The region where the sneutrino becomes the NLSP corresponds to a large down-type soft Higgs mass $m_{\tilde{h}_1}^2$ (cf. Figures IV.1 and IV.4). The sneutrino masses and lifetimes lie roughly in the same range as those of the staus, but with a somewhat larger minimal

mass. We find that the relic abundance for both $\tan\beta = 10$ and $\tan\beta = 20$ lies within the narrow window

$$1.3 \cdot 10^{-13} \leq Y_{\tilde{\nu}} \leq 4.6 \cdot 10^{-13} \ , \tag{V.30}$$

which is almost the same range as in the case of the stau NLSP. However, we expect that here the constraints from BBN are drastically relaxed in comparison to a charged NLSP.

Indeed, the BBN bounds on a sneutrino NLSP turn out to be rather weak, since the neutrinos emitted in the dominant two-body decay $\tilde{\nu} \to \nu\widetilde{G}$ interact much less with the light nuclei than charged particles. Nevertheless, the very energetic neutrinos may scatter off the background leptons via the weak interactions, leading to the pair production of several kinds of particles. Most of these particles induce only electromagnetic cascades, but processes like $\nu\bar{\nu}_{\mathrm{BG}} \to \pi^+\pi^-$ also provide pions, which in principle could induce processes like $\pi^+ n \to \pi^0 p$. However, as discussed before, interconversion effects are negligible at late times. The electromagnetic effects of the highly energetic neutrinos emitted in the two-body decay could potentially have a more severe effect on the light element abundances. For example the anti-neutrinos (neutrinos) produced in such a decay can annihilate with the background neutrinos (anti-neutrinos) and give rise to e^+e^- pairs which contribute to electromagnetic showers. The effects of highly energetic (anti-)neutrinos on BBN have been studied in [115, 116] and [117], but in the last reference only for the specific case of an unstable gravitino decaying into sneutrino and neutrino. Assuming $(n_{\mathrm{D}} + n_{^3\mathrm{He}})/n_{\mathrm{H}} \lesssim 4 \cdot 10^{-5}$ gives $Y_X \lesssim 4 \cdot 10^{-12}$ [116] for a general relic with mass around 200 GeV and lifetime 10^7 s decaying equally into neutrinos and anti-neutrinos. Shorter lifetimes are not discussed in this work, but according to [115] all constraints disappear for lifetimes shorter than 10^6 s, since at those earlier times high-energy photons thermalise efficiently scattering off the CMB before having the chance to interact with the light nuclei. Also the limits relax for longer lifetimes, since the density of background neutrinos becomes more diluted. The maximal abundance (V.30) is an order of magnitude below the limit of [116]. Therefore there are no restrictions on our parameterspace from energy released in the 2-body decay.

Nevertheless there could be constraints from three and four-body decay processes. For the electromagnetic case we have $\tilde{\nu} \to \nu\widetilde{G}\ell\bar{\ell}$, but as for the case of the $\tilde{\tau}$ NLSP, such a radiative decay producing $\ell\bar{\ell}$ pairs via an intermediate gauge boson has only a small branching ratio giving ϵ_{em} safely below 0.1 GeV. Therefore the effects of this decay channel is negligible even for our maximal value of $Y_{\tilde{\nu}}$.

This leaves the suppressed hadronic four-body decay $\tilde{\nu} \to \nu\widetilde{G}q\bar{q}$ as the only possible source for non-negligible constraints in our setup. Indeed, a recent analysis [118] found that despite the small branching ratio, the most stringent constraints on the sneutrino abundance is given by this process. For the case of a thermal relic density and $m_{3/2} = 50$ GeV the authors of [118] give an upper bound from Deuterium on the sneutrino mass of ~ 400 GeV. However, on the one hand they use an approximate expression similar to (V.22) to compute the sneutrino abundance, which always underestimates it in our

case, due to the importance of coannihilations. On the other hand the Deuterium bound they use is even more constraining than our severe bound. In their analysis the authors of [118] also show the hadronic branching ratios in the $m_{3/2} - m_{\widetilde{\nu}}$ plane. We can read off that for gravitino masses between 10 and 50 GeV and a sneutrino mass of 200 GeV the hadronic branching ratio is $B_{\rm had} \lesssim 10^{-4}$. Using this information to derive a strict upper bound on the maximal hadronic energy release in the sneutrino NLSP region we obtain

$$\epsilon_{\rm had} \cdot Y_{\widetilde{\nu}} \;<\; B_{\rm had} \cdot (m_{\widetilde{\nu}}^{\rm max} - m_{3/2}) \cdot Y_{\widetilde{\nu}}^{\rm max} \;\sim\; 10^{-14}\,{\rm GeV}\ . \tag{V.31}$$

Of course we made a rather cruel simplification here, since by far not all of the sneutrino energy ends up in the hadronic shower. Rather we would have to calculate the energy spectrum of the emitted quark-antiquark pairs. Taking this into account can lead to a large deviation from our rough approximation. Nevertheless our estimate is sufficient to see that at our benchmark point the hadronic energy release is well below the severe hadronic bound. For larger gaugino masses the hadronic energy release becomes more constraining. This is because the hadronic branching ratio increases fast with the sneutrino mass [118].

All in all, we can conclude that the $\widetilde{G}$-$\widetilde{\nu}$ scenario is essentially unconstrained. The severe hadronic limits could be marginally relevant and are worth a more careful investigation if the superpartners turn out to be heavier than considered here.

4.4. Constraints from the Dark Matter Density

Having discussed the constraints on the gravitino LSP scenario which originate from the observed light element abundances, we now turn to other astrophysical constraints. One constraint we already discussed for the case of the neutralino LSP is that the dark matter density has to be compatible with observations. Gravitinos are produced non-thermally via the NLSP decays. The corresponding energy density has to be smaller than the observed cold dark matter density,

$$\Omega_{3/2}^{\text{non-th}} h^2 = \frac{m_{3/2}}{m_{\rm NLSP}} \Omega_{\rm NLSP}^{\rm th} h^2 \leq \Omega_{\rm DM} < 0.123\ . \tag{V.32}$$

For $m_{1/2} = 500\,{\rm GeV}$ and $\tan\beta = 20$, we find

$$1.8 \cdot 10^{-3} \leq \Omega_{3/2}^{\text{non-th}} h^2 \leq 8.4 \cdot 10^{-3}\ . \tag{V.33}$$

For $\tan\beta = 10$ the maximal energy density is slightly smaller. Generally, $\Omega_{3/2}^{\text{non-th}}$ is largest in the part of the $\widetilde{\tau}$ NLSP region which is closest to the χ LSP region. Here we also find the largest NLSP abundance (cf. Figure V.3). In the $\widetilde{G}$-$\widetilde{\nu}$ scenario, the maximal value for $\Omega_{3/2}^{\text{non-th}} h^2$ is just slightly smaller than in the $\widetilde{\tau}$ NLSP case. All in all we find that the non-thermal gravitino energy density is far below the bound (V.32).

Note that a value of $\Omega_{3/2}^{\text{non-th}} h^2$ which is so much smaller than the observed cold dark matter density is unproblematic, since there are several potential gravitino production

mechanisms, such as thermal gravitino production.[9] Therefore the overall gravitino density can be much larger than the gravitino density resulting from NLSP decays and the observed dark matter density can be reached. Furthermore, as discussed in the case of a neutralino LSP, dark matter could be made up of several components and therefore even if there is no sizeable additional gravitino production, the scenario is still viable.

4.5. Constraints from CMB Distortions

In addition to bounds from the observed cold dark matter density there are constraints coming from distortions of the cosmic microwave background. These distortions can arise when part of the electromagnetic energy resulting from NLSP decays is transferred to background photons, because this changes the corresponding photon energy distribution. After the energy injection the CMB can re-thermalises through Compton scattering ($\gamma e \to \gamma e$), double-Compton scattering ($\gamma e \to \gamma\gamma e$) and bremsstrahlung ($eX \to eX\gamma$). Early NLSP decays can fully be thermalised, leading to a Planckian spectrum with vanishing chemical potential, however, distortions produced by late decays cannot. In particular, if the double-Compton scattering and bremsstrahlung processes become inefficient, the photon number will not be changed and electromagnetic energy release leads to a non-vanishing chemical potential.

From measurements of the FIRAS instrument aboard the COBE satellite it is well known that the CMB is very close to a blackbody distribution with zero chemical potential [119],

$$|\mu| < 9 \cdot 10^{-5} \text{ (at 95\% C.L.)}. \tag{V.34}$$

This upper limit on $|\mu|$ can be translated into an upper limit on late electromagnetic energy release ϵ_{em} [120]. However, the limit found in [120] is based on an approximation which turned out to be reliable only for stau masses above 500 GeV in an improved analysis [121]. For lighter staus, the bounds become considerably weaker. As a consequence, they are less constraining than the BBN bounds in our case [98].

4.6. Constraints on the Reheating Temperature

It is likely that in the early universe there was a period of inflation, driven by the non-vanishing potential energy of a scalar field, the inflaton. Assuming such an inflationary period any initial abundance of gravitinos is diluted away by the exponential expansion of the universe during the slow-roll phase. After the end of inflation the gravitino abundance is (re-)created in a phase of reheating in which a reheating temperature T_R is reached. In our scenario with gravitino masses $m_{3/2} \gtrsim 10\,\text{GeV}$ the gravitinos are extremely weakly coupled and are therefore not in thermal equilibrium with the

[9] In contrast, in many cosmological scenarios one often encounters a gravitino overproduction problem. To avoid the overproduction of gravitinos one has to restrict the allowed reheating temperatures, cf. Section 4.6.

primordial plasma for any reasonable value of the reheating temperature. Rather, the gravitinos are produced by thermal scatterings at these high temperatures. The resulting energy density has to be calculated in a consistent finite-temperature approach and is approximately given by [122, 123]

$$\Omega_{3/2}^{\mathrm{th}} h^2 \simeq 0.27 \left(\frac{T_{\mathrm{R}}}{10^{10}\,\mathrm{GeV}}\right) \left(\frac{100\,\mathrm{GeV}}{m_{3/2}}\right) \left(\frac{m_{\tilde{g}}}{1\,\mathrm{TeV}}\right)^2 , \tag{V.35}$$

where $m_{\tilde{g}}$ is the running gluino mass evaluated at low energy. It is obvious from (V.35) that if the gravitino energy density is known this relation can be used to derive an upper limit on the reheating temperature and that the maximal possible T_{R} is obtained for the heaviest allowed gravitino mass. The maximal reheating temperature in turn has profound implications on the generation of the observed baryon asymmetry in our universe. As with the gravitino relic density any initial baryon asymmetry is washed out after inflation. However, if the reheating temperature is high enough, heavy right-handed neutrinos can be produced by thermal reactions.[10] It is well known that the CP violating out-of-equilibrium decays of these heavy neutrinos can create a lepton asymmetry which then can be converted to a baryon asymmetry by sphaleron processes [125]. This mechanism is known as thermal leptogenesis and can explain the observed baryon asymmetry for reheating temperatures $T_R \gtrsim 2 \cdot 10^9\,\mathrm{GeV}$.

For our benchmark value of the unified gaugino mass, $m_{1/2} = 500\,\mathrm{GeV}$, the renormalisation group running results in a gluino mass of $m_{\tilde{g}} \simeq 1150\,\mathrm{GeV}$. We found that in the $\widetilde{G}$-$\widetilde{\tau}$ scenario, the gravitino mass is strongly constrained by BBN. The largest value consistent with our conservative constraint is around $m_{3/2} \simeq 70\,\mathrm{GeV}$. Using this upper limit and taking as lower bound $m_{3/2} = 10\,\mathrm{GeV}$, we can calculate an allowed range for the reheating temperature, assuming that all the dark matter is made up of gravitinos. Since the non-thermal contribution is negligible (cf. Eq. (V.33)), one obtains from $\Omega_{3/2}^{\mathrm{th}} \leq \Omega_{\mathrm{DM}}$ and Eq. (V.1)

$$3 \cdot 10^8\,\mathrm{GeV} \lesssim T_{\mathrm{R}} \lesssim 3 \cdot 10^9\,\mathrm{GeV} . \tag{V.36}$$

This is marginally compatible with the minimal temperature required for thermal leptogenesis [126]. Increasing the unified gaugino mass $m_{1/2}$ essentially leads to a rescaling of the gluino and gravitino masses, which lowers the upper bound on T_{R} as can be seen from (V.35). Therefore a small gaugino mass is needed for a high reheating temperature.

The $\widetilde{G}$-$\widetilde{\nu}$ scenario is less constrained by BBN and therefore allows for a much heavier gravitino. The only restriction is that the gravitino be lighter than the sneutrino, $m_{3/2} \lesssim 200\,\mathrm{GeV}$. This leads to a larger allowed range for the reheating temperature,

$$3 \cdot 10^8\,\mathrm{GeV} \lesssim T_{\mathrm{R}} \lesssim 7 \cdot 10^9\,\mathrm{GeV} , \tag{V.37}$$

which is consistent with thermal leptogenesis.

[10] A strong argument for the existence of these heavy right-handed neutrinos comes from the smallness of the left-handed neutrino masses, which can naturally be explained in terms of the see-saw mechanism [124].

Summary and Concluding Remarks

In this chapter we have investigated cosmological constraints on different scenarios in gaugino mediation. The leading constraints came from the observed cold dark matter density and from primordial nucleosynthesis. From the sparticle spectrum which was calculated in Chapter IV we knew that there were four possible different scenarios in our setup. The resulting viable dark matter candidates are summarised in Figure V.5 We found that although a neutralino NLSP is excluded by BBN, a neutralino LSP as the dominant component of dark matter is a viable possibility. Furthermore gravitino dark matter with a stau NLSP is strongly constrained and is consistent for a wide range of parameters only with the conservative BBN constraints. The severe BBN bounds require a gravitino mass close to the bound from naïve dimensional analysis. If the constraints from catalysed BBN are taken at face value, the gravitino stau scenario is ruled out, unless there is sizeable entropy production after the stau decoupling. Gravitino dark matter with a sneutrino NLSP can also be realised in gaugino mediation and is essentially unaffected by all constraints. We therefore conclude that the $\widetilde{G}$-$\widetilde{\nu}$ scenario seems more natural than the $\widetilde{G}$-$\widetilde{\tau}$ scenario in the framework of gaugino mediation. However one should keep in mind that we assumed strict R-parity conservation in our analysis. Relaxing this condition can considerably weaken the constraints while still allowing the LSP to make up all the dark matter.

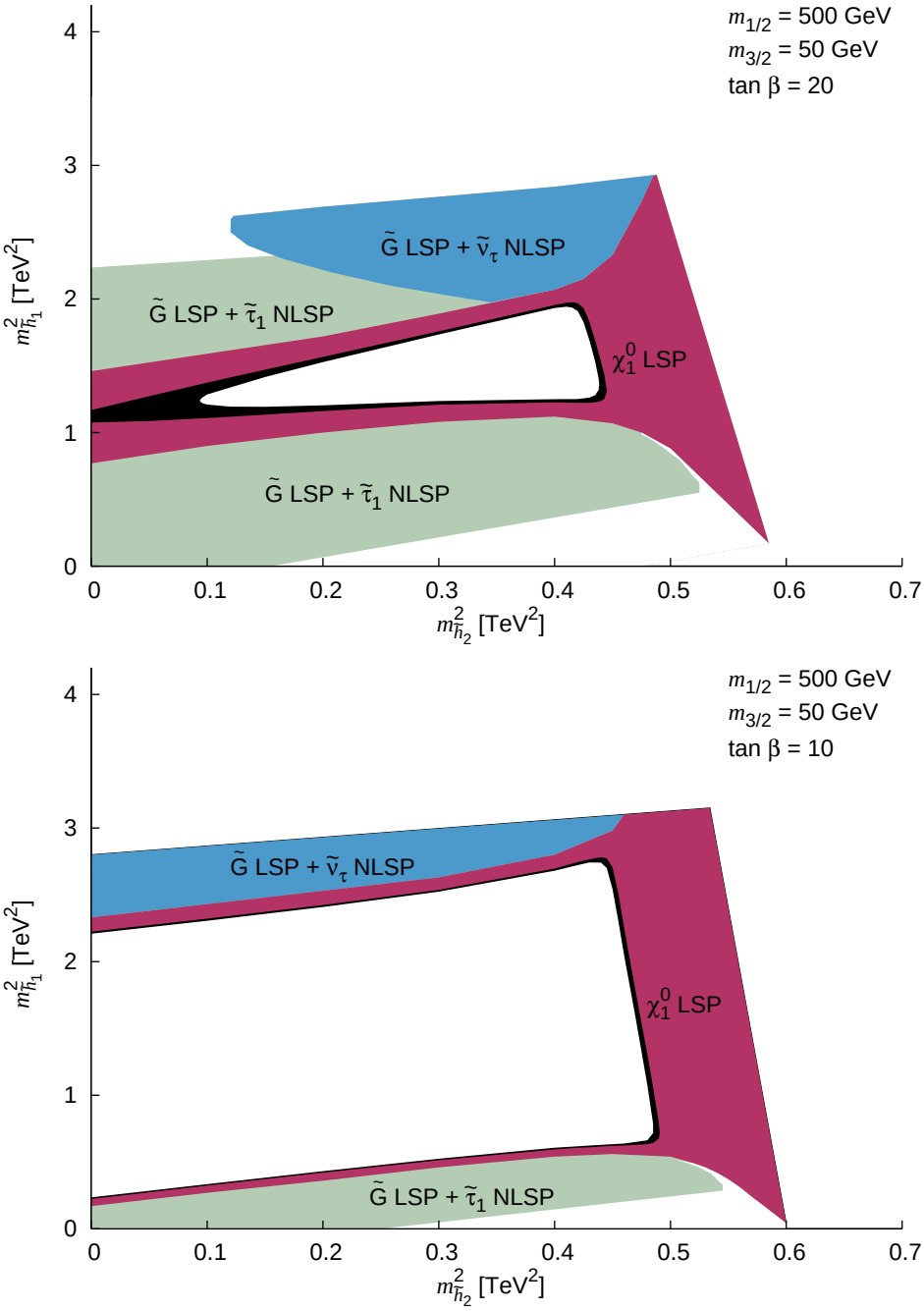

Figure V.5.: Allowed parameter space for the soft Higgs masses in gaugino mediation. In the black and magenta (dark-gray) coloured regions a neutralino is the LSP, whereas in the green (light-gray) and blue (medium-gray) regions the gravitino is the LSP with either a stau or a sneutrino being the NLSP. All white areas are excluded by bounds from the observed dark matter density and the "conservative" constraints from primordial nucleosynthesis.

VI. Conclusions and Outlook

This thesis was devoted to supersymmetric orbifold GUTs in six spacetime dimensions and their application to particle physics and cosmology. Symmetries and symmetry breaking effects are at the heart of high energy physics and theories with additional spacetime dimensions offer promising breaking schemes for supersymmetry as well as gauge symmetries. Nevertheless, despite these attractive features, there is one complication which is generic to all higher-dimensional theories: The volume and shape of the extra dimensions have to be stabilised in order to avoid severe phenomenological problems. An interesting possibility is that quantum effects induce a non-trivial potential for the extra-dimensional moduli fields. Following this line of thinking, we have calculated the Casimir energy due to a vector multiplet in the adjoint representation of $SO(10)$ on the toroidal orbifolds $T^2/\mathbb{Z}_2$ and $T^2/\left(\mathbb{Z}_2 \times \mathbb{Z}_2^{\mathrm{PS}} \times \mathbb{Z}_2^{\mathrm{GG}}\right)$. Expanding the result in a power series we found that the Casimir energy leads to an attractive force. To avoid a contraction of the extra-dimensional space down to the Planck length, additional contributions to the effective potential have to be taken into account. A detailed study of the modulus potential where our result for the Casimir energy will be essential is left for future work.

Having discussed one important contribution to the stabilisation potential, we turned to more phenomenological aspects of higher-dimensional theories. To this end we have investigated gaugino-mediated supersymmetry breaking in a six-dimensional $SO(10)$ orbifold GUT model where quarks and leptons are mixtures of brane and bulk fields. We found that the couplings of bulk matter fields to the SUSY breaking gauge singlet brane field have to be suppressed in order to avoid large FCNCs. The compatibility of the SUSY breaking mechanism and orbifold GUTs with brane and bulk matter fields is a generic problem which requires further studies. We have also determined bounds on the SUSY breaking parameters by naïve dimensional analysis, which turn out not to restrict the phenomenologically allowed parameter regions. The parameters relevant for the superparticle mass spectrum are the universal gaugino mass, the soft Higgs masses, $\tan\beta$ and the sign of μ. We have analysed their impact on the spectrum and determined the region in parameter space that results in a viable phenomenology. The model favours moderate values of $\tan\beta$ between about 10 and 25. The gaugino mass at the GUT scale should not be far below 500 GeV in order to satisfy the LEP bound on the Higgs mass. For a gaugino mass of 500 GeV, the lightest neutralino is typically bino-like with a mass of 200 GeV, and the gluino mass is about 1.2 TeV. For intermediate values of the down-type soft Higgs mass the neutralino is the LSP. For a small or large down-type soft Higgs mass either the right-handed or the left-handed sleptons can be lighter than the neutralinos. The corresponding region in parameter space grows with $\tan\beta$. In the region where sleptons are lighter than all other MSSM particles, the gravitino has to be

the LSP with the $\tilde{\tau}_1$ or the $\tilde{\nu}_{\tau \mathrm{L}}$ as the NLSP.

Motivated by the sparticle spectrum at low energies we also discussed dark matter candidates in theories with gaugino-mediated supersymmetry breaking. In particular we investigated constraints from the observed cold dark matter density and primordial nucleosynthesis on the different scenarios. The resulting viable dark matter candidates in gaugino mediation are summarised in Fig. V.5. A neutralino LSP as the dominant component of dark matter is a viable possibility. Gravitino dark matter with a $\widetilde{\tau}$ NLSP is marginally consistent for a wide range of parameters only with the "conservative" BBN constraints. Furthermore, if the constraints from catalysed ^{6}Li production are taken at face value the BBN bounds require either a gravitino mass close to the lower bound in gaugino mediation, entropy production after $\widetilde{\tau}$ decoupling or R parity violation. Finally, gravitino dark matter with a $\widetilde{\nu}$ NLSP can also be realised and is essentially unaffected by all constraints.

All in all we conclude that the framework of supersymmetric orbifold GUTs is theoretically very attractive and exhibits many phenomenologically appealing features. It can provide an interesting low-energy superpartner mass spectrum as well as promising candidates for cold dark matter, both of which could lead to distinct signatures at the upcoming Large Hadron Collider.

A. Appendix

1. Mode Expansion of Fields

1.1. Mode Expansion on $\mathbf{T^2}$

The mode expansion of fields which live on the product space $\mathcal{M} \times T^2$ where T^2 is a rectangular two torus can be written as

$$\Phi(x,y,z) = \frac{1}{\sqrt{4\pi^2 R_y R_z}} \sum_{m=-\infty}^{\infty} \sum_{n=-\infty}^{\infty} \phi^{(m,n)}(x) \exp\left\{ i \left(\frac{my}{R_y} + \frac{nz}{R_z} \right) \right\} ,$$

with the two radii R_y, R_z and $m, n \in \mathbb{Z}$. We now want to specialise this mode expansion to the case of an orbifold with reflection symmetries. In order to be able to apply the orbifold symmetries, it is convenient to rewrite the mode expansion on the torus in the following way,

$$\begin{aligned}
\Phi(x,y,z) = \frac{1}{\sqrt{2\pi^2 R_y R_z}} \frac{1}{\sqrt{2}} \Bigg\{ & \phi^{(0,0)}(x) + \sum_{n>0} \left[\phi^{(0,n)} e^{inz/R_z} + \phi^{(0,-n)} e^{-inz/R_z} \right] \\
& + \sum_{m>0} \left[\phi^{(m,0)}(x) e^{imy/R_y} + \phi^{(-m,0)} e^{-imy/R_y} \right] \\
& + \sum_{m>0} \sum_{n>0} \Bigg[\phi^{(m,n)}(x) e^{imy/R_y} e^{inz/R_z} + \phi^{(m,-n)}(x) e^{imy/R_y} e^{-inz/R_z} \\
& + \phi^{(-m,n)}(x) e^{-imy/R_y} e^{inz/R_z} + \phi^{(-m,-n)}(x) e^{-imy/R_y} e^{-inz/R_z} \Bigg] \Bigg\} \\
= \frac{1}{\sqrt{2\pi^2 R_y R_z}} \Bigg\{ & \frac{1}{\sqrt{2}} \phi_+^{(0,0)}(x) \\
& + \sum_{n>0} \left[\phi_+^{(0,n)} \cos\left(\frac{nz}{R_z} \right) + \phi_-^{(0,n)} \sin\left(\frac{nz}{R_z} \right) \right] \\
& + \sum_{m>0} \left[\phi_+^{(m,0)} \cos\left(\frac{my}{R_y} \right) + \phi_-^{(m,0)} \sin\left(\frac{my}{R_y} \right) \right] \\
& + \sum_{m>0} \sum_{n>0} \Bigg[\phi_+^{(m,n)} \cos\left(\frac{my}{R_y} + \frac{nz}{R_z} \right) + \phi_-^{(m,n)} \sin\left(\frac{my}{R_y} + \frac{nz}{R_z} \right) \\
& \qquad + \phi_+^{(m,-n)} \cos\left(\frac{my}{R_y} - \frac{nz}{R_z} \right) + \phi_-^{(m,-n)} \sin\left(\frac{my}{R_y} - \frac{nz}{R_z} \right) \Bigg] \Bigg\}
\end{aligned}$$

where we defined

$$\begin{aligned}
\phi_+^{(0,0)}(x) &= \phi^{(0,0)}(x) \\
\phi_+^{(m,n)}(x) &= \frac{1}{\sqrt{2}}\left(\phi^{(m,n)}(x) + \phi^{(-m,-n)}(x)\right) \\
\phi_-^{(m,n)}(x) &= \frac{i}{\sqrt{2}}\left(\phi^{(m,n)}(x) - \phi^{(-m,-n)}(x)\right) \ .
\end{aligned}$$

This rewriting in terms of sines and cosines is particularly useful to display the symmetry properties of the field. Having this expression at hand, it will be easy to obtain the mode expansion on an orbifold.

1.2. Mode Expansion on $\mathbf{T^2/\mathbb{Z}_2}$

We first consider fields which are even under the orbifold action. This leads to the following relation between the expansion coefficients

$$\phi^{(m,n)}(x) = \phi^{(-m,-n)}(x) \ ,$$

so that only $\phi_+^{(m,n)}(x)$ is nonzero. Using this relation we can write the mode expansion for even fields as follows,

$$\begin{aligned}
\Phi_+(x,y,z) =& \frac{1}{\sqrt{2\pi^2 R_y R_z}} \left\{ \frac{1}{\sqrt{2}}\phi_+^{(0,0)}(x) + \sum_{n>0} \phi_+^{(0,n)}(x) \cos\left(\frac{nz}{R_z}\right) \right. \\
&+ \sum_{m>0} \phi_+^{(m,0)}(x) \cos\left(\frac{my}{R_y}\right) + \sum_{m>0}\sum_{n>0} \left[\phi_+^{(m,n)}(x) \cos\left(\frac{my}{R_y} + \frac{nz}{R_z}\right) \right. \\
&\left. \left. + \phi_+^{(m,-n)}(x) \cos\left(\frac{my}{R_y} - \frac{nz}{R_z}\right) \right] \right\} \\
=& \frac{1}{\sqrt{2\pi^2 R_y R_z}} \left\{ \frac{1}{\sqrt{2}}\phi_+^{(0,0)}(x) + \sum_{n>0} \phi_+^{(0,n)}(x) \cos\left(\frac{nz}{R_z}\right) \right. \\
&\left. + \sum_{m>0}\sum_{n=-\infty}^{\infty} \phi_+^{(m,n)}(x) \cos\left(\frac{my}{R_y} + \frac{nz}{R_z}\right) \right\} \\
=& \frac{1}{\sqrt{2\pi^2 R_y R_z}} \left\{ \sum_{n\geq 0} \phi_+^{(0,n)}(x) \frac{1}{\sqrt{2^{\delta_{n,0}}}} \cos\left(\frac{nz}{R_z}\right) \right. \\
&\left. + \sum_{m>0}\sum_{n=-\infty}^{\infty} \phi_+^{(m,n)}(x) \cos\left(\frac{my}{R_y} + \frac{nz}{R_z}\right) \right\}
\end{aligned}$$

so that we can finally write the mode expansion for even fields as

$$\Phi_+(x,y,z) = \frac{1}{\sqrt{2\pi^2 R_y R_z 2^{\delta_{n,0}\delta_{m,0}}}} \left[\delta_{0,m}\sum_{n\geq 0} + \sum_{m>0}\sum_{n=-\infty}^{\infty}\right] \times \phi_+^{(m,n)}(x)\cos\left(\frac{my}{R_y}+\frac{nz}{R_z}\right) . \tag{A.1}$$

Now we consider the mode expansion of fields which are odd under the orbifold action. The corresponding coefficients satisfy

$$\phi^{(m,n)}(x) = \phi^{(-m,-n)}(x)$$

so that only $\phi_-^{(m,n)}(x)$ is nonzero. Performing a similar analysis as before we obtain

$$\Phi_-(x,y,z) = \frac{1}{\sqrt{2\pi^2 R_y R_z}} \left[\delta_{0,m}\sum_{n\geq 0} + \sum_{m>0}\sum_{n=-\infty}^{\infty}\right] \times \phi_-^{(m,n)}(x)\sin\left(\frac{my}{R_y}+\frac{nz}{R_z}\right) . \tag{A.2}$$

1.3. Mode Expansion on $\mathbf{T^2}/\left(\mathbb{Z}_\mathbf{2}\times\mathbb{Z}_\mathbf{2}^{\mathrm{PS}}\times\mathbb{Z}_\mathbf{2}^{\mathrm{GG}}\right)$

Let us now consider the action of the two additional $\mathbb{Z}_2$-parities on the mode expansion. The action of the other two $\mathbb{Z}_2$-symmetries on bulk fields is given by a reflection around $y' = y + \frac{\pi}{2}R_y$ for $\mathbb{Z}_2^{\mathrm{PS}}$ and a reflection around $z' = z + \frac{\pi}{2}R_z$ for $\mathbb{Z}_2^{\mathrm{GG}}$ respectively. Lets start with the $\mathbb{Z}_2^{\mathrm{PS}}$ reflection. Using the result for Φ_+ and rewriting it in terms of y' in order to see the action of the orbifold symmetry we obtain

$$\Phi_+(x,y,z) = \frac{1}{\sqrt{2\pi^2 R_y R_z 2^{\delta_{n,0}\delta_{m,0}}}} \left[\delta_{0,m}\sum_{n=0}^{\infty} + \sum_{m=1}^{\infty}\sum_{n=-\infty}^{\infty}\right] \times \phi_+^{(m,n)}(x)\cos\left(\frac{my'}{R_y}+\frac{nz}{R_z}-\frac{m\pi}{2}\right) .$$

It is obvious that this will be even under $y' \to -y'$ if m is an even integer and odd if m is an odd integer. Therefore the mode expansion for fields which are even under the first $\mathbb{Z}_2$-symmetry and even or odd with respect to the second $\mathbb{Z}_2$-symmetry can be written as

$$\Phi_{++}(x,y,z) = \frac{1}{\sqrt{2\pi^2 R_y R_z 2^{\delta_{n,0}\delta_{m,0}}}} \left[\delta_{0,m}\sum_{n\geq 0} + \sum_{m>0}\sum_{n=-\infty}^{\infty}\right] \times \phi_{++}^{(2m,n)}(x)\cos\left(\frac{2my}{R_y}+\frac{nz}{R_z}\right)$$

$$\Phi_{+-}(x,y,z) = \frac{1}{\sqrt{2\pi^2 R_y R_z}} \left[\sum_{m=0}^{\infty}\sum_{n=-\infty}^{\infty}\right] \phi_{+-}^{(2m+1,n)}(x)\cos\left(\frac{(2m+1)y}{R_y}+\frac{nz}{R_z}\right)$$

Performing an analogous approach for all other combinations of parities we finally obtain for the mode expansion on $T^2/\left(\mathbb{Z}_2 \times \mathbb{Z}_2^{\mathrm{PS}} \times \mathbb{Z}_2^{\mathrm{GG}}\right)$

$$\Phi_{+++}(x,y,z) = \frac{1}{\sqrt{2\pi R_y R_z 2^{\delta_{n,0}\delta_{m,0}}}} \left[\delta_{0,m}\sum_{n=0}^{\infty} + \sum_{m=1}^{\infty}\sum_{n=-\infty}^{\infty}\right] \phi_{+++}^{(2m,2n)}(x) \times \cos\left(\frac{2my}{R_y} + \frac{2nz}{R_z}\right), \tag{A.3a}$$

$$\Phi_{++-}(x,y,z) = \frac{1}{\sqrt{2\pi R_y R_z}} \left[\delta_{0,m}\sum_{n=0}^{\infty} + \sum_{m=1}^{\infty}\sum_{n=-\infty}^{\infty}\right] \phi_{++-}^{(2m,2n+1)}(x) \times \cos\left(\frac{2my}{R_y} + \frac{(2n+1)z}{R_z}\right), \tag{A.3b}$$

$$\Phi_{+-+}(x,y,z) = \frac{1}{\sqrt{2\pi R_y R_z}} \left[\sum_{m=0}^{\infty}\sum_{n=-\infty}^{\infty}\right] \phi_{+-+}^{(2m+1,2n)}(x) \times \cos\left(\frac{(2m+1)y}{R_y} + \frac{(2n)z}{R_z}\right), \tag{A.3c}$$

$$\Phi_{+--}(x,y,z) = \frac{1}{\sqrt{2\pi R_y R_z}} \left[\sum_{m=0}^{\infty}\sum_{n=-\infty}^{\infty}\right] \phi_{+--}^{(2m+1,2n+1)}(x) \times \cos\left(\frac{(2m+1)y}{R_y} + \frac{(2n+1)z}{R_z}\right), \tag{A.3d}$$

$$\Phi_{-++}(x,y,z) = \frac{1}{\sqrt{2\pi R_y R_z}} \left[\sum_{m=0}^{\infty}\sum_{n=-\infty}^{\infty}\right] \phi_{-++}^{(2m+1,2n+1)}(x) \times \sin\left(\frac{(2m+1)y}{R_y} + \frac{(2n+1)z}{R_z}\right), \tag{A.3e}$$

$$\Phi_{-+-}(x,y,z) = \frac{1}{\sqrt{2\pi R_y R_z}} \left[\sum_{m=0}^{\infty}\sum_{n=-\infty}^{\infty}\right] \phi_{-+-}^{(2m+1,2n)}(x) \times \sin\left(\frac{(2m+1)y}{R_y} + \frac{2nz}{R_z}\right), \tag{A.3f}$$

$$\Phi_{--+}(x,y,z) = \frac{1}{\sqrt{2\pi R_y R_z}} \left[\delta_{0,m}\sum_{n=0}^{\infty} + \sum_{m=1}^{\infty}\sum_{n=-\infty}^{\infty}\right] \phi_{++-}^{(2m,2n+1)}(x) \times \sin\left(\frac{2my}{R_y} + \frac{(2n+1)z}{R_z}\right), \tag{A.3g}$$

$$\Phi_{---}(x,y,z) = \frac{1}{\sqrt{2\pi R_y R_z}} \left[\delta_{0,m}\sum_{n=0}^{\infty} + \sum_{m=1}^{\infty}\sum_{n=-\infty}^{\infty}\right] \phi_{---}^{(2m,2n)}(x) \times \sin\left(\frac{2my}{R_y} + \frac{(2n)z}{R_z}\right). \tag{A.3h}$$

2. Evaluation of the Casimir Sums

Before we evaluate the Casimir sums, let us consider two sums which will prove particularly useful for this calculation.

$\widetilde{\mathbf{F}}(\mathbf{s};\mathbf{a},\mathbf{c})$

The first sum which we will need is given by

$$\widetilde{F}(s;a,c) \equiv \sum_{m=0}^{\infty} \frac{1}{\left[(m+a)^2+c^2\right]^s}$$

This is a series of the generalised Epstein-Hurwitz zeta type. The result can be found in [127] and is given by

$$\begin{aligned}\widetilde{F}(s;a,c) =& \frac{c^{-2s}}{\Gamma(s)} \sum_{m=0}^{\infty} \frac{(-1)^m \Gamma(m+s)}{m!} c^{-2m} \zeta_H(-2m,a) \\ &+ \sqrt{\pi} \frac{\Gamma(s-\frac{1}{2})}{2\Gamma(s)} c^{1-2s} \\ &+ \frac{2\pi^s}{\Gamma(s)} c^{1/2-s} \sum_{p=1}^{\infty} p^{s-1/2} \cos(2\pi p a) K_{s-1/2}(2\pi p c)\end{aligned}$$

where $\zeta_H(s,a)$ is the Hurwitz zeta function. For us it will be important that $\zeta_H(-2m,0) = \zeta_H(-2n,1/2) = 0$ for $m \in \mathbb{N}$ and $n \in \mathbb{N}_0$. Therefore the first term in $\widetilde{F}(s;a,c)$ collapses in our case. For $a = 1/2$ we can drop the first term completely and for $a = 0$ only the first term in the sum contributes with $\zeta_H(0,0) = +1/2$. In this case the first line is simply given by $+1/2c^{-2s}$.

$\mathbf{F}(\mathbf{s};\mathbf{a},\mathbf{c})$

A related sum which we will also need frequently is

$$F(s;a,c) \equiv \sum_{m=-\infty}^{\infty} \frac{1}{\left[(m+a)^2+c^2\right]^s} \ .$$

By observing that

$$\zeta_H(-2m,a) = -\zeta_H(-2m,1-a)$$

for $m \in \mathbb{N}$ and that

$$F(s;a,c) = \widetilde{F}(s;a,c) + \widetilde{F}(s;1-a,c)$$

we can easily obtain $F(s;a,c)$ as a particular case of $\widetilde{F}(s;a,c)$,

$$F(s;a,c)=\frac{\sqrt{\pi}}{\Gamma(s)}|c|^{1-2s}\left[\Gamma\left(s-\tfrac{1}{2}\right)+4\sum_{p=1}^{+\infty}\cos(2\pi pa)(\pi\,p\,|c|)^{s-\frac{1}{2}}K_{s-\frac{1}{2}}(2\pi\,p\,|c|)\right]\,.$$

Equipped with these formulas we come back to the calculation of the Casimir energy in our specific setup. Let us start with the Casimir energy on $T^2/\left(\mathbb{Z}_2\times\mathbb{Z}_2^{\rm PS}\times\mathbb{Z}_2^{\rm GG}\right)$. Albeit more involved, we can easily restrict the result to the case of $T^2/\mathbb{Z}_2$.

2.1. Casimir Sum on $\mathbf{T^2/\left(\mathbb{Z}_2\times\mathbb{Z}_2^{PS}\times\mathbb{Z}_2^{GG}\right)}$

Case 1

We first consider the case where

$$\Big[\sum\Big]_{m,n}=\sum_{m=0}^{\infty}\sum_{n=-\infty}^{\infty}\,.$$

In this case the sum can be written as

$$\sum_{m=0}^{\infty}\sum_{n=-\infty}^{\infty}\left[e^2(m+\alpha)^2+(n+\beta)^2)+\mu^2\right]^{-s}\,.$$

where we rescaled $s\to s+2$ and defined $\mu^2=\frac{R_z^2}{4}M^2$. Using the expression of $F(s;a,c)$ we can perform the sum over n,

$$\begin{aligned}
&\sum_{m=0}^{\infty}\sum_{n=-\infty}^{\infty}\left[e^2(m+\alpha)^2+(n+\beta)^2)+\mu^2\right]^{-s}\\
=&\sum_{m=0}^{\infty}\left\{\frac{\sqrt{\pi}}{\Gamma(s)}(\sqrt{e^2(m+\alpha)^2+\mu^2})^{1-2s}\left[\Gamma(s-\frac{1}{2})\right.\right.\\
&\left.\left.+4\sum_{p=1}^{+\infty}\cos(2\pi p\beta)\left(\pi\,p\,\sqrt{e^2(m+\alpha)^2+\mu^2}\right)^{s-\frac{1}{2}}K_{s-\frac{1}{2}}(2\pi\,p\,\sqrt{e^2(m+\alpha)^2+\mu^2})\right]\right\}\\
=&\sqrt{\pi}\frac{\Gamma(s-\frac{1}{2})}{\Gamma(s)}\sum_{m=0}^{\infty}(e^2(m+\alpha)^2+\mu^2)^{1/2-s}\\
&+\frac{4\sqrt{\pi}}{\Gamma(s)}\sum_{p=1}^{+\infty}\cos(2\pi p\beta)\sum_{m=0}^{\infty}(\pi\,p)^{s-\frac{1}{2}}\left(\sqrt{e^2(m+\alpha)^2+\mu^2}\right)^{\frac{1}{2}-s}\\
&\qquad\qquad K_{s-\frac{1}{2}}(2\pi\,p\,\sqrt{e^2(m+\alpha)^2+\mu^2})\\
\equiv&f_1(s)+f_2(s)\,.
\end{aligned}$$

Let us concentrate on $f_1(s)$ for now. The sum over m can be performed with the help of $\widetilde{F}(s;a,c)$,

$$\begin{aligned}
f_1(s) =&\sqrt{\pi}\frac{\Gamma(s-\frac{1}{2})}{\Gamma(s)}\sum_{m=0}^{\infty}(e^2(m+\alpha)^2+\mu^2)^{1/2-s}\\
=&\sqrt{\pi}\frac{\Gamma(s-\frac{1}{2})}{\Gamma(s)}e^{1-2s}\Bigg\{\left(\frac{\mu}{e}\right)^{1-2s}\zeta_H(0,\alpha)\\
&+\sqrt{\pi}\frac{\Gamma(s-1)}{2\Gamma(s-1/2)}\left(\tfrac{\mu}{e}\right)^{2-2s}\\
&+\frac{2\pi^{s-1/2}}{\Gamma(s-1/2)}\left(\tfrac{\mu}{e}\right)^{1-s}\sum_{p=1}^{\infty}p^{s-1}\cos(2\pi p\alpha)K_{s-1}(2\pi p\left(\tfrac{\mu}{e}\right))\Bigg\}\\
=&\sqrt{\pi}\frac{\Gamma(s-1/2)}{\Gamma(s)}\mu^{1-2s}\zeta_H(0,\alpha)\\
&+\frac{\pi}{2(s-1)}\frac{\mu^{2-2s}}{e}\\
&+\frac{2\pi^s}{\Gamma(s)}e^{-s}\mu^{1-s}\sum_{p=1}^{\infty}p^{s-1}\cos(2\pi p\alpha)K_{s-1}(2\pi p\left(\tfrac{\mu}{e}\right))
\end{aligned}$$

Remembering the shift in s we can now write $\zeta(s)$ as

$$\begin{aligned}
\zeta(s) =&\frac{1}{32\pi^2}\left(\frac{4}{R_z^2}\right)^{-s}\frac{1}{(s)(s+1)}\Bigg\{\sqrt{\pi}\frac{\Gamma(s-1/2)}{\Gamma(s)}\mu^{1-2s}\zeta_H(0,\alpha)\\
&+\frac{\pi}{2(s-1)}\frac{\mu^{2-2s}}{e}\\
&+\frac{2\pi^s}{\Gamma(s)}e^{-s}\mu^{1-s}\sum_{p=1}^{\infty}p^{s-1}\cos(2\pi p\alpha)K_{s-1}(2\pi p\left(\tfrac{\mu}{e}\right))\\
&+\frac{4\sqrt{\pi}}{\Gamma(s)}\sum_{p=1}^{+\infty}\cos(2\pi p\beta)\sum_{m=0}^{\infty}(\pi\,p)^{s-\frac{1}{2}}\left(\sqrt{e^2(m+\alpha)^2+\mu^2}\right)^{\frac{1}{2}-s}\\
&K_{s-\frac{1}{2}}(2\pi\,p\,\sqrt{e^2(m+\alpha)^2+\mu^2})\Bigg\}
\end{aligned}$$

Now we have to differentiate with respect to s and set $s=-2$. Since $\Gamma(-2)=\infty$, the derivative only has to act on $\Gamma(s)$ if the corresponding term is inversely proportional to $\Gamma(s)$. Note that

$$\frac{\mathrm{d}}{\mathrm{d}s}\frac{1}{\Gamma(s)}\bigg|_{s=-2}=-\frac{\Gamma'(s)}{\Gamma(s)^2}\bigg|_{s=-2}=+2$$

Performing the differentiation we obtain

$$\begin{aligned}
&\frac{\mathrm{d}}{\mathrm{d}s}\zeta(s)\Big|_{s=-2} \\
=&\frac{1}{2\pi^2 R_z^4}\frac{1}{2}\Bigg\{ -\frac{16\pi}{15}\mu^5\zeta_H(0,\alpha) \\
&+\frac{\pi\mu^6}{36e}\left[-11+6\log(4/R_z^2)+12\log(\mu)\right] \\
&+\frac{4}{\pi^2}e^2\mu^3\sum_{p=1}^{\infty}\frac{\cos(2\pi p\alpha)}{p^3}K_3(2\pi p\left(\tfrac{\mu}{e}\right)) \\
&+\frac{8}{\pi^2}\sum_{p=1}^{+\infty}\frac{\cos(2\pi p\beta)}{p^{5/2}}\sum_{m=0}^{\infty}\left(e^2(m+\alpha)^2+\mu^2\right)^{\frac{5}{4}}K_{5/2}(2\pi\, p\sqrt{e^2(m+\alpha)^2+\mu^2})\Bigg\}
\end{aligned}$$

where we used $K_a(z)=K_{-a}(z)$. Replacing again $e=R_z/R_y$ and $\mu=R_zM/2$ we finally obtain for the Casimir energy in the case 1

$$\begin{aligned}
V_{s,\mathrm{I}}^{\alpha,\beta,M} =& -\frac{1}{4\pi^2R_z^4}\Bigg\{ -\frac{16\pi}{15}\frac{M^5R_z^5}{32}\zeta_H(0,\alpha) \\
&+\pi\frac{R_yR_z^5M^6}{2304}\left[-11+12\log(M)\right] \\
&+\frac{4}{\pi^2}\frac{R_z^5M^3}{8R_y^2}\sum_{p=1}^{\infty}\frac{\cos(2\pi p\alpha)}{p^3}K_3(\pi pMR_y) \\
&+\frac{8}{\pi^2}\left(\frac{R_z}{R_y}\right)^{5/2}\sum_{p=1}^{+\infty}\frac{\cos(2\pi p\beta)}{p^{5/2}}\sum_{m=0}^{\infty}\left((m+\alpha)^2+\tfrac{M^2R_y^2}{4}\right)^{\frac{5}{4}} \\
&\qquad K_{5/2}\left(2\pi\, p\,\tfrac{R_z}{R_y}\sqrt{(m+\alpha)^2+M^2R_y^2/4}\right)\Bigg\}. \qquad \text{(A.4)}
\end{aligned}$$

Case 2

This time we consider the case where

$$\Big[\sum\Big]_{m,n} = \left[\delta_{0,m}\sum_{n=0}^{\infty} + \sum_{m=1}^{\infty}\sum_{n=-\infty}^{\infty}\right] .$$

In this case the sum can be written as

$$\begin{aligned}
&\left[\delta_{0,m}\sum_{n=0}^{\infty} + \sum_{m=1}^{\infty}\sum_{n=-\infty}^{\infty}\right]\left[e^2(m+\alpha)^2 + (n+\beta)^2 + \mu^2\right]^{-s} \\
=&\sum_{n=0}^{\infty}\left[e^2\alpha^2 + (n+\beta)^2 + \mu^2\right]^{-s} \\
&+\left[\sum_{m=0}^{\infty}\sum_{n=-\infty}^{\infty} - \delta_{m,0}\sum_{n=-\infty}^{\infty}\right]\left[e^2(m+\alpha)^2 + (n+\beta)^2 + \mu^2\right]^{-s} ,
\end{aligned}$$

where we again rescaled $s \to s+2$ and set $\mu^2 = \frac{R_z^2}{4}M^2$. The double sum corresponds to the case 1 we already calculated. Let us now evaluate the additional piece, which we denote by $f_3(s)$. Note that

$$\begin{aligned}
&\sum_{n=-\infty}^{\infty}\left[(n+\beta)^2 + e^2\alpha^2 + \mu^2\right]^{-s} \\
=&\sum_{n=0}^{\infty}\left[(n+\beta)^2 + e^2\alpha^2 + \mu^2\right]^{-s} + \sum_{n=0}^{\infty}\left[(n+1-\beta)^2 + e^2\alpha^2 + \mu^2\right]^{-s} .
\end{aligned}$$

Then it is easy to see that $f_3(s)$ can be written as[1]

$$\begin{aligned}
f_3(s) &= -\sum_{n=0}^{\infty}\left[(n+1-\beta)^2 + e^2\alpha^2 + \mu^2\right]^{-s} \\
&= -\left(e^2\alpha^2 + \mu^2\right)^{-s}\zeta_H(0, 1-\beta) \\
&\quad -\sqrt{\pi}\frac{\Gamma(s-\frac{1}{2})}{2\Gamma(s)}\left(e^2\alpha^2 + \mu^2\right)^{1/2-s} \\
&\quad -\frac{2\pi^s}{\Gamma(s)}\left(e^2\alpha^2 + \mu^2\right)^{1/4-s/2}\sum_{p=1}^{\infty} p^{s-1/2}\cos(2\pi p(1-\beta))K_{s-1/2}(2\pi p\sqrt{e^2\alpha^2+\mu^2}) .
\end{aligned}$$

[1] Note that $\zeta_H(0,1) = -1/2$ and $\zeta_H(-2m,1) = 0$

We will now evaluate the contribution of $f_3(s)$ to $\zeta(s)$ and denote it $\zeta_3(s)$.

$$\begin{aligned}\zeta_3(s) = &-\frac{1}{32\pi^2}\frac{1}{s(s+1)}\left(\frac{4}{R_z^2}\right)^{-s}\Bigg\{\left(e^2\alpha^2+\mu^2\right)^{-s}\zeta_H(0,1-\beta)\\ &+\sqrt{\pi}\frac{\Gamma(s-\frac{1}{2})}{2\Gamma(s)}\sqrt{e^2\alpha^2+\mu^2}^{1-2s}\\ &+\frac{2\pi^s}{\Gamma(s)}\sqrt{e^2\alpha^2+\mu^2}^{1/2-s}\sum_{p=1}^{\infty}p^{s-1/2}\cos(2\pi p(1-\beta))K_{s-1/2}(2\pi p\sqrt{e^2\alpha^2+\mu^2})\Bigg\}\end{aligned}$$

Now we perform the differentiation again and set $s=-2$. For terms which are proportional to the inverse of $\Gamma(s)$ the derivative has to act only on the Gamma function as before.

$$\begin{aligned}&\left.\frac{\mathrm{d}\zeta_3(s)}{ds}\right|_{s=-2}\\ =&-\frac{1}{4\pi^2R_z^4}\Bigg\{(e^2\alpha^2+\mu^2)^2\left[\frac{3}{2}-\log(e^2\alpha^2+\mu^2)-\log(4/R_z^2)\right]\zeta_H(0,1-\beta)\\ &-\frac{8\pi}{15}\left(e^2\alpha^2+\mu^2\right)^{5/2}\\ &+\frac{4}{\pi^2}\left(e^2\alpha^2+\mu^2\right)^{5/4}\sum_{p=1}^{\infty}\frac{\cos(2\pi p(1-\beta))}{p^{5/2}}K_{5/2}(2\pi p\sqrt{e^2\alpha^2+\mu^2})\Bigg\}\end{aligned}$$

where we used $\Gamma(-5/2)=-8/15\sqrt{\pi}$. Replacing again $e=R_z/R_y$ and $\mu=R_zM/2$ we finally obtain for the Casimir energy in the case 2

$$\begin{aligned}V_{s,\mathrm{II}}^{\alpha,\beta,M} =&V_{s,\mathrm{I}}^{\alpha,\beta,M}\\ &-\frac{1}{4\pi^2R_z^4}\Bigg\{-\frac{R_z^4}{R_y^4}\left(\alpha^2+\frac{M^2R_y^2}{4}\right)^2\left[\frac{3}{2}-\log\left(\tfrac{4\alpha^2}{R_y^2}+M^2\right)\right]\zeta_H(0,1-\beta)\\ &+\frac{8\pi}{15}\frac{R_z^5}{R_y^5}\left(\alpha^2+\frac{M^2R_y^2}{4}\right)^{5/2}\\ &-\frac{4}{\pi^2}\left(\frac{R_z}{R_y}\right)^{5/2}\left(\alpha^2+\tfrac{M^2R_y^2}{4}\right)^{5/4}\sum_{p=1}^{\infty}\frac{\cos(2\pi p(1-\beta))}{p^{5/2}}\\ &\qquad K_{5/2}\left(2\pi p\tfrac{R_z}{R_y}\sqrt{\alpha^2+M^2R_y^2/4}\right)\Bigg\}. \qquad (A.5)\end{aligned}$$

2.2. Casimir Sum on $\mathbf{T^2/\mathbb{Z}_2}$

The summation can be performed exactly as in the case of $T^2/\left(\mathbb{Z}_2 \times \mathbb{Z}_2^{\rm PS} \times \mathbb{Z}_2^{\rm GG}\right)$. However, since we already evaluated the more involved case, this will not be necessary for all terms which are proportional to $\Gamma(s)$[1]. In this case we see by comparison that the result for the Casimir energy of the scalar field Φ_+ on $T^2/\mathbb{Z}_2$ can be obtained from the corresponding expression on $T^2/\left(\mathbb{Z}_2 \times \mathbb{Z}_2^{\rm PS} \times \mathbb{Z}_2^{\rm GG}\right)$. We just have to rescale $V_{s,\rm II}^{(\alpha,\beta,M)}$ by $1/16$ replace M by $2M$ and set $\alpha = \beta = 0$. The remaining two terms are also easily calculated.

3. Power Series of the Casimir Energy

Here we will perform the power series of the Casimir energy in $x = M\sqrt{R_y R_z} \ll 1$. The leading terms will be $\mathcal{O}(x^0)$, but they will cancel within one supermultiplet. The first non-vanishing terms will be $\mathcal{O}(x^2)$.

3.1. $\mathbf{T^2/\mathbb{Z}_2}$

We denote the terms of the Casimir energy by V^i, $i = 1, ..., 5$. Clearly, only the second, third and fifth term will give a contribution which is $\mathcal{O}(x^2)$. Let us look at these three cases in turn.

$\mathbf{V^2}$

To expand the V^2 we use that

$$K_3\left(2\pi p e^{-1/2} x\right) = \frac{e^{3/2}}{p^3\pi^3 x^3} - \frac{e^{1/2}}{2p\pi x} + \mathcal{O}(x) \ .$$

We concentrate on the second term in the expansion which will lead to a term $\mathcal{O}(x^2)$. Using the expansion given above, V^2 can be written as

$$V^2 = +\frac{1}{2880\pi R_y^4} M^2 R_y R_z \ , \tag{A.6}$$

where we used

$$\sum_{p=1}^{\infty} \frac{1}{p^4} = \frac{\pi^4}{90} \ .$$

$\mathbf{V^3}$

We can expand the Bessel function including its prefactor as

$$\begin{aligned}&\left(m^2+\frac{x^2}{e}\right)^{\frac{5}{4}} K_{5/2}\left(2\pi\, p\, e^{1/2}\sqrt{em^2+x^2}\right)\\&= e^{-2\pi pme}\left\{\frac{3+6\pi pme+4\pi^2p^2m^2e^2}{8\pi^2p^{5/2}e^{5/2}}-\frac{1+2\pi pme}{4p^{1/2}e^{3/2}}x^2+\mathcal{O}(x^4)\right\}\,.\end{aligned}$$

Inserting this expansion, the corresponding term can be written as

$$\begin{aligned}V^3 &= +\frac{1}{64\pi^2R_z^4}\frac{8}{\pi^2}\left(\frac{R_z}{R_y}\right)^{5/2}\sum_{p=1}^{+\infty}\frac{1}{p^{5/2}}\sum_{m=0}^{\infty}e^{-2\pi pme}\frac{1+2\pi pme}{4p^{1/2}e^{3/2}}x^2\\&= +\frac{1}{64\pi^2R_z^4}\frac{8}{\pi^2}\left(\frac{R_z}{R_y}\right)^{5/2}\sum_{p=1}^{+\infty}\frac{1}{p^3}x^2e^{2\pi pe}\frac{-1+e^{2\pi pe}+2\pi pe}{4e^{3/2}(-1+e^{2\pi pe})^2}\\&= +\frac{M^2}{64\pi^4R_z^2}\sum_{p=1}^{+\infty}\frac{1}{p^3}\left\{1+\coth(\pi pR_z/R_y)+\frac{R_z}{R_y}\frac{\pi p}{\sinh^2(\pi pR_z/R_y)}\right\}\\&= +\frac{M^2}{64\pi^4R_z^2}\left\{\zeta(3)+\sum_{p=1}^{+\infty}\frac{1}{p^3}\left[\coth(\pi pR_z/R_y)\right.\right.\\&\qquad\left.\left.+\frac{R_z}{R_y}\frac{\pi p}{\sinh^2(\pi pR_z/R_y)}\right]\right\}\,.\end{aligned}\tag{A.7}$$

$\mathbf{V^5}$

With the help of

$$K_{5/2}(2\pi pe^{1/2}x)=\frac{3}{8\pi^2p^{5/2}e^{5/4}}x^{-5/2}-\frac{1}{4p^{1/2}e^{1/4}}x^{-1/2}+\mathcal{O}(x^{3/2})$$

the last term can be written as

$$V^5=+\frac{\zeta(3)}{64\pi^4R_yR_z^3}M^2R_yR_z\tag{A.8}$$

where we used

$$\sum_{p=1}^{\infty}\frac{1}{p^3}=\zeta(3)\,.$$

Collecting all terms and remembering the factor 90, the Casimir energy of the vector-multiplet on $T^2/\mathbb{Z}_2$ is given to leading order in $x = M\sqrt{R_y R_z}$ by

$$V_V = -\frac{1}{32\pi R_y^4} M^2 R_y R_z - \frac{45M^2}{32\pi^4 R_z^2} \sum_{p=1}^{+\infty} \frac{1}{p^3} \left\{ \frac{R_z}{R_y} \frac{\pi p}{\sinh^2(\pi p R_z/R_y)} + \coth(\pi p R_z/R_y) \right\} . \tag{A.9}$$

3.2. $\mathbf{T^2/\left(\mathbb{Z}_2 \times \mathbb{Z}_2^{PS} \times \mathbb{Z}_2^{GG}\right)}$

As before we denote the terms of the Casimir energy by V^i, $i = 1, ..., 7$. The first two terms of the Casimir energy clearly do not contribute.

$\mathbf{V^3}$

For the third term we need the expansion

$$K_3\left(\pi p e^{-1/2} x\right) = \frac{8e^{3/2}}{p^3\pi^3 x^3} - \frac{e^{1/2}}{p\pi x} + \mathcal{O}(x)$$

Inserting this expression into the third term and performing the sum over p we obtain

$$V^3 = +\frac{1}{16\pi^5 R_z^4} \left(\frac{R_z}{R_y}\right)^4 M^2 R_y R_z \left[\mathrm{Li}_4(e^{-2\pi i\alpha}) + \mathrm{Li}_4(e^{2\pi i\alpha})\right]$$

where we used

$$\sum_{p=1}^{\infty} \frac{\cos(2\pi p\alpha)}{p^4} = \frac{1}{2}\left[\mathrm{Li}_4(e^{-2\pi i\alpha}) + \mathrm{Li}_4(e^{2\pi i\alpha})\right] .$$

Here Li_4 a polylogarithm. From this expression we can extract the expressions for $\alpha = 0, 1/2$,

$$V^3_{\alpha=0} = +\frac{1}{720\pi R_y^4} M^2 R_y R_z , \tag{A.10}$$

$$V^3_{\alpha=1/2} = -\frac{7}{5760\pi R_y^4} M^2 R_y R_z . \tag{A.11}$$

$\mathbf{V^4}$

Here we need the expansion

$$\begin{aligned}&\left((m+\alpha)^2+x^2\tfrac{R_y}{4R_z}\right)^{5/4}K_{5/2}\left(2\pi p\tfrac{R_z}{R_y}\sqrt{(m+\alpha)^2+x^2\tfrac{R_y}{4R_z}}\right)\\&=e^{-2\pi p(m+\alpha)R_z/R_y}\left\{\frac{3+6\pi p(R_z/R_y)(m+\alpha)+4\pi^2p^2(R_z/R_y)^2(m+\alpha)^2}{8\pi^2p^{5/2}(R_z/R_y)^{5/2}}\right.\\&\qquad\left.-\frac{1+2\pi pe(m+\alpha)}{16p^{1/2}(R_z/R_y)^{3/2}}x^2+\mathcal{O}(x^4)\right\}.\end{aligned}$$

Plugging the second term of this expansion back in we obtain

$$\begin{aligned}V^4=&\frac{1}{4\pi^2R_z^4}\frac{8}{\pi^2}\left(\frac{R_z}{R_y}\right)^{5/2}\sum_{p=1}^{+\infty}\frac{\cos(2\pi p\beta)}{p^{5/2}}\sum_{m=0}^{\infty}e^{-2\pi p(m+\alpha)R_z/R_y}\frac{1+2\pi pe(m+\alpha)}{16p^{1/2}(R_z/R_y)^{3/2}}x^2\\=&\frac{1}{4\pi^2R_z^4}\frac{8}{\pi^2}\left(\frac{R_z}{R_y}\right)^{5/2}\sum_{p=1}^{+\infty}\frac{\cos(2\pi p\beta)}{p^{5/2}}x^2\sqrt{R_y}e^{-2\pi p(\alpha-1)R_z/R_y}\\&\frac{2\pi pR_z(1-\alpha)-R_y+e^{2\pi pR_z/R_y}(R_y+2\pi p\alpha R_z)}{16p^{1/2}R_z^{3/2}(e^{2\pi pR_z/R_y}-1)^2}\end{aligned}$$

Let us now come to the particular values of α and β.

- $\alpha,\beta=(0,0)$

$$V^4_{\alpha=0,\beta=0}=\frac{M^2}{16\pi^4R_z^2}\sum_{p=1}^{\infty}\frac{1}{p^3}\left\{1+\coth(\pi pR_z/R_y)+\pi p\frac{R_z}{R_y}\frac{1}{\sinh^2(\pi pR_z/R_y)}\right\}\quad(A.12)$$

- $\alpha,\beta=(1/2,0)$

$$V^4_{\alpha=1/2,\beta=0}=\frac{M^2}{16\pi^4R_z^2}\sum_{p=1}^{\infty}\frac{1}{p^3}\left\{\frac{1}{\sinh(\pi pR_z/R_y)})+\pi p\frac{R_z}{R_y}\frac{\coth(\pi pR_z/R_y)}{\sinh(\pi pR_z/R_y)}\right\}\quad(A.13)$$

- $\alpha,\beta=(0,1/2)$

$$\begin{aligned}V^4_{\alpha=0,\beta=1/2}=\frac{M^2}{16\pi^4R_z^2}\sum_{p=1}^{\infty}\frac{1}{p^3}\Big\{&\cos(\pi p)\left[1+\coth(\pi pR_z/R_y)\right]\\&+\pi p\frac{R_z}{R_y}\frac{\cos(\pi p)}{\sinh^2(\pi pR_z/R_y)}\Big\}\end{aligned}\quad(A.14)$$

- $\alpha, \beta = (1/2, 1/2)$

$$V^4_{\alpha=1/2,\beta=1/2} = \frac{M^2}{16\pi^4 R_z^2}\sum_{p=1}^{\infty}\frac{1}{p^3}\Bigg\{\frac{\cos(\pi p)}{\sinh(\pi p R_z/R_y)}) + \pi p\frac{R_z}{R_y}\frac{\cos(\pi p)\coth(\pi p R_z/R_y)}{\sinh(\pi p R_z/R_y)}\Bigg\} \tag{A.15}$$

$\mathbf{V^{5,6}}$

The fifth and sixth term are only non-zero for $\alpha = 1/2$ and therefore do not contribute to the Casimir energy.

$\mathbf{V^7}$

For the last term we need the expansion

$$\begin{aligned}&\left(\alpha^2 + \frac{x^2}{4e}\right)^{5/4} K_{5/2}(\pi p e^{1/2}\sqrt{4e\alpha^2 + x^2}) \\ &= e^{-2\pi p e\alpha}\left\{\frac{3 + 6\pi p e\alpha + 4\pi^2 p^2 e^2\alpha^2}{8\pi^2 p^{5/2} e^{5/2}} - \frac{1 + 2\pi p e\alpha}{16 p^{1/2} e^{3/2}}x^2 + \mathcal{O}(x^4)\right\}\ .\end{aligned}$$

Then V^7 can be written as

$$\begin{aligned}V^7 &= -\frac{1}{16\pi^4 R_z^4}\frac{R_z}{R_y}x^2\sum_{p=1}^{\infty}\frac{\cos[2\pi p(1-\beta)]}{p^3}e^{-2\pi p e\alpha}(1 + 2\pi p e\alpha) \\ &= -\frac{1}{16\pi^4 R_z^4}\frac{R_z}{R_y}x^2\Big\{\pi e\alpha\left(\mathrm{Li}_2(e^{-2\pi(e\alpha + i\beta)}) + \mathrm{Li}_2(e^{-2\pi(e\alpha - i\beta)})\right) \\ &\qquad + \frac{1}{2}\left(\mathrm{Li}_3(e^{-2\pi(e\alpha + i\beta)}) + \mathrm{Li}_3(e^{-2\pi(e\alpha - i\beta)})\right)\Big\}\ .\end{aligned}$$

We only have to consider the case $\alpha = 0$ here. Choosing $\beta = 0, 1/2$ we obtain

$$V^7_{\beta=0} = -\frac{M^2}{16\pi^4 R_z^2}\zeta(3)\ , \tag{A.16}$$

$$V^7_{\beta=1/2} = +\frac{3M^2}{64\pi^4 R_z^2}\zeta(3)\ . \tag{A.17}$$

Collecting all the terms and taking into account that the fermionic contribution comes with a minus sign we obtain

$$
\begin{aligned}
&\left(V_{s,\mathrm{II}}^{(0,0)} - V_{s,\mathrm{II}}^{(0,0),M}\right) \\
=&-\frac{1}{720\pi R_y^4} M^2 R_y R_z + \frac{1}{16\pi^4 R_z^2} M^2 \zeta(3) \\
&-\frac{M^2}{16\pi^4 R_z^2} \sum_{p=1}^{\infty} \frac{1}{p^3} \left\{ 1 + \coth(\pi p R_z/R_y) + \pi p \frac{R_z}{R_y} \frac{1}{\sinh^2(\pi p R_z/R_y)} \right\} \\
&\left(V_{s,\mathrm{II}}^{(0,1/2)} - V_{s,\mathrm{II}}^{(0,1/2),M}\right) \\
=&-\frac{1}{720\pi R_y^4} M^2 R_y R_z - \frac{3}{64\pi^4 R_z^2} M^2 \zeta(3) \\
&-\frac{M^2}{16\pi^4 R_z^2} \sum_{p=1}^{\infty} \frac{1}{p^3} \left\{ \frac{1}{\sinh(\pi p R_z/R_y)}) + \pi p \frac{R_z}{R_y} \frac{\coth(\pi p R_z/R_y)}{\sinh(\pi p R_z/R_y)} \right\} \\
&\left(V_{s,\mathrm{I}}^{(1/2,0)} - V_{s,\mathrm{I}}^{(1/2,0),M}\right) \\
=&\frac{7}{5760\pi R_y^4} M^2 R_y R_z \\
&-\frac{M^2}{16\pi^4 R_z^2} \sum_{p=1}^{\infty} \frac{1}{p^3} \left\{ \cos(\pi p) \left[1 + \coth(\pi p R_z/R_y)\right] + \pi p \frac{R_z}{R_y} \frac{\cos(\pi p)}{\sinh^2(\pi p R_z/R_y)} \right\} \\
&\left(V_{s,\mathrm{I}}^{(1/2,1/2)} - V_{s,\mathrm{I}}^{(1/2,1/2),M}\right) \\
=&\frac{7}{5760\pi R_y^4} M^2 R_y R_z \\
&-\frac{M^2}{16\pi^4 R_z^2} \sum_{p=1}^{\infty} \frac{1}{p^3} \left\{ \frac{\cos(\pi p)}{\sinh(\pi p R_z/R_y)}) + \pi p \frac{R_z}{R_y} \frac{\cos(\pi p) \coth(\pi p R_z/R_y)}{\sinh(\pi p R_z/R_y)} \right\} .
\end{aligned}
$$

With these expressions the final result for the Casimir energy of the vector multiplet on $T^2/\left(\mathbb{Z}_2 \times \mathbb{Z}_2^{\mathrm{PS}} \times \mathbb{Z}_2^{\mathrm{GG}}\right)$ to leading order in $x = M\sqrt{R_y R_z}$ is given by

$$
\begin{aligned}
V_V =& -\frac{1}{48\pi R_y^4} M^2 R_y R_z + \frac{1}{2\pi^4 R_z^2} M^2 \zeta(3) \\
&-\frac{M^2}{8\pi^2 R_z^2} \sum_{p=1}^{\infty} \frac{1}{p^3} \Bigg\{ \left[13 + 8\cos(\pi p)\right] \left[1 + \coth(\pi p R_z/R_y)\right] \\
&+ 12[1 + \cos(\pi p)] \left(1 + \pi \tfrac{R_z}{R_y} \coth(\pi p R_z/R_y)\right) \frac{1}{\sinh(\pi p R_z/R_y)} \\
&+ \pi \tfrac{R_z}{R_y} \left(13 + 8\cos(\pi p)\right) \frac{1}{\sinh^2(\pi p R_z/R_y)} \Bigg\} .
\end{aligned} \tag{A.18}
$$

This expression still looks quite complicated. However, in practice only the first few terms of the sum contribute.

Bibliography

[1] M. F. Sohnius, *Introducing supersymmetry*, Phys. Rept. **128** (1985), 39–204.

[2] S. P. Martin, *A supersymmetry primer*, (1997), hep-ph/9709356.

[3] A. Hebecker and M. Trapletti, *Gauge unification in highly anisotropic string compactifications*, Nucl. Phys. **B713** (2005), 173–203, hep-th/0411131.

[4] L. J. Dixon, J. A. Harvey, C. Vafa, and E. Witten, *Strings on orbifolds*, Nucl. Phys. **B261** (1985), 678–686.

[5] L. J. Dixon, J. A. Harvey, C. Vafa, and E. Witten, *Strings on orbifolds. 2*, Nucl. Phys. **B274** (1986), 285–314.

[6] Y. Kawamura, *Gauge symmetry reduction from the extra space S(1)/Z(2)*, Prog. Theor. Phys. **103** (2000), 613–619, hep-ph/9902423.

[7] Y. Kawamura, *Triplet-doublet splitting, proton stability and an extra dimension*, Prog. Theor. Phys. **105** (2001), 999–1006, hep-ph/0012125.

[8] G. Altarelli and F. Feruglio, *SU(5) grand unification in extra dimensions and proton decay*, Phys. Lett. **B511** (2001), 257–264, hep-ph/0102301.

[9] L. J. Hall and Y. Nomura, *Gauge unification in higher dimensions*, Phys. Rev. **D64** (2001), 055003, hep-ph/0103125.

[10] A. Hebecker and J. March-Russell, *A minimal S(1)/(Z(2) × Z'(2)) orbifold GUT*, Nucl. Phys. **B613** (2001), 3–16, hep-ph/0106166.

[11] T. Asaka, W. Buchmuller, and L. Covi, *Gauge unification in six dimensions*, Phys. Lett. **B523** (2001), 199–204, hep-ph/0108021.

[12] L. J. Hall, Y. Nomura, T. Okui, and D. R. Smith, *SO(10) unified theories in six dimensions*, Phys. Rev. **D65** (2002), 035008, hep-ph/0108071.

[13] T. Appelquist and A. Chodos, *Quantum effects in kaluza-klein theories*, Phys. Rev. Lett. **50** (1983), 141.

[14] T. Appelquist and A. Chodos, *The quantum dynamics of kaluza-klein theories*, Phys. Rev. **D28** (1983), 772.

[15] A. Anisimov, M. Dine, M. Graesser, and S. D. Thomas, *Brane world susy breaking*, Phys. Rev. **D65** (2002), 105011, hep-th/0111235.

[16] D. E. Kaplan, G. D. Kribs, and M. Schmaltz, *Supersymmetry breaking through transparent extra dimensions*, Phys. Rev. **D62** (2000), 035010, hep-ph/9911293.

[17] Z. Chacko, M. A. Luty, A. E. Nelson, and E. Ponton, *Gaugino mediated supersymmetry breaking*, JHEP **01** (2000), 003, hep-ph/9911323.

[18] T. Asaka, W. Buchmüller, and L. Covi, *Exceptional coset spaces and unification in six dimensions*, Phys. Lett. **B540** (2002), 295–300, hep-ph/0204358.

[19] T. Asaka, W. Buchmüller, and L. Covi, *Bulk and brane anomalies in six dimensions*, Nucl. Phys. **B648** (2003), 231–253, hep-ph/0209144.

[20] T. Asaka, W. Buchmüller, and L. Covi, *Quarks and leptons between branes and bulk*, Phys. Lett. **B563** (2003), 209–216, hep-ph/0304142.

[21] Z. Chacko, M. A. Luty, and E. Ponton, *Massive higher-dimensional gauge fields as messengers of supersymmetry breaking*, JHEP **07** (2000), 036, hep-ph/9909248.

[22] W. Buchmüller, K. Hamaguchi, and J. Kersten, *The gravitino in gaugino mediation*, Phys. Lett. **B632** (2006), 366–370, hep-ph/0506105.

[23] T. Falk, K. A. Olive, and M. Srednicki, *Heavy sneutrinos as dark matter*, Phys. Lett. **B339** (1994), 248–251, hep-ph/9409270.

[24] Particle Data Group, S. Eidelman et al., *Review of particle physics*, Phys. Lett. **B592** (2004), 1.

[25] W. Buchmüller, K. Hamaguchi, M. Ratz, and T. Yanagida, *Supergravity at colliders*, Phys. Lett. **B588** (2004), 90–98, hep-ph/0402179.

[26] K. Hamaguchi, Y. Kuno, T. Nakaya, and M. M. Nojiri, *A study of late decaying charged particles at future colliders*, Phys. Rev. **D70** (2004), 115007, hep-ph/0409248.

[27] J. L. Feng and B. T. Smith, *Slepton trapping at the large hadron and international linear colliders*, Phys. Rev. **D71** (2005), 015004, hep-ph/0409278.

[28] A. Brandenburg, L. Covi, K. Hamaguchi, L. Roszkowski, and F. D. Steffen, *Signatures of axinos and gravitinos at colliders*, Phys. Lett. **B617** (2005), 99–111, hep-ph/0501287.

[29] H.-U. Martyn, *Detecting metastable staus and gravitinos at the ILC*, (2006), hep-ph/0605257.

[30] J. R. Ellis, A. R. Raklev, and O. K. Øye, *Gravitino dark matter scenarios with massive metastable charged sparticles at the LHC*, (2006), hep-ph/0607261.

[31] J. L. Feng, A. Rajaraman, and F. Takayama, *SuperWIMP dark matter signals from the early universe*, Phys. Rev. **D68** (2003), 063504, hep-ph/0306024.

[32] M. Fujii, M. Ibe, and T. Yanagida, *Upper bound on gluino mass from thermal leptogenesis*, Phys. Lett. **B579** (2004), 6–12, hep-ph/0310142.

[33] J. L. Feng, S. Su, and F. Takayama, *Supergravity with a gravitino LSP*, Phys. Rev. **D70** (2004), 075019, hep-ph/0404231.

[34] J. R. Ellis, K. A. Olive, Y. Santoso, and V. C. Spanos, *Gravitino dark matter in the CMSSM*, Phys. Lett. **B588** (2004), 7–16, hep-ph/0312262.

[35] L. Roszkowski, R. Ruiz de Austri, and K.-Y. Choi, *Gravitino dark matter in the CMSSM and implications for leptogenesis and the LHC*, JHEP **08** (2005), 080, hep-ph/0408227.

[36] W. Buchmüller, J. Kersten, and K. Schmidt-Hoberg, *Squarks and sleptons between branes and bulk*, JHEP **02** (2006), 069, hep-ph/0512152.

[37] W. Buchmuller, L. Covi, J. Kersten, and K. Schmidt-Hoberg, *Dark matter from gaugino mediation*, JCAP **0611** (2006), 007, hep-ph/0609142.

[38] T. Kaluza, *On the problem of unity in physics*, Sitzungsber. Preuss. Akad. Wiss. Berlin (Math. Phys.) **1921** (1921), 966–972.

[39] O. Klein, *Quantum theory and five-dimensional theory of relativity*, Z. Phys. **37** (1926), 895–906.

[40] M. B. Green, J. H. Schwarz, and E. Witten, *Superstring theory. vol. 1: Introduction*, Cambridge, Uk: Univ. Pr. (1987) 469 P. (Cambridge Monographs On Mathematical Physics).

[41] M. B. Green, J. H. Schwarz, and E. Witten, *Superstring theory. vol. 2: Loop amplitudes, anomalies and phenomenology*, Cambridge, Uk: Univ. Pr. (1987) 596 P. (Cambridge Monographs On Mathematical Physics).

[42] N. Arkani-Hamed, S. Dimopoulos, and G. R. Dvali, *The hierarchy problem and new dimensions at a millimeter*, Phys. Lett. **B429** (1998), 263–272, hep-ph/9803315.

[43] J. Scherk and J. H. Schwarz, *How to get masses from extra dimensions*, Nucl. Phys. **B153** (1979), 61–88.

[44] H. Georgi, A. K. Grant, and G. Hailu, *Brane couplings from bulk loops*, Phys. Lett. **B506** (2001), 207–214, hep-ph/0012379.

[45] A. Hebecker and J. March-Russell, *The structure of gut breaking by orbifolding*, Nucl. Phys. **B625** (2002), 128–150, hep-ph/0107039.

[46] C. Csaki, *Tasi lectures on extra dimensions and branes*, (2004), hep-ph/0404096.

[47] W. D. Goldberger and M. B. Wise, *Modulus stabilization with bulk fields*, Phys. Rev. Lett. **83** (1999), 4922–4925, hep-ph/9907447.

[48] H. B. G. Casimir, *On the attraction between two perfectly conducting plates*, Indag. Math. **10** (1948), 261–263.

[49] B. V. Deriagin and I. I. Abrikosova, *Direct measurement of the molecular attraction of solid bodies. I. statement of the problem and method of measuring forces by using negative feedback*, Sov. Phys. JETP **3** (1957), 819–829.

[50] M. J. Sparnaay, *Measurements of attractive forces between flat plates*, Physica **24** (1958), 751–764.

[51] G. Plunien, B. Muller, and W. Greiner, *The casimir effect*, Phys. Rept. **134** (1986), 87–193.

[52] J. S. Dowker and R. Critchley, *Effective lagrangian and energy momentum tensor in de sitter space*, Phys. Rev. **D13** (1976), 3224.

[53] S. W. Hawking, *Zeta function regularization of path integrals in curved space-time*, Commun. Math. Phys. **55** (1977), 133.

[54] E. Elizalde, *Ten physical applications of spectral zeta functions*, Springer, Berlin.

[55] E. Ponton and E. Poppitz, *Casimir energy and radius stabilization in five and six dimensional orbifolds*, JHEP **06** (2001), 019, hep-ph/0105021.

[56] M. Ito, *Casimir forces due to matters in compactified six dimensions*, Nucl. Phys. **B668** (2003), 322–334, hep-ph/0301168.

[57] D. M. Ghilencea, D. Hoover, C. P. Burgess, and F. Quevedo, *Casimir energies for 6d supergravities compactified on t(2)/z(n) with wilson lines*, JHEP **09** (2005), 050, hep-th/0506164.

[58] M. E. Peskin and D. V. Schroeder, *An introduction to quantum field theory*, Reading, USA: Addison-Wesley (1995) 842 p.

[59] S. Dimopoulos, S. Raby, and F. Wilczek, *Supersymmetry and the scale of unification*, Phys. Rev. **D24** (1981), 1681–1683.

[60] T. Fukuyama, A. Ilakovac, T. Kikuchi, S. Meljanac, and N. Okada, *So(10) group theory for the unified model building*, J. Math. Phys. **46** (2005), 033505, hep-ph/0405300.

[61] G. F. Giudice and A. Masiero, *A natural solution to the mu problem in supergravity theories*, Phys. Lett. **B206** (1988), 480–484.

[62] M. Drees, *Intermediate scale symmetry breaking and the spectrum of super partners in superstring inspired supergravity models*, Phys. Lett. **B181** (1986), 279.

[63] C. F. Kolda and S. P. Martin, *Low-energy supersymmetry with D term contributions to scalar masses*, Phys. Rev. **D53** (1996), 3871–3883, hep-ph/9503445.

[64] MEGA, M. Ahmed et al., *Search for the lepton-family-number nonconserving decay mu+ -> e+ gamma*, Phys. Rev. **D65** (2002), 112002, hep-ex/0111030.

[65] A. G. Cohen, D. B. Kaplan, and A. E. Nelson, *The more minimal supersymmetric standard model*, Phys. Lett. **B388** (1996), 588–598, hep-ph/9607394.

[66] W. Buchmüller, L. Covi, D. Emmanuel-Costa, and S. Wiesenfeldt, *Flavour structure and proton decay in 6D orbifold GUTs*, JHEP **09** (2004), 004, hep-ph/0407070.

[67] W. Buchmüller, K. Hamaguchi, O. Lebedev, and M. Ratz, *The supersymmetric standard model from the heterotic string*, (2005), hep-ph/0511035.

[68] M. Dine and N. Seiberg, *Is the superstring semiclassical?*, Presented at Unified String Theories Workshop, Santa Barbara, CA, Jul 29 - Aug 16, 1985.

[69] B. C. Allanach, *SOFTSUSY: A C++ program for calculating supersymmetric spectra*, Comput. Phys. Commun. **143** (2002), 305–331, hep-ph/0104145.

[70] D. M. Ghilencea, H. M. Lee, and K. Schmidt-Hoberg, *Higher derivatives and brane-localised kinetic terms in gauge theories on orbifolds*, JHEP **08** (2006), 009, hep-ph/0604215.

[71] J. R. Ellis, C. Kounnas, and D. V. Nanopoulos, *No-scale supersymmetric GUTs*, Nucl. Phys. **B247** (1984), 373–395.

[72] K. Inoue, M. Kawasaki, M. Yamaguchi, and T. Yanagida, *Vanishing squark and slepton masses in a class of supergravity models*, Phys. Rev. **D45** (1992), 328–337.

[73] CDF Collaboration, D0 Collaboration, and Tevatron Electroweak Working Group, *Combination of CDF and D0 results on the top-quark mass*, (2005), hep-ex/0507091.

[74] K. Inoue, A. Kakuto, H. Komatsu, and S. Takeshita, *Aspects of grand unified models with softly broken supersymmetry*, Prog. Theor. Phys. **68** (1982), 927.

[75] K. Inoue, A. Kakuto, H. Komatsu, and S. Takeshita, *Renormalization of supersymmetry breaking parameters revisited*, Prog. Theor. Phys. **71** (1984), 413.

[76] J. L. Evans, D. E. Morrissey, and J. D. Wells, *Higgs boson exempt no-scale supersymmetry and its collider and cosmology implications*, Phys. Rev. **D75** (2007), 055017, hep-ph/0611185.

[77] A. Lleyda and C. Muñoz, *Non-universal soft scalar masses in supersymmetric theories*, Phys. Lett. **B317** (1993), 82–91, hep-ph/9308208.

[78] D. E. Kaplan and T. M. P. Tait, *Supersymmetry breaking, fermion masses and a small extra dimension*, JHEP **06** (2000), 020, hep-ph/0004200.

[79] M. Schmaltz and W. Skiba, *The superpartner spectrum of gaugino mediation*, Phys. Rev. **D62** (2000), 095004, hep-ph/0004210.

[80] M. Kawasaki, K. Kohri, and T. Moroi, *Big-bang nucleosynthesis and hadronic decay of long-lived massive particles*, Phys. Rev. **D71** (2005), 083502, astro-ph/0408426.

[81] D. G. Cerdeño, K.-Y. Choi, K. Jedamzik, L. Roszkowski, and R. Ruiz de Austri, *Gravitino dark matter in the CMSSM with improved constraints from BBN*, JCAP **0606** (2006), 005, hep-ph/0509275.

[82] H. Baer, A. Belyaev, T. Krupovnickas, and X. Tata, *The reach of the Fermilab Tevatron and CERN LHC for gaugino mediated SUSY breaking models*, Phys. Rev. **D65** (2002), 075024, hep-ph/0110270.

[83] D. Clowe et al., *A direct empirical proof of the existence of dark matter*, (2006), astro-ph/0608407.

[84] U. Seljak, A. Slosar, and P. McDonald, *Cosmological parameters from combining the Lyman-alpha forest with CMB, galaxy clustering and SN constraints*, JCAP **0610** (2006), 014, astro-ph/0604335.

[85] M. Bartelmann and P. Schneider, *Weak gravitational lensing*, Phys. Rept. **340** (2001), 291–472, astro-ph/9912508.

[86] W. Buchmuller, L. Covi, K. Hamaguchi, A. Ibarra, and T. Yanagida, *Gravitino dark matter in r-parity breaking vacua*, (2007), hep-ph/0702184.

[87] E. W. Kolb and M. S. Turner, *The early universe*, Frontiers in Physics (1990).

[88] K. Griest and D. Seckel, *Three exceptions in the calculation of relic abundances*, Phys. Rev. **D43** (1991), 3191–3203.

[89] T. Asaka, K. Hamaguchi, and K. Suzuki, *Cosmological gravitino problem in gauge mediated supersymmetry breaking models*, Phys. Lett. **B490** (2000), 136–146, hep-ph/0005136.

[90] P. Gondolo and G. Gelmini, *Cosmic abundances of stable particles: Improved analysis*, Nucl. Phys. **B360** (1991), 145–179.

[91] G. Belanger, F. Boudjema, A. Pukhov, and A. Semenov, *micrOMEGAs: A program for calculating the relic density in the MSSM*, Comput. Phys. Commun. **149** (2002), 103–120, hep-ph/0112278.

[92] G. Belanger, F. Boudjema, A. Pukhov, and A. Semenov, *micrOMEGAs: Version 1.3*, Comput. Phys. Commun. **174** (2006), 577–604, hep-ph/0405253.

[93] CDF and D0 Collaborations, Tevatron Electroweak Working Group, *Combination of CDF and D0 results on the mass of the top quark*, (2006), hep-ex/0603039.

[94] R. H. Cyburt, B. D. Fields, and K. A. Olive, *Primordial nucleosynthesis in light of wmap*, Phys. Lett. **B567** (2003), 227–234, astro-ph/0302431.

[95] R. H. Cyburt, J. R. Ellis, B. D. Fields, and K. A. Olive, *Updated nucleosynthesis constraints on unstable relic particles*, Phys. Rev. **D67** (2003), 103521, astro-ph/0211258.

[96] K. Jedamzik, *Big bang nucleosynthesis constraints on hadronically and electromagnetically decaying relic particles*, (2006), hep-ph/0604251.

[97] M. Kawasaki and T. Moroi, *Electromagnetic cascade in the early universe and its application to the big bang nucleosynthesis*, Astrophys. J. **452** (1995), 506, astro-ph/9412055.

[98] F. D. Steffen, *Gravitino dark matter and cosmological constraints*, JCAP **09** (2006), 001, hep-ph/0605306.

[99] S. Dimopoulos, R. Esmailzadeh, L. J. Hall, and G. D. Starkman, *Limits on late decaying particles from nucleosynthesis*, Nucl. Phys. **B311** (1989), 699.

[100] T. Jittoh, J. Sato, T. Shimomura, and M. Yamanaka, *Long life stau*, Phys. Rev. **D73** (2006), 055009, hep-ph/0512197.

[101] M. E. Gomez, T. Ibrahim, P. Nath, and S. Skadhauge, *Sensitivity of supersymmetric dark matter to the b quark mass*, Phys. Rev. **D70** (2004), 035014, hep-ph/0404025.

[102] J. R. Ellis, S. Heinemeyer, K. A. Olive, and G. Weiglein, *Indirect sensitivities to the scale of supersymmetry*, JHEP **02** (2005), 013, hep-ph/0411216.

[103] A. Djouadi, M. Drees, and J.-L. Kneur, *Updated constraints on the minimal supergravity model*, JHEP **03** (2006), 033, hep-ph/0602001.

[104] G. Jungman, M. Kamionkowski, and K. Griest, *Supersymmetric dark matter*, Phys. Rept. **267** (1996), 195–373, hep-ph/9506380.

[105] N. Fornengo, private communication.

[106] CDMS Collaboration, D. S. Akerib et al., *Limits on spin-independent WIMP nucleon interactions from the two-tower run of the Cryogenic Dark Matter Search*, Phys. Rev. Lett. **96** (2006), 011302, astro-ph/0509259.

[107] CDMS-II Collaboration, D. A. Bauer, *Current and future searches for dark matter*, AIP Conf. Proc. **815** (2006), 105–114.

[108] M. H. Reno and D. Seckel, *Primordial nucleosynthesis: The effects of injecting hadrons*, Phys. Rev. **D37** (1988), 3441.

[109] M. Pospelov, *Particle physics catalysis of thermal big bang nucleosynthesis*, (2006), hep-ph/0605215.

[110] K. Kohri and F. Takayama, *Big bang nucleosynthesis with long lived charged massive particles*, (2006), hep-ph/0605243.

[111] M. Kaplinghat and A. Rajaraman, *Big bang nucleosynthesis with bound states of long-lived charged particles*, (2006), astro-ph/0606209.

[112] K. Hamaguchi, T. Hatsuda, M. Kamimura, Y. Kino, and T. T. Yanagida, *Stau-catalyzed li-6 production in big-bang nucleosynthesis*, (2007), hep-ph/0702274.

[113] R. H. Cyburt, J. Ellis, B. D. Fields, K. A. Olive, and V. C. Spanos, *Bound-state effects on light-element abundances in gravitino dark matter scenarios*, (2006), astro-ph/0608562.

[114] W. Buchmuller, K. Hamaguchi, M. Ibe, and T. T. Yanagida, *Eluding the bbn constraints on the stable gravitino*, Phys. Lett. **B643** (2006), 124–126, hep-ph/0605164.

[115] J. Gratsias, R. J. Scherrer, and D. N. Spergel, *Indirect photofission of light elements from high-energy neutrinos in the early universe*, Phys. Lett. **B262** (1991), 298–302.

[116] A. A. de Laix and R. J. Scherrer, *Improved cosmological constraints on neutrino producing decaying particles*, Phys. Rev. **D48** (1993), 562–566.

[117] M. Kawasaki and T. Moroi, *Gravitino decay into a neutrino and a sneutrino in the inflationary universe*, Phys. Lett. **B346** (1995), 27–34, hep-ph/9408321.

[118] T. Kanzaki, M. Kawasaki, K. Kohri, and T. Moroi, *Cosmological constraints on gravitino lsp scenario with sneutrino nlsp*, Phys. Rev. **D75** (2007), 025011, hep-ph/0609246.

[119] D. J. Fixsen et al., *The cosmic microwave background spectrum from the full COBE/FIRAS data set*, Astrophys. J. **473** (1996), 576, astro-ph/9605054.

[120] W. Hu and J. Silk, *Thermalization and spectral distortions of the cosmic background radiation*, Phys. Rev. **D48** (1993), 485–502.

[121] R. Lamon and R. Durrer, *Constraining gravitino dark matter with the cosmic microwave background*, Phys. Rev. **D73** (2006), 023507, hep-ph/0506229.

[122] M. Bolz, A. Brandenburg, and W. Buchmüller, *Thermal production of gravitinos*, Nucl. Phys. **B606** (2001), 518–544, hep-ph/0012052.

[123] J. Pradler and F. D. Steffen, *Thermal gravitino production and collider tests of leptogenesis*, (2006), hep-ph/0608344.

[124] T. Yanagida, *Horizontal gauge symmetry and masses of neutrinos*, In Proceedings of the Workshop on the Baryon Number of the Universe and Unified Theories, Tsukuba, Japan, 13-14 Feb 1979.

[125] M. Fukugita and T. Yanagida, *Baryogenesis without grand unification*, Phys. Lett. **B174** (1986), 45.

[126] W. Buchmüller, P. Di Bari, and M. Plümacher, *Leptogenesis for pedestrians*, Ann. Phys. **315** (2005), 305–351, hep-ph/0401240.

[127] E. Elizalde, *Analysis of an inhomogeneous generalized epstein-hurwitz zeta function with physical applications*, J. Math. Phys. **35** (1994), 6100–6122.

Acknowledgments

I am very grateful to Wilfried Buchmüller for the supervision of my thesis, his advice throughout the years and many helpful discussions. I also would like to thank Jan Louis and Jochen Bartels for their co-supervision. Thanks to my collaborators, Riccardo Catena, Laura Covi, Dumitru Ghilencea, Jörn Kersten and Hyun Min Lee, without whom this thesis would not have been possible. Furthermore I want to thank Jan Hamann and Jonas Schmidt for proofreading, Dirk Brömmel for 'technical support' and my 'Um die Ecke gedacht' collaborators, Tobias Kleinschmidt and Toffi Lüdeling, as well as the DESY Theory Group for an enjoyable time. Finally I would like to thank my parents, who always supportet me in every possible way, and of course Marcia ♡